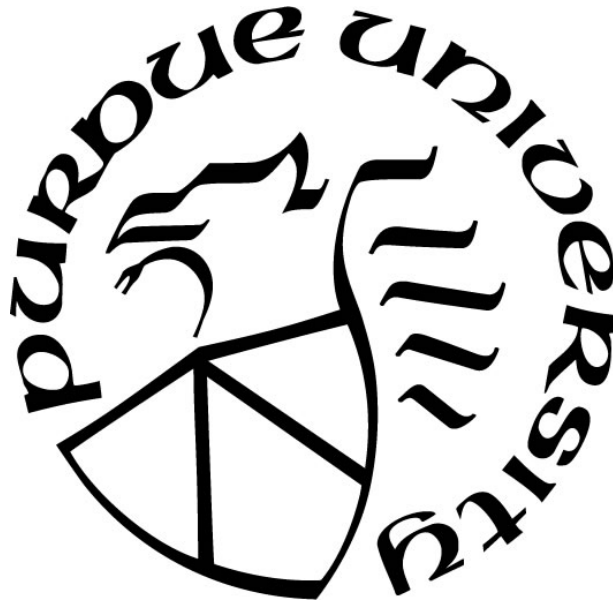# STOCHASTIC MODEL GENERATION AND SELECTION FOR DEVICE EMULATING STRUCTURAL MATERIAL NONLINEARITY

by

Sunny A. Sharma

A Thesis

Submitted to the Faculty of Purdue University

In Partial Fulfillment of the Requirements for the degree of

Master of Science in Civil Engineering

Lyles School of Civil Engineering

West Lafayette, Indiana

May 2021

THE PURDUE UNIVERSITY GRADUATE SCHOOL
STATEMENT OF COMMITTEE APPROVAL

Dr. Shirley Dyke, Chair

Department of Mechanical Engineering and Lyles School of Civil Engineering

Dr. Ayhan Irfanoglu

Lyles School of Civil Engineering

Dr. Mohammad Jahanshahi

Lyles School of Civil Engineering

Approved by:

Dr. Dulcy Abraham

To my family

ACKNOWLEDGMENTS

TABLE OF CONTENTS

LIST OF TABLES

LIST OF FIGURES

NOMENCLATURE

A	Bouc-Wen model parameter determining shape of hysteresis curve
A_{max}	Maximum amplitude (mm)
A_n	Linearization constant
c	Damping coefficient $(N \cdot s/m)$
e	Exponential constant (2.718)
E_t	Error in force with respect to time
E_x	Error in force with respect to displacement
$E_{\dot{x}}$	Error in force with respect to velocity
$E[\mathrm{X}]$	Expected value of matrix X
f	MR damper restoring force (N)
f_0	Initial force in the MR damper (N)
F_d	Coulomb frictional force (N)
f_{exp}	Experimental value of force (N)
f_{max}	Maximum frequency (Hz)
f_{pre}	Predicted value of force (N)
j	Numeric coefficient
k	Stiffness coefficient (N/m)
k_s	Post-yield stiffness (N/m)
k_z	Initial stiffness
l_x	Dimension of original state vector
m	Mass (kg)
N	Final time step (sec)
n	Bouc-Wen model parameter determining shape of hysteresis curve
n_f	Final value of parameter n
n_k	Measurement noise
$O(h^n)$	Error of order (n)
$\mathbf{P}_0$	Covariance of prior distribution
P_0	Initial covariance matrix

$p(x_0)$	Initial probability distribution
Q	Process noise covariance matrix
R	Measurement noise covariance matrix
r_0	Normalization constant
$r(t)$	Bouc-Wen model hysteretic component
S	Scaling factor
T	Time (sec)
$\mathbf{u}(t)$	Known input of the system
v_k	Process noise
$\mathbf{v}(t)$	Measurement noise
$W_i^{(c)}$	Weights for the covariance matrix
$W_i^{(m)}$	Weights for the mean
$\mathbf{w}(t)$	Process noise vector
x	MR Damper$_x$
$\mathbf{X}^a$	Augmented state vector
$\widehat{\mathbf{X}}_0$	Mean of prior distribution
x_k	State of the system at time step, k
$x(t)$	Displacement at time step, t
$\dot{x}(t)$	Velocity at time step, t
$\ddot{x}(t)$	Acceleration at time step, t
y	MR Damper$_y$
y_k	Measurement from sensors at time step, k
y_o	Observation equation
Z	Total number of observations
z	MR Damper$_z$
z	Internal hysteresis variable
α	Generalized stiffness parameter $(1/m)$
α_1	Ratio of post-yield to pre-yield
α_h	Spread of sigma points
β	Generalized stiffness parameter (N/m)

β_1	Bouc-Wen model parameter determining shape of hysteresis curve
β_h	Coefficient considering higher order effects and prior knowledge
γ	Bouc-Wen model parameter determining shape of hysteresis curve
ε	Generalized damping parameter $(N \cdot s/m)$
$\varepsilon_{\dot{x}}$	Coefficient for force error with respect to velocity
ε_t	Coefficient for force error with respect to time
ε_x	Coefficient for force error with respect to displacement
κ	Secondary scaling parameter
λ	Scaling parameter
μ_0	Initial mean matrix
μ_F	Mean of force (N)
ρ	Initial stiffness of z
σ	Parameter determining shape of hysteresis loop
σ_a^2	Variance in acceleration noise
σ_d^2	Variance in displacement noise
σ_f	Variance of experimental force
σ_j	Initial covariance estimates on parameters
τ	Index of dispersion
Δt	Time step (sec)

ABSTRACT

Structural identification is a useful tool for detecting damage and damage evolution in a structure. The initiation of damage in a structure and its subsequent growth are mainly associated with nonlinear behaviors. While linear dynamics of a structure are easy to simulate, nonlinear structural dynamics have more complex dynamics and amplitude dependence that do require more sophisticated simulation tools and identification methods compared to linear systems. Additionally, there are generally many more parameters in nonlinear models and the responses may not be sensitive to all of them for all inputs. To develop model selection methods, an experiment is conducted that uses an existing device with repeatable behavior and having an expected model from the literature. In this case, an MR damper is selected as the experimental device. The objective of this research is to develop and demonstrate a method to select the most appropriate model from a set of identified stochastic models of a nonlinear device. The method is developed using numerical example of a common nonlinear system, and is then implemented on an experimental structural system with unknown nonlinear properties. Bayesian methods are used because they provide a distinct advantage over many other existing methods due to their ability to provide confidence on answers given the observed data and initial uncertainty. These methods generate a description of the parameters of the system given a set of observations. First, the selected model of the MR damper is simulated and used for demonstrating the results on a numerical example. Second, the model selection process is demonstrated on an experimental structure based on experimental data. This study explores the use of the Bayesian approach for nonlinear structural identification and identifies a number of lessons for others aiming to employ Bayesian inference.

1. INTRODUCTION

1.1 Background

Structures are often subjected to different types of loads. The factor of safety accounted for during the design of a structure plays an important role in protecting the structure when subjected to excessive loads. However, structures are still prone to damage. Some of the reasons that contribute to the damage are extreme loading conditions that are not accounted for in the design, modifications on the existing structure, or due to the factors that were not accounted for in the design. The study of damage to these structures often follows a conventional linear approach. However, the linear analysis of some of the components of the structure often tend to be inadequate and points to the nonlinear dynamic analysis of the structure. Several incidents like the collapse of Tacoma Narrows Bridge in 1940 showed that there is a need to consider nonlinear effects during the design process and while investigating the cause of damage to the structure.

Identification of nonlinearity in experimental structure plays a major role in the study of nonlinear collapse mechanisms. It is evident from literature that several methods are efficacious in quickly identifying nonlinearity in experiments. Some of these methods include restoring force identification, static testing, Bayesian model identification, etc. Bayesian structural identification is a prominent approach when identifying nonlinearities in highly noisy data environments. When using technique of recursive identification, filtering methods adopted include the particle filter and the Kalman filter.

The current study focuses on the application of Bayesian structural identification methods, specifically the Kalman filter family of algorithms, to a scaled-down model of a building with a device simulating material nonlinearity. Though this building is small-scale, the dimensionality of the identification problem will be analogous to the full-scale system, without undue model uncertainty. The identification approach followed for the scaled-down model can then be extended to the identification of nonlinearity on actual structures. The findings of this research will contribute to the process of model selection for a nonlinear device installed on an experimental structure.

1.2 Objective

The primary objectives of this thesis can be described as:

- Choose a device that exhibits a repeatable nonlinearity in an experimental structure. The device simulating nonlinearity is selected based on comparative literature study of different types of devices. The most appropriate device for experimental purpose is selected based on its feasibility in terms of controllability, repeatability and the ability to quantify its behavior physically.

- Provide a numerical example of the identification method using the selected nonlinear device with a computational structural model. This example will verify the code and illustrate the behavior of the device when connected to the experimental structure.

- Conduct tests with the device on the experimental structure and implement a generalized model selection procedure to select the most suitable model of the nonlinear device that represents the experimental behavior. The experiments are performed in different sets and the response of the structure with and without the nonlinear device is studied.

1.3 Organization

The thesis has been organized into six chapters. A detailed literature study on the nonlinear structural identification method and the selection of nonlinear device is provided in Chapter 2. This chapter reviews different nonlinear devices that can be used for the study and identifies the most appropriate device based on the current experimental setup. Chapter 3 gives an overview of model selection methods and demonstrates the method selected using a computational model of the selected nonlinear device and structure. This chapter lays the foundation for the model selection process performed on the experimental structure in the subsequent chapters. The setup of the selected nonlinear device is described in Chapter 4. The nonlinear device is installed on a SDOF scaled-down experimental structure. This chapter explains the overall test setup for the experiment. Chapter 5 explains the test input used for the experiment. This chapter continues the model selection process from Chapter 3 and with the added challenge of applying the method to experimental results in which the true model of the device is not known. The most appropriate model is then selected for the experimental device used. Chapter 6 concludes the research findings and discusses the future work.

2. LITERATURE REVIEW

2.1   Nonlinear Structural Identification

Nonlinear structural identification is usually done with different methods like sequential Monte Carlo, H_∞ filter, extended Kalman filter (EKF), least square estimation (LSE), etc. The Bayesian method for nonlinear estimation of states characterizes the uncertainty in the identification process using a probability density function (PDF) created from the available data. The Kalman filter is normally used to estimate the linear behavior using a Gaussian distribution (Kalman, 1960). It is a process of inferring the hidden states of the dynamic system from experimental measurements of the systems behavior, which are noise-contaminated. The method represents the optimal filter for linear systems, and uses a theoretical model of the system to infer the posterior probability of the states for each measurement step. The application of Kalman filter in complex structural health monitoring problems under varying environmental conditions has been successfully studied by Erazo et al. (2019). However, parameter estimation is an inherently nonlinear problem and cannot be addressed by standard linear inference techniques like Kalman filter. For nonlinear estimation of unknown variables, a recursive estimation method using EKF is used. The EKF uses a Taylor series expansion for the functions and has widely been used for civil engineering applications involving vibration measurements. Gordon et al. (1993) proposed a recursive algorithm that used random samples to represent the PDF. A roughening prior editing procedure was used to prevent the truly distinct values from collapsing in the sample. It is evident that the results are better when compared with an extended Kalman filter application.

Wan & van der Merwe (2000) used the Unscented Kalman Filter (UKF) for the nonlinear state and parameter estimation. The authors indicated the drawbacks of using EKF. The joint parameter estimation and state estimation problems considered in the study revealed that the UKF produced better results when compared to the EKF. The approximation of states by a Gaussian random variable (GRV) while using an EKF propagates error throughout the nonlinear system. This error is averted by the usage of sample points while approximating states by a GRV in the UKF approach. Also, the EKF method relies on calculation of a Jacobian matrix and complex linearized functions. The UKF incorporates functional nonlinearity of variables and eliminates the calculation of a Jacobian matrix. The posterior from the Bayes theorem is directly dependent on

likelihood and prior. The UKF approach helps to identify the posterior mean and covariance matrices using the true mean and covariance of the GRV generated from the sample points. Wu and Smyth (2007) while studying the application of EKF and UKF for real-time identification of nonlinear systems showcased that the UKF produced better state estimates and provided better identification of parameters of the nonlinear system. This was concluded from the results of EKF and UKF implementation on single degree-of-freedom (SDOF) and multi DOF structures with hysteresis behavior. Olivier and Smyth (2017) concluded that the UKF seemed to be efficient for identifiable systems and unidentifiable parameters. However, the use of particle filter was recommended for locally identifiable systems when sufficient particles were available for the approximation.

Several modifications to the conventional EKF and UKF methods have been done recently. A structured black box variational inference method for models with latent time series was introduced by Bamler and Mandt (2017). Wan and Nelson (1997) demonstrated the use of dual Kalman filters and provided several updates for nonlinear prediction of neural networks. These filters are useful to estimate both the states and parameters of the system. Lei et al. (2019) presented an updated UKF method for nonlinear identification methods where the input excitation is absent. A damped least squares method was used in their approach to interpolate between the Gauss-Newton algorithm and the method of gradient descent while trying to find the minimum in nonlinear optimization problems. The proposed method was validated numerically for a six-story hysteretic chain subjected to unknown force excitation. The method successfully identified the unknown states and input excitation using the modified approach. Chatzi and Smyth (2009) studied a combination of displacement and acceleration data from sensors for degrees of freedom of a structure. A Gaussian mixture sigma-point particle filter developed in this study turned out to be more robust when compared to the UKF. This was demonstrated with the results from the estimation of time invariant model parameters in the nonlinear system. A complex nonlinear UKF introduced by Olivier and Smyth (2017) is computationally efficient for posteriors with complex distributions. The updated filter was capable to tackle complex Gaussian noise terms. Lund et al. (2019) performed a Sobol sensitivity analysis and demonstrated its application by identifying an experimental nonlinear energy sink (NES) device. The degree of identifiability was influenced by the magnitude of sensitivity and the duration of regions with high sensitivity.

The application of UKF in model selection and assessment has been extensively studied by several researchers. The Bayesian method of model selection comprises of updating current model classes for the prediction of structural response to compare between the available classes of the model. It selects a best fit model from a set of many stochastic models of the device dynamics. An online identification scheme for the estimation of states and parameters along with Bayesian model assessment was combined by Kontoroupi and Smyth (2017) to provide one unique method for the health monitoring of structures. This method was then demonstrated for different hysteretic candidate models. Muto and Beck (2008) performed a Bayesian updating and model class selection on a Masing hysteretic structural model. The study indicated that the comparisons for different model classes should consider the complexity of the model along with the quality of data fit by the model. This is in line with Occam's razor principle that states the model with a simpler implementation should be preferred over models with complex implementation if very little improvement in data fit is obtained from the more complex model. A best fit class of models based on the largest probability of the model class conditional on data was implemented by Beck and Yuen (2004). The Bayesian probabilistic approach used in the study was dependent on the evidence of the class of models available from the data. Lund et al. (2020) while demonstrating the method for the dentification of a NES device using the UKF and experimental data discovered that slight variations in prior distribution of parameters leads to variation in the identified models. The sensitivity of training signals for the parameters plays an important role in identifying the most appropriate model.

2.2   Selection of Nonlinear Device

Experiments aiming to study nonlinear dynamics of structures often require components in structures that induce nonlinearity. The goal of the experimental process in this study is to generate a rich set of experimental data with known variations in nonlinearity, such that the abilities of the Bayesian identification algorithm can be comparatively evaluated on a sufficiently complex case study. Nonlinearity in structures is studied through a nonlinear stress versus strain relation (called material nonlinearity), through a nonlinear displacement versus strain relation (called geometric nonlinearity) or through contact surfaces (via friction, sliding). While it is easy to induce these nonlinearities in an experimental structure through different methods (nonlinear springs, NES, magnetorheological dampers, etc.), it is imperative to deliberate between these devices for better

controllability, repeatability and efficiency. These nonlinear devices can be selected depending upon various properties they propagate to the experimental structure.

With this as the goal, the ideal nonlinear mechanism to produce these effects in an experimental structure should be controllable, repeatable, and adequately reactive to the level of disturbance in the structure. The controllability provided by such device will play a vital role in performing range of experiments over similar models and simulate controlled damage in the structure. Repeatability, in this context, suggests a nonlinear device that is resistant to changes in its inherent dynamic properties due to dynamic excitations performed on the main structure. Depending upon the complexities allowed in modelling of these structures, their equation of motion (EOM) play a critical role in this decision. The cost of the devices also plays a major role in determining the viability of these devices for each experiment. At the same time the device should be capable of producing complexity in the given structure with or without simulation of damage.

As the purpose of this study is not to develop new nonlinear devices, but rather to use them to enhance the study of nonlinear identification approach, a candidate device is selected based on a review of the literature on nonlinear structural mechanisms. This section systematically considers and compares different nonlinear devices in terms of their ease of implementation, complexities in their EOM, their cost and controllability. The most suitable device is then tested on an experimental structure. The implementation of the device on the experimental structure is discussed in Chapter 4.

A literature review for twelve active, semi-active and passive damping devices revealed different ways these devices simulate nonlinearity to the structure. The active and semi-active damping devices comprised of a magnetorheological (MR) damper, a bicycle brake, a variable friction damper, a semi-active tuned mass damper (STMD) and an electromagnetic friction damper. The passive damping devices reviewed in the study comprised of a coupled oscillator, a NES, a nonlinear negative magnetic stiffness system (NNMS), a unit cell, a cantilever beam and a spring. Though active devices would be more helpful in benchmarking the identification techniques, passive devices are simpler to design and build and are therefore considered as potential mechanisms. The next two sections identify these active, semi-active and passive devices. This is followed by a section on device selection that helps to identify the most appropriate device based on some key factors associated with this study.

2.2.1 Active and semi-active devices

A nonlinear system identification for multi-input, multi-output system has been performed by Kim et al. (2009). The study comprised of structures equipped with MR dampers. The MR damper acts as a semi-active system and holds advantages over traditional active controlled systems. A benefit of semi-active devices is that these devices offer adaptability of active control devices without any large power sources. The MR dampers continue to act as a passive damping system in case of failure of some of its components. The governing differential equations for MR damper in this study were based on modified Bouc-Wen model. The MR dampers act nonlinearly when used for energy dissipation in structural systems and hence, these controllable devices become viable when cost is not a concern. Figure 2.1 shows a schematic of these dampers in a high-rise building system. These MR dampers are the best fit if controllable nonlinearity is a priority in an experiment.

Brakes can help in a significant way for inducing nonlinearity in structures. The friction force generated by the application of a brake is of nonlinear type. The modelling of frictional forces in a brake has been performed by various researchers. Chang and Hu (2016) developed a simplified 2 DOF model for generating EOM of a brake. The model considered in this study is shown in Figure 2.2. The application of the model directly to the current structure depends on the accuracy of this simplified model. More complex equations might be required for detailed study of these brakes on a structure.
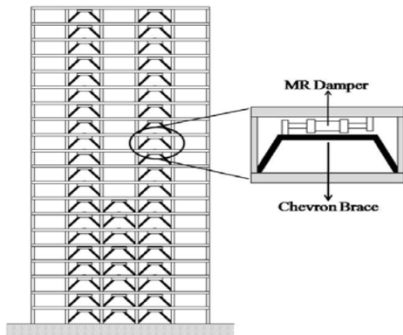
Figure 2.1. MR Damper
(Kim et al., 2009)
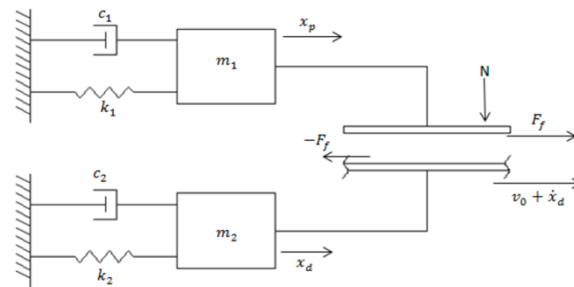
Figure 2.2. 2 DOF Model of Brake
(Chang & Hu, 2016)

A variable friction damper has been actively used in structural control applications. This device has been studied by Nishitani et al. (1999) while discussing a methodology for semi-active structural control. The nonlinear friction force is generated in these devices with the help of surface friction. The SDOF system considered in this study is shown in Figure 2.3. The use of friction dampers is possible for the structure if complexity of equation is not of any concern. In the research related to the seismic isolation of buildings from earthquake, Ealangi (2010) studied different devices used for seismic isolation. Flat slider bearings and curved slider bearings are some of the friction type devices studied in this research.

A MR damper can be controlled by the motion of hydraulic actuator and provides passive damping to the structure. The friction force in a bike brake can be varied by changing the application of brake pressure and thereby leading to changing nonlinearity. A variable friction damper works on the same principle as a bicycle brake and the force is produced using surface friction. Thus, these devices induce controllable nonlinearity in the structure and at the same time are repeatable due to their robust equipment over the course of the test.

The presence of material nonlinearity in STMD has been studied by Karami et al. (2019). The nonlinearity is generated when STMD is subjected to strong dynamic excitations. The STMD used in this study was developed on the lines of a semi-active independently variable stiffness (SAIVS) device. The device consists of four linear springs attached in a rhomboid configuration and is shown in Figure 2.4. Variation in stiffness and response of this device becomes feasible by changing the angle, θ. Application of such device becomes feasible in areas of structural control. The STMD can be used for the current research by installing it directly over the top of the structural system.
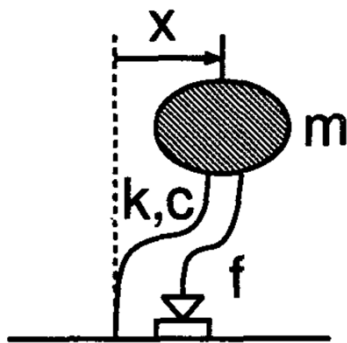
Figure 2.3. Variable Friction
Damper (Nishitani et al., 1999)
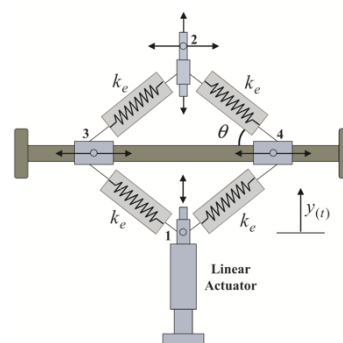
Figure 2.4. Semi-active Tuned
Mass Damper (Karami et al., 2019)

A seismic response study on a multi-story building has been done by Amjadian and Agrawal (2019). An electromagnetic friction damper developed for the study was used as a base isolator for the building. The device was made of a ferromagnetic plate and two thick rectangular ferromagnetic coils arranged in series. These coils were installed on the sides of plate using two non-magnetic friction pads. A semi-active controller was then used to control the magnitude of force generated from friction between friction pads and ferromagnetic plates. It was studied that the arrangement of coils according to the direction of their poles led to an increase or decrease in the magnitude of the force. The setup of this device is shown in Figure 2.5.
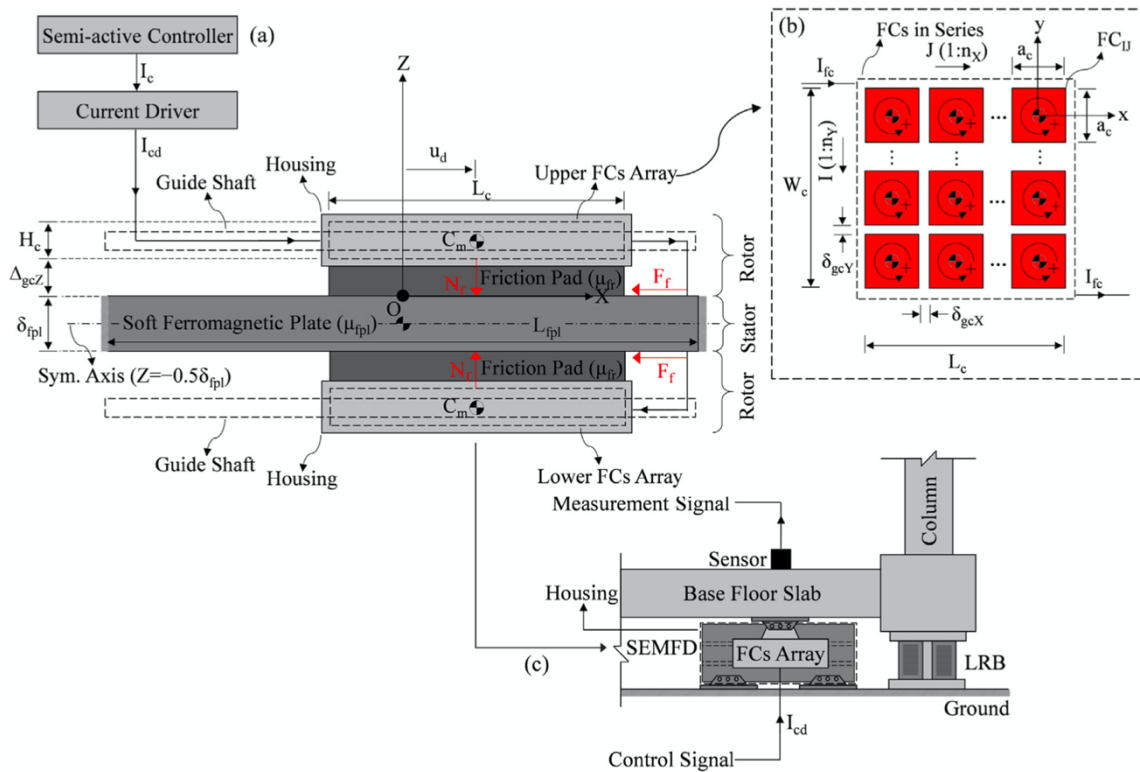
Figure 2.5. Electromagnetic Friction Damper (Amjadian & Agrawal, 2019)

2.2.2   Passive devices

A two degree-of-freedom system with combined nonlinear stiffness and damping has been developed by Andersen et al. (2012) while studying dynamic instabilities in coupled oscillators. The generated nonlinearity was induced by geometrically nonlinear damping in the system. The

top small mass in the system was subjected to geometrical nonlinearity due to the vertical component of the force acting on it from inclined spring and dampers. Figure 2.6 shows the general configuration of this device. The vibration of this device under dynamic excitations cannot be controlled. This type of nonlinearity becomes feasible for the current research if controllability is not required.

A NES is a passive device used to absorb generated energy due to vibrations in a structure. Starosvetsky and Gendelman (2008) while studying this device compared the nonlinear vibration with the best-tuned linear vibration. A NES consists of a small mass with a spring and a damper connected to the main system. In the present case, this NES can be installed on the linear system and nonlinearity can be induced by attaching a nonlinear spring to this NES. A NES connected to a linear subsystem is shown in Figure 2.7.
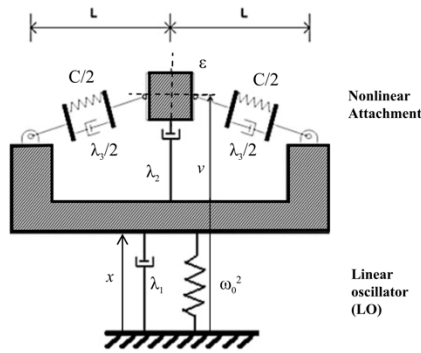
Figure 2.6. Coupled Oscillator
(Andersen et al., 2012)
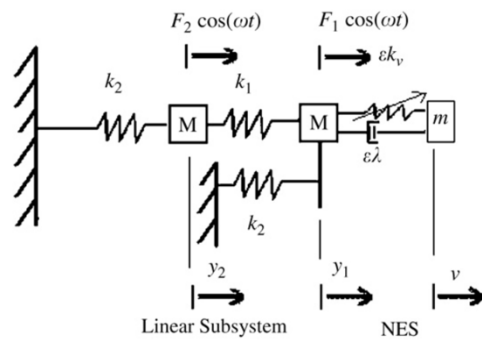
Figure 2.7. Nonlinear Energy Sink
(Starosvetsky & Gendelman, 2008)

Oyelade (2020) developed springs with negative stiffness using repelling magnets. A strong and variable nonlinearity is generated by changing the spacing between the magnets. The study demonstrates the behavior of these magnets by comparing with Duffing's equation, an equation for approximating cubic nonlinear stiffness. The configuration of this NNMS system is shown in Figure 2.8. An advantage of using this system is that no additional mass is attached to the main structural system. However, setting magnets at appropriate spacing and non-controllability propels away from using this system for the current application.
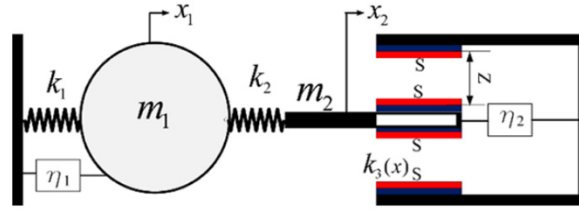
Figure 2.8. Nonlinear Negative Magnetic
Stiffness System (Oyelade, 2020)

An experimental modal analysis by the extraction of nonlinear normal modes has been performed by Peeters et al. (2011). The experimental validation has been performed using a cantilever beam with geometrical nonlinearity. Geometric nonlinearity was induced due to stiffening of a thin beam attached towards one end of the main beam. The experimental setup was excited in a direction parallel to the ground to avoid gravitational effects on the structure. This type of nonlinearity can be induced in a structure if it is feasible to change geometry of the structure in a direction perpendicular to gravitational force. However, such a type of nonlinearity is not controllable. Figure 2.9 shows top view of the experimental setup. The periodic response of this system is developed using complex Fourier series.

A nonlinear energy pumping phenomenon has been studied by McFarland et al. (2005). One of the 2 DOF oscillators in this study comprised of a nonlinear spring of cubic nonlinearity attached to a NES. The cubic nonlinearity was achieved by transverse vibration at the center of an initially unstretched thin rod clamped at both the ends. This method provides a repeatable method for inducing nonlinearity in structure. Figure 2.10 shows the schematic of thin rod. The EOM for the rod was generated from a Taylor series expansion. The analysis of this system when attached to the main structure depends upon the force acting at its center.

Figure 2.9. Ductility in Cantilever Beam
(Peeters et al., 2011)

Bunyan et al. (2018) developed nonlinearity in one-dimensional asymmetric lattice made of three cells. The experimental system was made of linearly coupled unit cells where each unit cell comprised of series coupling of oscillators. The nonlinearity was induced by strong stiffness of each unit cell. A strong cubic nonlinearity was obtained by coupling a large-scale model to an ungrounded oscillator of small mass with two parallel steel wires of 0.035 in. Figure 2.11 shows reduced order model of the asymmetric lattice. The complex EOM and sensitive wires make this system difficult for use in the current research. In addition to the above devices, a break-away element can also be considered to simulate nonlinearity in the structure. The break-away element is an element designed to be weaker than other elements in the structure and provides uncontrollable nonlinearity.
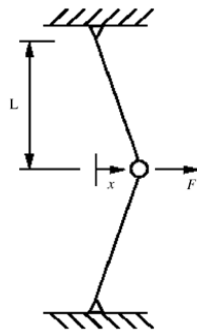
Figure 2.10. Cubic Nonlinearity using Thin Rod (McFarland et al., 2005)
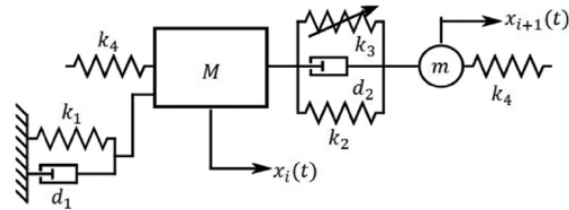
Figure 2.11. Unit Cell (Bunyan et al., 2018)

Spencer and Nagarajaiah (2003) reviewed many types of semi active control systems for controlling structures against earthquakes and wind loading. Some of the devices studied were variable-orifice fluid dampers, tuned liquid dampers, controllable fluid dampers and controllable impact dampers. A controllable nonlinearity can be produced by using an electromechanical variable-orifice damper. Controllable fluid dampers hold an advantage of reversibly changing their viscous fluid from free-flowing linear viscous fluid to a semisolid on an exposure to a magnetic field. The models of STMD, variable-stiffness device using SAIVS device has already been demonstrated here while the MR Damper was demonstrated in section 2.2.1.

2.2.3 Device Selection

Though the key factors in the selection of a device for this experimental study are the repeatability and controllability of the device, it will also be beneficial to work with a device whose dynamic behavior is relatively simple to understand. The dependence of models on large number of parameters and complex EOM makes understanding their behavior difficult. Thus, for an easy understanding of the behavior of nonlinear devices, it is important to select models with less complex EOM. The literature review reveals that a coupled oscillator, NES, NNMS system, spring and unit cells can be studied using simple EOM. However, it should be noted that the resulting EOM in case of a spring with thin rod can increase the complexity if it is attached to the main structural system. The remaining four devices pose an advantage of strong cubic nonlinearity with simple EOM but, are not controllable.

Although models with simpler EOM are easier to analyze in preliminary step of uncertainty quantification, the devices might not be repeatable for experimental phase. Based on the current study, a coupled oscillator and a NES consist of a sensitive spring attachment for their effective functioning. A spring might be subjected to tensioning before the start of the experiment and the usage of a spring with thin rod might not be viable. The unit cells are coupled with a series of oscillators and their application is dependent on sensitive steel wires. Therefore, usage of these devices on the main structure will lead to less reliable results and the devices might fail in some configurations. As the final criteria, the selection of a nonlinear device will be governed by the ease of installation of these devices on the main structure.

The above study for the selection of a nonlinear device reveals that it might not be possible to select a device that check marks all the possible factors. Therefore, it is important to assign priority to these factors for the selection of a suitable device for the experimental structure. On the lines of current goals of the study, a controllable and repeatable nonlinear device with less sensitive equipment can be used with complex EOM. Such a device will be helpful for the experimental study and its computational model will be based on complex EOM. It shows that a MR damper is controllable and repeatable with less sensitive equipment. The analytical studies of this device can be done by using EOM from previous studies. Thus, the MR damper (controllable, repeatable and complex nonlinearity) is selected for the current study. The properties of the MR damper used for further study along with other devices are summarized in Table 1.

Table 2.1: Summary of Nonlinear Component Selection

Sr. No.	Device	Nonlinearity	Controllable	Cost	Installation Complexity
1	MR Damper	Complex	Yes	High	Moderate
2	Variable Friction Damper	Complex	Yes	Moderate	Moderate
3	Break-away Element	Simple	No	Low	Easy
4	Coupled Oscillator	Cubic	No	Moderate	Moderate
5	NES	Cubic	No	Low	Easy
6	NNMS System	Cubic	No	High	Difficult
7	STMD	Trigonometric	No	Very High	Difficult
8	Cantilever Beam	Complex	No	Moderate	Moderate
9	Spring	Cubic	No	Low	Easy
10	Unit Cells	Cubic	No	Moderate	Moderate
11	Brake	Complex	Yes	Moderate	Difficult
12	Electromagnetic Friction Damper	Complex	Yes	Moderate	Moderate

2.3 Summary

The findings from the literature review of this chapter can be summarized as:

- A UKF is commonly used for nonlinear identification and model selection for civil engineering structures. (Section 2.1)
- Bayesian model selection technique selects a best fit model from a set of stochastic dynamic models. (Section 2.1)
- Along with the quality of data fit, the complexity of the model plays an important role in selecting the most appropriate model. (Section 2.1)
- The MR damper has been selected to propagate nonlinearity into the existing structural system. (Section 2.2)
- An MR damper is a controllable and repeatable device that can propagate nonlinearity into a structural system. Its modelling is based on complex EOM. (Section 2.2)

3. NUMERICAL STUDY OF MODEL SELECTION

3.1 Introduction

Kalman filters are normally used to approximate properties of linear and nonlinear systems. In particular, EKF and UKF are used for systems with nonlinear properties. The algorithms for these filters are based on Bayesian filtering equations. For highly nonlinear systems, UKF can provide a good approximation of the system states and model parameters. An overview of the filtering techniques along with a description of Bayesian filtering equations is given in this chapter. The application of the UKF for both parameter and state estimation to a basic SDOF Bouc-Wen model is demonstrated in Section 3.5. This study is followed by an explanation of the model selection procedure used for the current research in Section 3.6. The procedure is demonstrated by performing numerical model selection on three different models of the MR damper in Section 3.8. The best model for the MR damper is selected based on both the results of implementing both training and validation of the models, and on the specific criteria explained in this section.

3.2 Bayesian Filtering Equations

The Bayesian filtering method is used to approximate states of general probabilistic state space models that are represented by sequence consisting of conditional probability distributions. Consider the general probabilistic state space model for $k = 1, 2, ...,$

$$x_k \sim p(x_k|x_{k-1}) \tag{3-1}$$

$$y_k \sim p(y_k|x_k) \tag{3-2}$$

where the state of the system and the measurement from the sensors at time step $t_k = k\Delta t$ is represented by x_k and y_k, respectively. $p(x_k|x_{k-1})$ is a dynamical model of the system that gives information on stochastic dynamics of the system. The distribution of measurements used to estimate this information is given by the measurement model, $p(y_k|x_k)$. The model follows a Markovian property of states which means that the state x_k given x_{k-1} are independent of the prior

states of the system $(x_{k-2}, x_{k-3} \dots)$. Also, the current measurement of the system y_k given the state x_k is independent of any past measurements and states.

The Bayesian filtering equation aims to calculate the marginal posterior distribution of state x_k at each time step k provided the history of measurement is available until time step k. This term can be denoted by $p(x_k|y_{1:k})$. With an initial distribution $p(x_0)$, the recursive equation for Bayesian filtering gives the future distribution of state x_k at the time step k by Chapman-Kolmogorov equation given by,

$$p(x_k|y_{1:k-1}) = \int p(x_k|x_{k-1}) \, p(x_{k-1}|y_{1:k-1}) \, dx_{k-1}. \tag{3-3}$$

The predicted distribution is then updated from the measurement of the system y_k at time step k. The posterior distribution for state x_k is calculated using Bayes' theorem. This equation is given by,

$$p(x_k|y_{1:k}) = \frac{p(y_k|x_k) \, p(x_k|y_{1:k-1})}{\int p(y_k|x_k) \, p(x_k|y_{1:k-1}) \, dx_k}. \tag{3-4}$$

3.3 Kalman Filter

A Kalman filter is widely used to predict the linear behavior of a system. It gives a closed form solution for linear Gaussian problems comprising of Bayesian filtering equations. The filter assumes a Gaussian distribution with zero mean and follows a two-step recursive process. The first step is called the prediction step and the second step is called the update step. In the prediction step, the filter predicts the states of the system. It considers the noise in the system in order to account for any uncertainties. The predicted states are then corrected using the measurements from the system in the next step. The correction for the predicted states is based on an average of weights in the system. The predicted system state with a lower uncertainty is assigned a higher weight. A Kalman filter in its basic form cannot be used for systems exhibiting nonlinearities in either states or measurement and hence, its use is only limited to systems exhibiting linear behavior.

3.4   Extended Kalman Filter

An EKF has been developed to address the limitations of using a Kalman filter. These limitations have been indicated in Section 2.1. The EKF uses Taylor series expansion to approximate a nonlinear behavior by the linear approach. It provides results based on first-order approximations. The optimal state predictions in this approach are dependent on prior mean of the estimates. The nonlinear dynamic equations x_{k+1} and y_k are linearized as $x_{k+1} \approx A_1 x_k + A_2 v_k$ and $y_k \approx A_3 x_k + A_4 n_k$. The posterior covariance matrices are then calculated for the linear system. However, the approximation made by EKF may sometimes propagate errors in the true posterior mean and covariance of the transformed GRV. In addition, the EKF does not put constraints on the estimations of states. As a result, the estimations are sometimes obtained outside the domain defined for the states. Ungarala et al. (2007) presented a constrained EKF (CEKF) algorithm for putting linear constraints on the states. The use of CEKF for parameter identification was further demonstrated by Li and Wang (2021). It is inferred that the identification by CEKF gives better estimation than the conventional EKF. The CEKF makes sure that the parameter and state values lie in the physical domain. However, the CEKF still needs a differentiable system for the algorithm to work. As a result, the use of CEKF for non-differentiable systems becomes difficult. In addition, the comparison of the CEKF with the UKF algorithm for differentiable systems is yet to be studied.

3.5   Unscented Kalman Filter

A UKF uses the unscented transform (UT) to calculate a true posterior mean and covariance of a system to an accuracy of 3rd order Taylor series expansion (Wan & van der Merwe, 2000). Like the other two filters described above, it also uses a GRV to represent the state distribution of the system. However, for the UKF, the GRV is now specified using a set of deterministic sample points known as sigma points. The sigma points completely capture the true mean and covariance of the GRV. These sigma points are then propagated through the nonlinear system and the mean and covariance of the nonlinear system are calculated based on certain weights. The UKF also approximates the states for a system with non-Gaussian inputs, however, the accuracy for such systems depend on the value of parameters of the UKF. The approximations are accurate to at least second-order and become more accurate depending upon the values of the parameters chosen.

Figure 3.1 shows a comparison of predicted states by an EKF and a UKF. It is evident that the UKF approximations predict the behavior of the system more closely to the true mean and covariance (Wan & van der Merwe, 2000). A comparison of the three nonlinear algorithms based on different aspects is made in Table 3.1. The superiority of the UKF is evident due to its inherent property of estimating highly nonlinear differentiable systems without the requirement of partial derivatives. Although the UKF is the slowest of the three algorithms, the advantages mentioned here make it the best overall choice for the current nonlinear identification study.
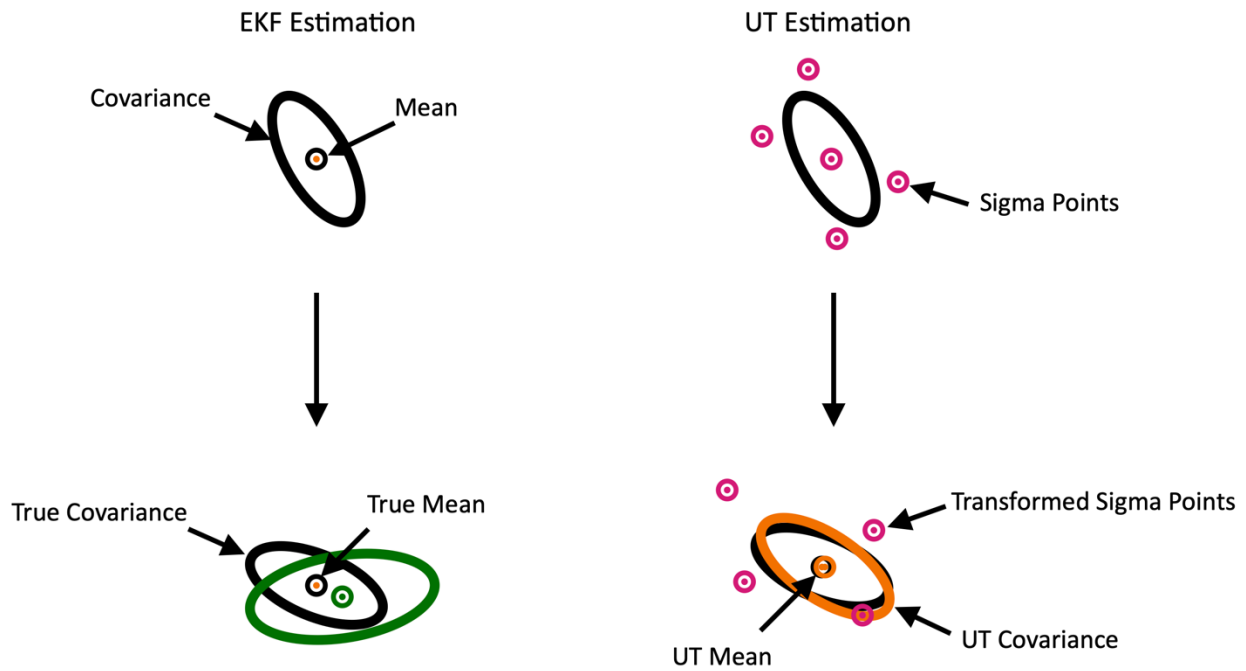
Figure 3.1. Comparison of Approximations

Table 3.1. Summary of Nonlinear Algorithms

Type	EKF	Constrained EKF	UKF
Operation Principle	Linearization	Linearization	Unscented transform
Accuracy	Low	Medium	High
Partial Derivatives	Required	Required	Not required
Speed	Fastest	Slightly slower	Slowest
Application	Nonlinear	Constrained nonlinear problems	Highly nonlinear

3.5.1 UKF Equations

Let a nonlinear continuous state-space equation and measurement equation of a general dynamic system be represented by,

$$\dot{\mathbf{X}} = \mathbf{f}(\mathbf{X}(t), \mathbf{u}(t), \mathbf{w}(t)) \tag{3-5}$$

$$\mathbf{Y}(t) = \mathbf{h}(\mathbf{X}(t), \mathbf{v}(t)) \tag{3-6}$$

where, the known input of the system is represented by $\mathbf{u}(t)$, the process noise vector in the system is represented by $\mathbf{w}(t)$ and the measurement noise is given by $\mathbf{v}(t)$. The discretized forms of Equations 3-5 and 3-6 are

$$\mathbf{X}_{k+1} = \mathbf{F}(\mathbf{X}_k, \mathbf{u}_k, \mathbf{w}_k) \tag{3-7}$$

$$\mathbf{Y}_k = \mathbf{H}(\mathbf{X}_k, \mathbf{v}_k). \tag{3-8}$$

Equations 3-7 and 3-8 give the discrete nonlinear difference state space equation. In the equation, the discrete process noise is represented by $w_k \sim N(0, \mathbf{Q}_k)$ and is kept as a Gaussian white noise having mean equal to zero and covariance matrix equal to Q. The measurement noise which is again assumed to be Gaussian white noise with mean equal to zero and covariance matrix equal to R is represented as $v_k \sim N(0, \mathbf{R}_k)$. For a time-step Δt belonging to the sampling time, Equation 3-5 can be used to calculate the following function F as,

$$\mathbf{F}(\mathbf{X}_k, \mathbf{u}_k, \mathbf{w}_k) = \mathbf{X}_k + \int_{k\Delta t}^{(k+1)\Delta t} \mathbf{f}(\mathbf{X}(t), \mathbf{u}(t), \mathbf{w}(t)) \mathrm{d}t. \tag{3-9}$$

The solution to the above Equation 3-9 can be calculated by numerical approximation method like the fourth-order Runge-Kutta method, also known as the 'classic Runge-Kutta method'. In this method, the solution at time step $(k + 1)\Delta t$ is found using the value available at the time step $k\Delta t$ and the average of the weights of four increments. These increments are calculated using the product of the increment time interval, Δt and the approximate slope of the function at the current

time step, at half of the time step Δt and at the time step Δt. The local truncation error in the fourth-order Runge-Kutta method is of the order $O(h^5)$ and the total accumulated error is of the order $O(h^4)$. In order to use the UKF algorithm for state and parameter estimation, we first concatenate the state vector to the original state vector and the noise variables. This equation is given by,

$$\mathbf{X}_k^a = [\mathbf{X}_k^T \ \mathbf{w}_k^T \ \mathbf{v}_k^T]^T. \tag{3-10}$$

The algorithm starts with the initialization step as,

$$\widehat{\mathbf{X}}_0 = E[\mathbf{X}_0] \tag{3-11}$$

$$\mathbf{P}_0 = E\left[(\mathbf{X}_0 - \widehat{\mathbf{X}}_0)(\mathbf{X}_0 - \widehat{\mathbf{X}}_0)^T\right] \tag{3-12}$$

$$\widehat{\mathbf{X}}_0^a = E[\mathbf{X}^a] = [\widehat{\mathbf{X}}_0^T \ \mathbf{0} \ \mathbf{0}]^T \tag{3-13}$$

$$\mathbf{P}_0^a = E\left[(\mathbf{X}_0^a - \widehat{\mathbf{X}}_0^a)(\mathbf{X}_0^a - \widehat{\mathbf{X}}_0^a)^T\right] = \begin{bmatrix} \mathbf{P_0} & \mathbf{0} & \mathbf{0} \\ \mathbf{0} & \mathbf{Q} & \mathbf{0} \\ \mathbf{0} & \mathbf{0} & \mathbf{R} \end{bmatrix}. \tag{3-14}$$

The sigma points are calculated at time step k for $k \in \{1, 2 \ldots \infty\}$ as,

$$\mathfrak{X}_{k+1|k}^X = \left[(\widehat{\mathbf{X}}_k^a) \ \left(\widehat{\mathbf{X}}_k^a + \sqrt{(L+\lambda)\mathbf{P}_k^a}\right) \left(\widehat{\mathbf{X}}_k^a - \sqrt{(L+\lambda)\mathbf{P}_k^a}\right)\right]. \tag{3-15}$$

The scaling parameter λ in the Equation 3-15 is given by,

$$\lambda = \alpha_h^2(l_x + \kappa) - l_x \tag{3-16}$$

where, the augmented state vector $\mathbf{X}^a$ has the dimension L and the original state vector $\mathbf{X}$ has the dimension l_x. The spread of sigma points around $\widehat{\mathbf{X}}_k^a$ is given by α_h. The value of α_h is normally set to a small positive number ranging between 0 and 1. The secondary scaling parameter κ in the Equation 3-16 is set to $(3 - l_x)$. For the current nonlinear identification study, the value of α_h is set as 0.0001 and the value of κ is set to 0. After the calculation of sigma points from Equation 3-

15, the prediction for the state vector $\widehat{\mathbf{X}}_{k+1}^-$ and the prediction for the covariance matrix $\mathbf{P}_{k+1}^-$ is made in the time update step. These equations are given by,

$$\mathfrak{X}_{k+1|k}^{\mathbf{X}} = \mathbf{F}(\mathfrak{X}_k^{\mathbf{X}}, \mathbf{u}_k, \mathfrak{X}_k^{\mathbf{w}}) \tag{3-17}$$

$$\widehat{\mathbf{X}}_{k+1}^- = \sum_{i=0}^{2L} W_i^{(m)} \mathfrak{X}_{i,k+1|k}^{\mathbf{X}} \tag{3-18}$$

$$\mathbf{P}_{k+1}^- = \sum_{i=0}^{2L} W_i^{(c)} \left[\mathfrak{X}_{i,k+1|k}^{\mathbf{X}} - \widehat{\mathbf{X}}_{k+1}^-\right]\left[\mathfrak{X}_{i,k+1|k}^{\mathbf{X}} - \widehat{\mathbf{X}}_{k+1}^-\right]^{\mathrm{T}}. \tag{3-19}$$

The time update step also calculates the prediction for the measurement vector $\widehat{\mathbf{Y}}_{k+1}^-$ and its covariance matrix $\mathbf{P}_{k+1}^{YY}$. These equations are given by,

$$\boldsymbol{\mathcal{Y}}_{k+1|k} = \mathbf{H}\left(\mathfrak{X}_{i,k+1|k}^{\mathbf{X}}, \mathfrak{X}_k^{\mathbf{v}}\right) \tag{3-20}$$

$$\widehat{\mathbf{Y}}_{k+1}^- = \sum_{i=0}^{2L} W_i^{(m)} \boldsymbol{\mathcal{Y}}_{i,k+1|k} \tag{3-21}$$

$$\mathbf{P}_{k+1}^{YY} = \sum_{i=0}^{2L} W_i^{(c)} \left[\boldsymbol{\mathcal{Y}}_{i,k+1|k} - \widehat{\mathbf{Y}}_{k+1}^-\right]\left[\boldsymbol{\mathcal{Y}}_{i,k+1|k} - \widehat{\mathbf{Y}}_{k+1}^-\right]^{\mathrm{T}}. \tag{3-22}$$

The weights for the mean and covariance matrices in the above equations are $W_i^{(m)}$ and $W_i^{(c)}$. These weights are calculated as,

$$W_0^{(m)} = \frac{\lambda}{l_x + \lambda} \tag{3-23}$$

$$W_0^{(c)} = \frac{\lambda}{l_x + \lambda} + (1 - \alpha_h^2 + \beta_h) \tag{3-24}$$

$$W_i^{(m)} = W_i^{(c)} = \frac{1}{2(l_x + \lambda)}, \qquad i = 1, \dots, 2l_x. \tag{3-25}$$

The higher order effects and the prior knowledge of the system in above equations is considered by β_h in Equation 3-24. The β_h is added to the weight of zeroth sigma point. The value of β_h is set to 2 for optimal solutions from Gaussian distribution and hence, has been set to this value for the current nonlinear identification study. The time update step is followed by the measurement step and is given by,

$$\mathbf{P}_{k+1}^{XY} = \sum_{i=0}^{2L} W_i^{(c)} \left[\mathbf{X}_{i,k+1|k}^X - \widehat{\mathbf{X}}_{k+1}^-\right]\left[\mathbf{y}_{i,k+1|k} - \widehat{\mathbf{Y}}_{k+1}^-\right]^T \tag{3-26}$$

$$\mathcal{K}_{k+1} = \mathbf{P}_{k+1}^{XY} \left(\mathbf{P}_{k+1}^{YY}\right)^{-1} \tag{3-27}$$

$$\widehat{\mathbf{X}}_{k+1} = \widehat{\mathbf{X}}_{k+1}^- + \mathcal{K}_{k+1}(\mathbf{Y}_{k+1} - \widehat{\mathbf{Y}}_{k+1}^-) \tag{3-28}$$

$$\mathbf{P}_{k+1} = \mathbf{P}_{k+1}^- - \mathcal{K}_{k+1}\mathbf{P}_{k+1}^{YY} \mathcal{K}_{k+1}^T \tag{3-29}$$

where,

$$\mathbf{X}^a = [(\mathbf{X}^X)^T \ (\mathbf{X}^w)^T \ (\mathbf{X}^v)^T]^T. \tag{3-30}$$

The above UKF algorithm can be explained using Figure 3.2. The filter starts with the initialization step as indicated in step (i). The mean for the prior distribution on the states is kept as $\widehat{\mathbf{X}}_0$ and the covariance is set as $\mathbf{P}_0$. The distribution of states is shown by the generation of sigma points in step (ii). The sigma points are then transformed to the nonlinear model in step (iii) to predict the future state, $p(x_k|y_{1:k-1})$. This prediction on the future distribution of states is made using the prior information from the system and the measurement. In step (iv), the distribution of the estimated measurement is made by using the predicted future state distribution in the system observation function. The predicted distribution is then compared with the true measured response of the system in step (v) and the corrected distribution of states, $p(x_k|y_{1:k})$ is calculated. The UKF thus uses the prediction and correction algorithm and proceeds to the next time step and finally predicts the system states and measurements at time step N.
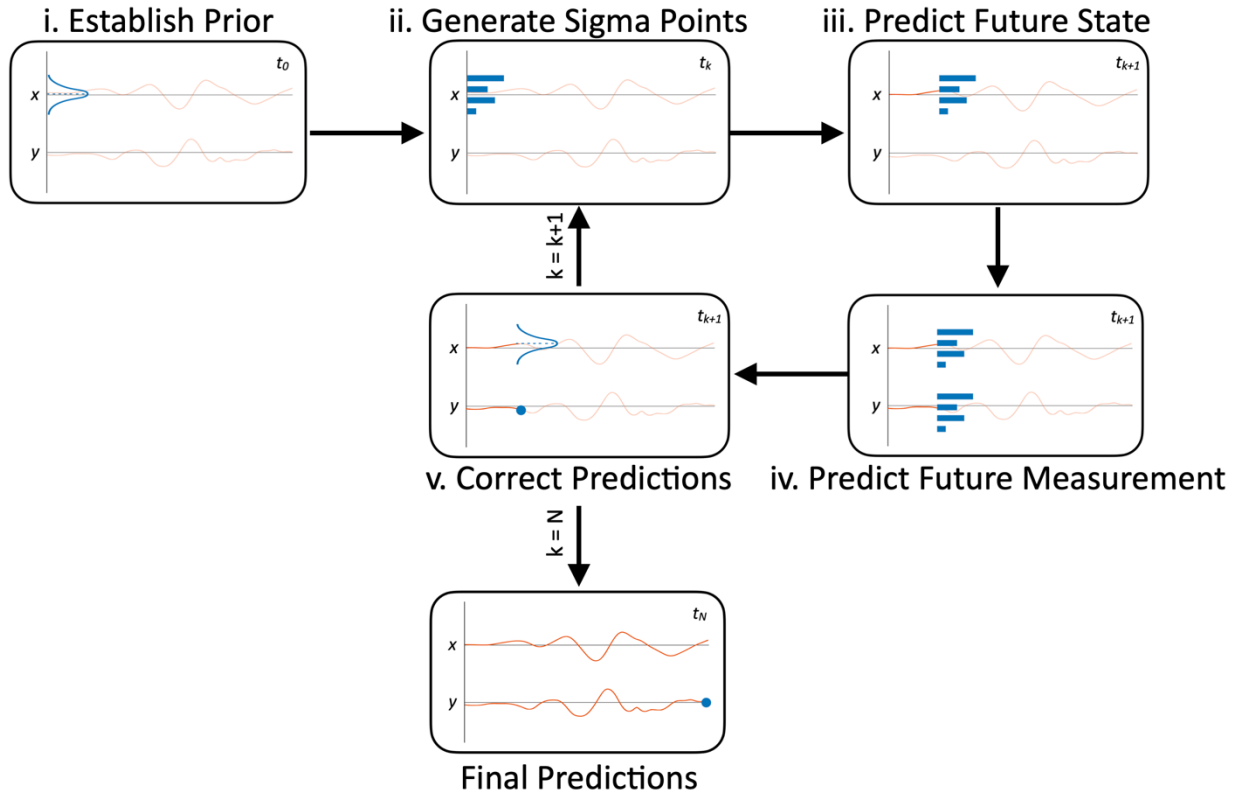
Figure 3.2. Procedure for the UKF algorithm

3.5.2 System State and Parameter Identification using UKF

The application of UKF for system state and parameter identification can be demonstrated with a computational Bouc-Wen model. This example will serve as a basis for developing the model selection process described in Section 3.6. A nonlinear Bouc-Wen model of hysteresis is a most commonly used model to represent hysteretic response in a system. A MR damper exhibits a hysteresis behavior for the force and displacement and hence, it can be represented using a Bouc-Wen model. A SDOF mechanical model of the MR Damper represented by nonlinear Bouc-Wen model is shown in Figure 3.3. The EOM of the SDOF model represented in Figure 3.3 is given by,

$$m\ddot{x}(t) + c\dot{x}(t) + kx(t) + kr(t) = -m\ddot{x}_g(t) \tag{3-31}$$

where, m is the mass of the system, c is the damping and k is the stiffness in the system. The displacement, velocity and acceleration at time t are given by $x(t)$, $\dot{x}(t)$ and $\ddot{x}(t)$. The hysteretic component in the Bouc-Wen model is represented by $r(t)$. The relation of $\dot{r}(t)$ with other parameters is given by,

$$\dot{r} = \dot{x} - \beta_1 |\dot{x}||r|^{n-1}r - \gamma\dot{x}|r|^n. \tag{3-32}$$
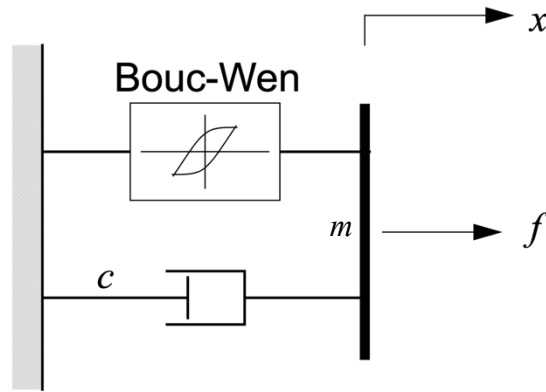
Figure 3.3. Mechanical Model of the Shear Mode MR Damper

The system parameters are set at values $m = 0.2$, $c = 0.3$, $k = 9$, $\beta_1 = 2$, $\gamma = 1$, and $n = 2$. An El-Centro earthquake signal at a sampling frequency of 50 Hz is used for the state and parameter estimation of this SDOF Bouc-Wen model. The input signal is shown in Figure 3.4. The augmented state vector for the UKF identification calculated from Equation 3-31 is represented as,

$$X = [x, \dot{x}, r, c, k, \beta_1, \gamma, n]^T. \tag{3-33}$$

The state space representation of the system is developed from Equations 3-31 and 3-32. It is given by,

$$\dot{\mathbf{X}} = f(\mathbf{X}(t), \mathbf{u}(t)) \tag{3-34}$$

where,

41

$$
f(X(t), u(t)) = \begin{bmatrix} \dot{x} \\ -\ddot{x}_g - (c\dot{x} + kr + kx)/m \\ \dot{x} - \beta_1|\dot{x}||r|^{n-1}r - \gamma\dot{x}|r|^n \\ 0 \\ 0 \\ 0 \\ 0 \\ 0 \end{bmatrix}. \tag{3-35}
$$

The observation equation based on the measured acceleration response and excitation signal can be given by,

$$
y_o = \ddot{x} + \ddot{x}_g + \mathrm{v} = -\frac{(c\dot{x}+kr)}{\mathrm{m}} + \mathrm{v}. \tag{3-36}
$$
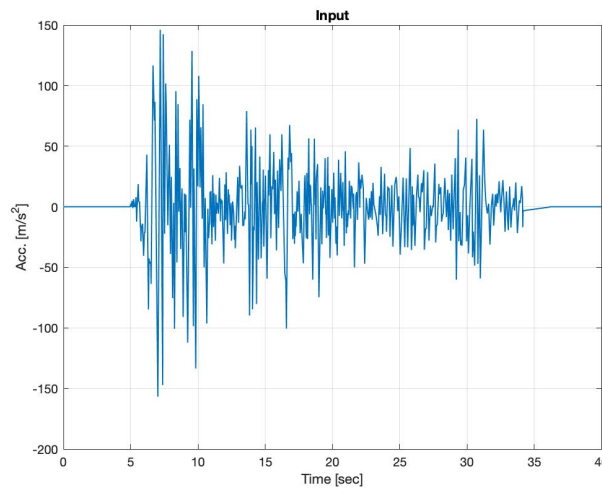
Figure 3.4. El-Centro Earthquake Input Signal

The UKF algorithm described in Section 3.5.1 starts for the Bouc-Wen model by taking the initial estimates at the mean of the system parameters. In order to replicate the true system response to the experimental signal, a random, band-limited white noise (BLWN) with the root mean square (RMS) value set at 1%, 2% and 5% is used. This noise is imposed on the displacement and acceleration measurements generated from the response of the computational model without noise. In addition, the noise is also added to the input earthquake signal. The noise in the displacement and acceleration response is due to the inherent sensor measurement error and is called measurement noise. The noise in the input signal is due to the actual actuator performance

and is called process noise. The process and measurement noise can vary and are usually not equal. However, for the current example, these values are set equal.

The estimated system response for the displacement, velocity and acceleration using the UKF algorithm is shown in Figure 3.5. These estimations are compared with the simulated system response at the true value of the parameters. It is observed that the UKF is capable of estimating the true state of the system with a very high accuracy. When the Bouc-Wen system starts showing hysteretic behavior, the contribution of the hysteretic component towards the total resisting force in the system increases. Figure 3.6 shows the contribution of viscous force, elastic force and hysteretic force towards the total force in the system. This figure shows a considerable amount of hysteretic contribution and confirms the presence of hysteresis in the system. The estimated hysteresis loop of the Bouc-Wen system is compared with the simulated case in Figure 3.7. The UKF estimation for the hysteretic response is close to the true hysteretic response of the computational model. It should be noted that the system parameters and the response are unitless. This example demonstrates the UKF implementation on a non-physical model. The more realistic values of the model and the system parameters will be taken for the numerical model selection process performed in Section 3.8 and the experimental model selection performed in Chapter 5. The convergence history of the parameters over the length of the input signal is shown in Figure 3.8. It is observed that the UKF converges towards the correct value of the parameters between 5 and 10 seconds. The input signal excites the structure at around 5 seconds and the parameters converge in the first 5 seconds of the excitations. The parameter estimations then remain near the true value and correct towards the true value for the remaining part of the excitation. The final estimation of the five parameters at the end of the input signal is compared with their true value in Table 3.2. An error for each of the parameter estimation is calculated by the difference between the exact value and the final estimated value of these parameters. This error is shown in Table 3.2 in terms of the percentage relative to the true value of the parameters.

The sensitivity of the UKF estimation results to different noise levels is studied by introducing both a 2% and a 5% RMS random, band-limited white noise. Again, the noise levels are introduced for both process and measurement and the UKF system state and parameter estimation is studied. Figures 3.9 and 3.10 show the comparison of state estimates and hysteresis loops using UKF for a noise level of 2% RMS. The comparison of state estimates and hysteresis loops using UKF for a noise level of 5% is shown in Figures 3.11 and 3.12, respectively. Figures

3.13 and 3.14 show the convergence history of parameters for noise levels of 2% and 5% RMS, respectively. It is again observed that the parameters come towards the true value during initial 5 seconds of the input and then converge towards the true value for the rest of the signal input. The state estimation and hysteresis loops tend to fall slightly away from the true response as the RMS noise level increases. This finding is evident from the figures for 1%, 2% and 5% noise levels. The comparison of error in parameter estimation from Table 3.2 shows that the estimation is more accurate for lower level of RMS noise. However, due to its approximation, the UKF might sometime show more error in parameter estimation for lesser level of RMS noise. This finding is evident from the error in estimation of β_1 for RMS noise levels of 1%, 2% and 5%. The error decreases as the noise level increases. This behavior is in contrast to what is expected from the parameter estimation. This behavior is mostly attributed to the fact the UKF approximates
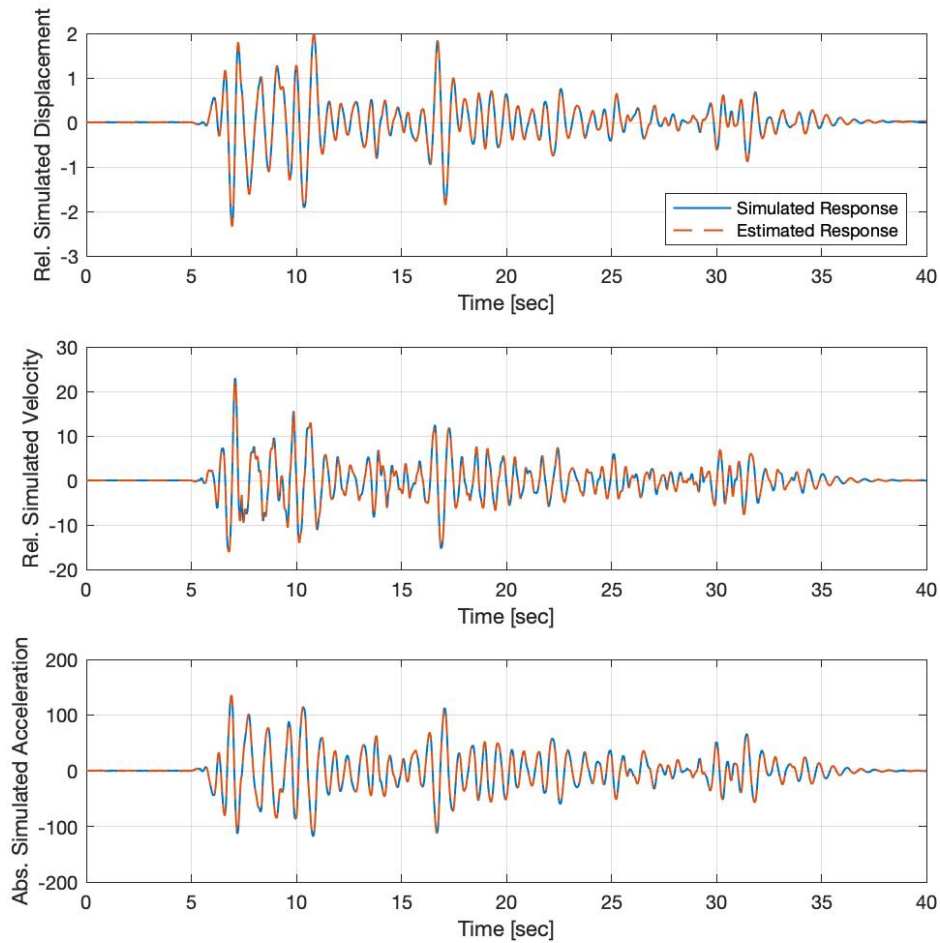
Figure 3.5. Comparison of State Estimates for Non-Physical Model using UKF at a Noise of 1% RMS

parameters only to a certain degree (third order Taylor series expansion in this case). Any error in estimation of parameters that is less than 5% should be considered as a good result. For the current scenario, the error was over 5% only for γ at RMS noise level of 5%, while it was less than 5% for the rest of the parameters.
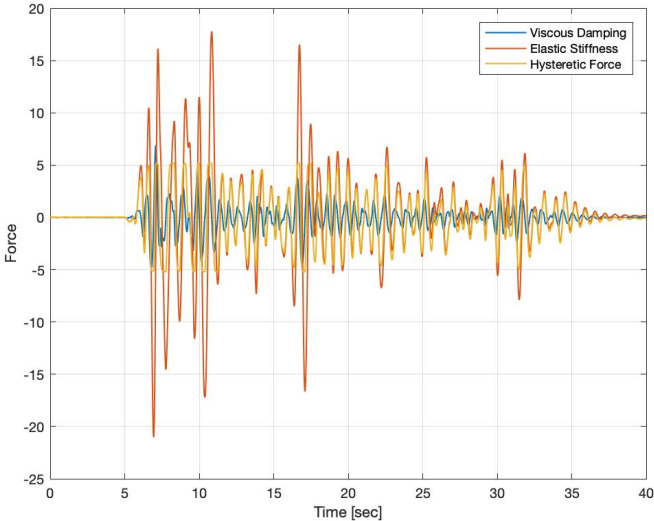
Figure 3.6. Contribution Towards Total Force for the Non-Physical Model
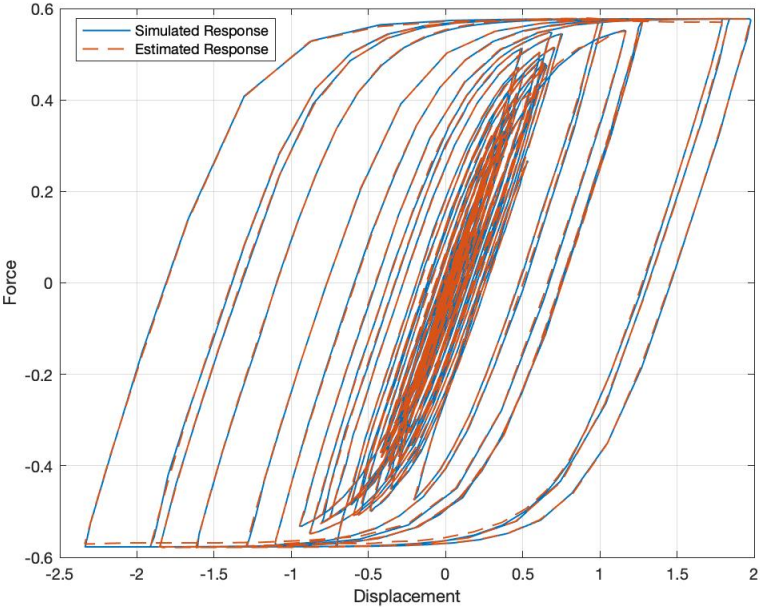
Figure 3.7. Comparison of Hysteresis Loops for Non-Physical Model
using UKF at a Noise of 1% RMS
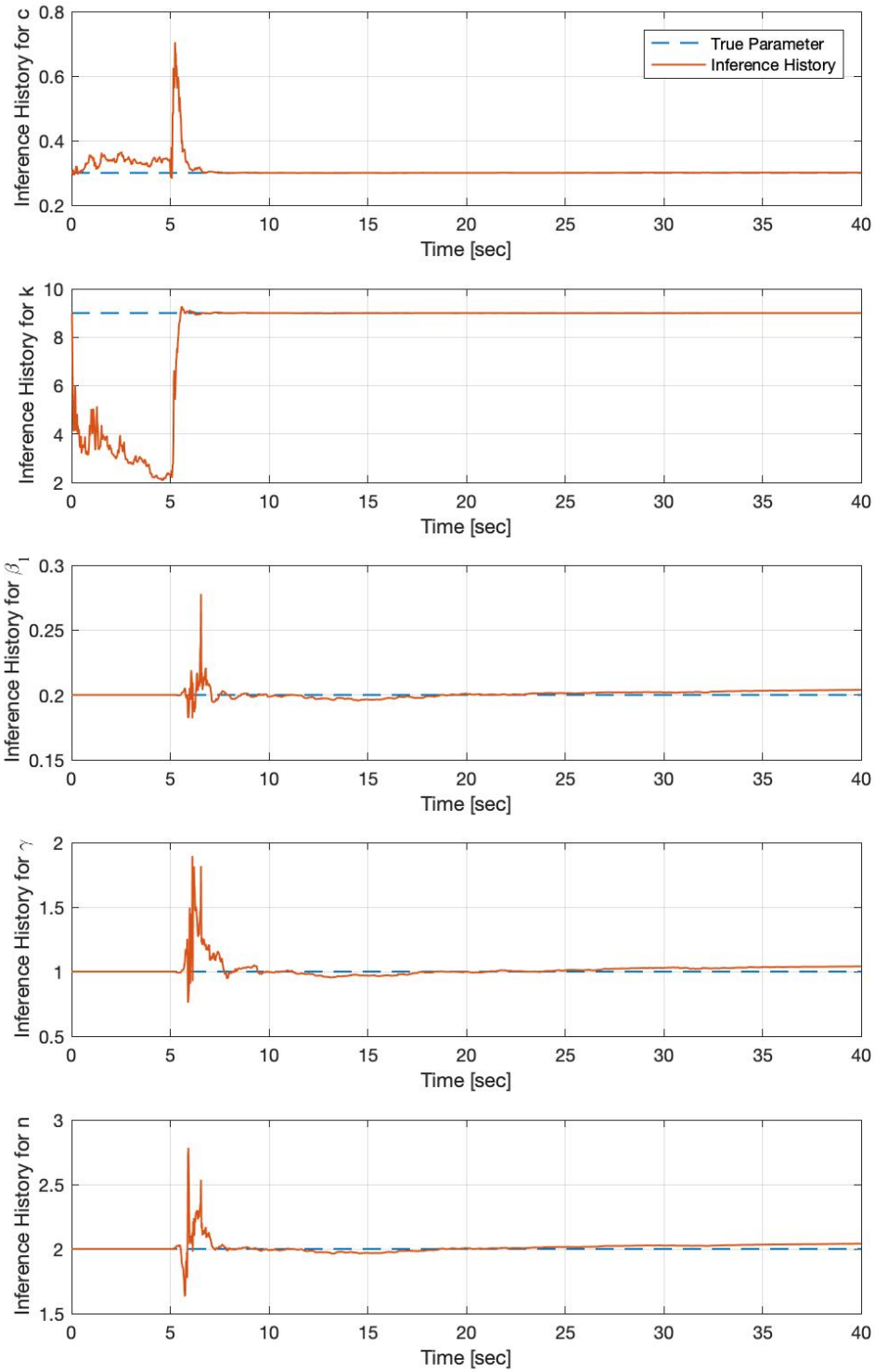
Figure 3.8. Convergence History of Parameters for Non-Physical Model using UKF at a Noise of 1% RMS
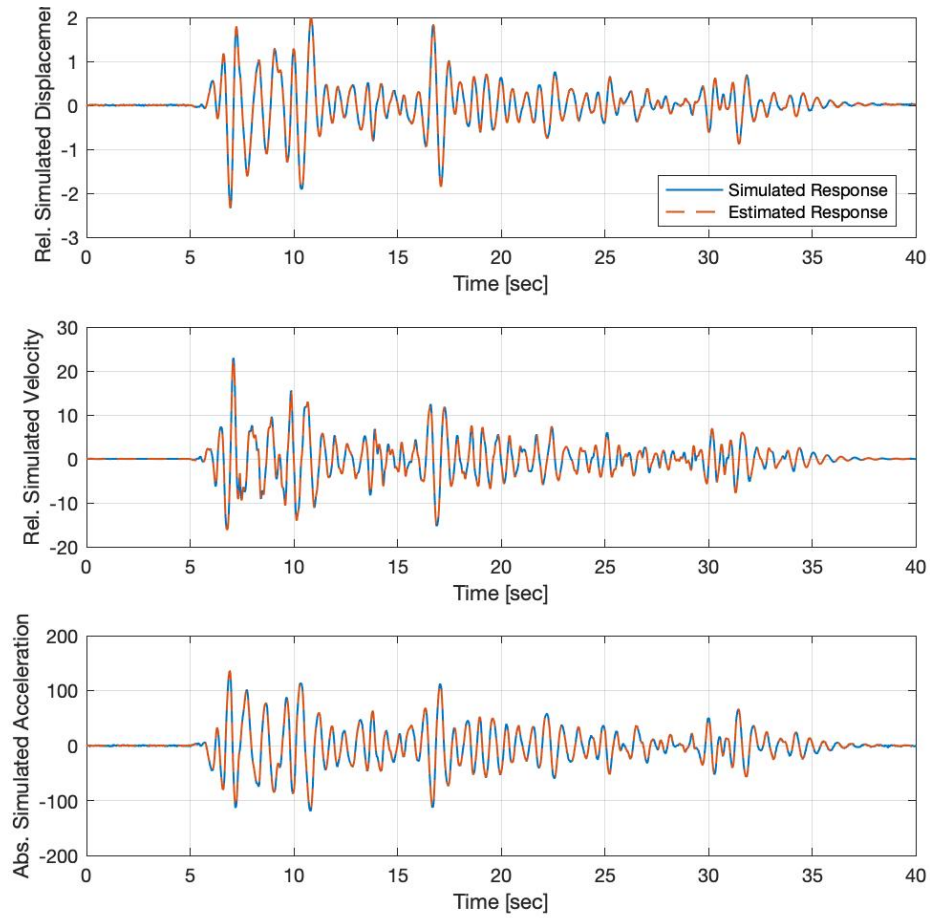
Figure 3.9. Comparison of State Estimates for Non-Physical Model using UKF at a Noise of 2% RMS
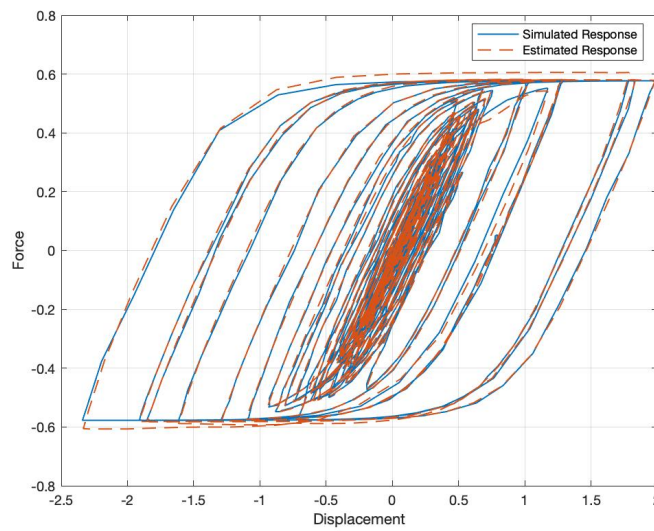
Figure 3.10. Comparison of Hysteresis Loops for Non-Physical Model using UKF at a Noise of 2% RMS
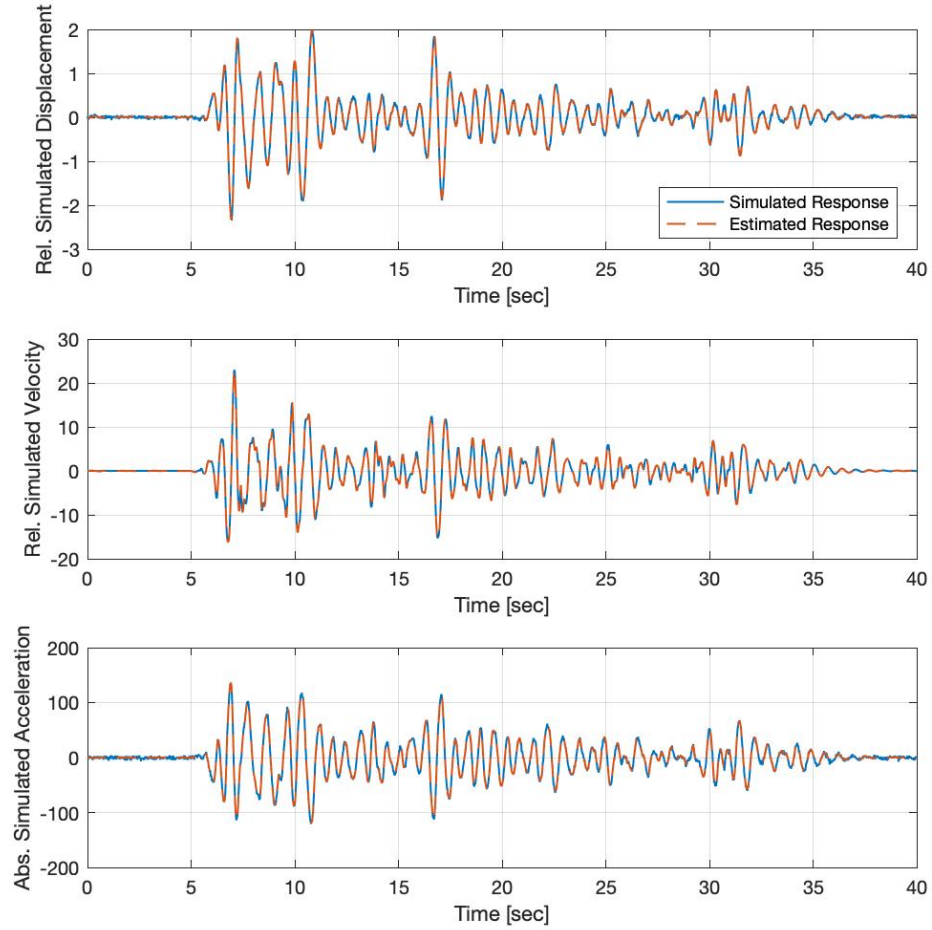
Figure 3.11. Comparison of State Estimates for Non-Physical Model using UKF at a Noise of 5% RMS
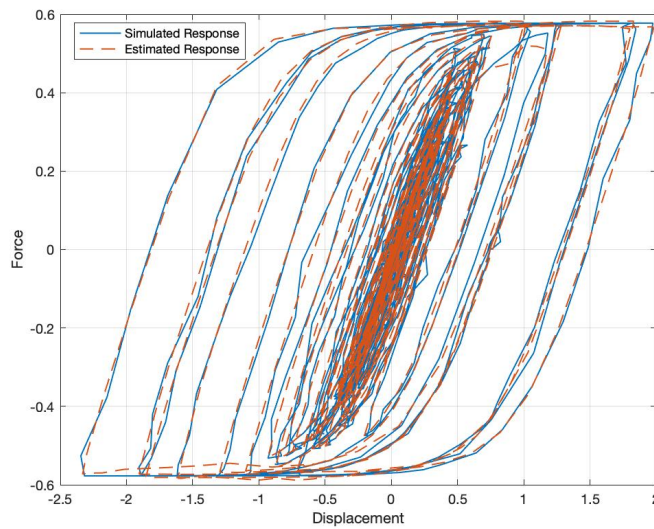
Figure 3.12. Comparison of Hysteresis Loops for Non-Physical Model using UKF at a Noise of 5% RMS
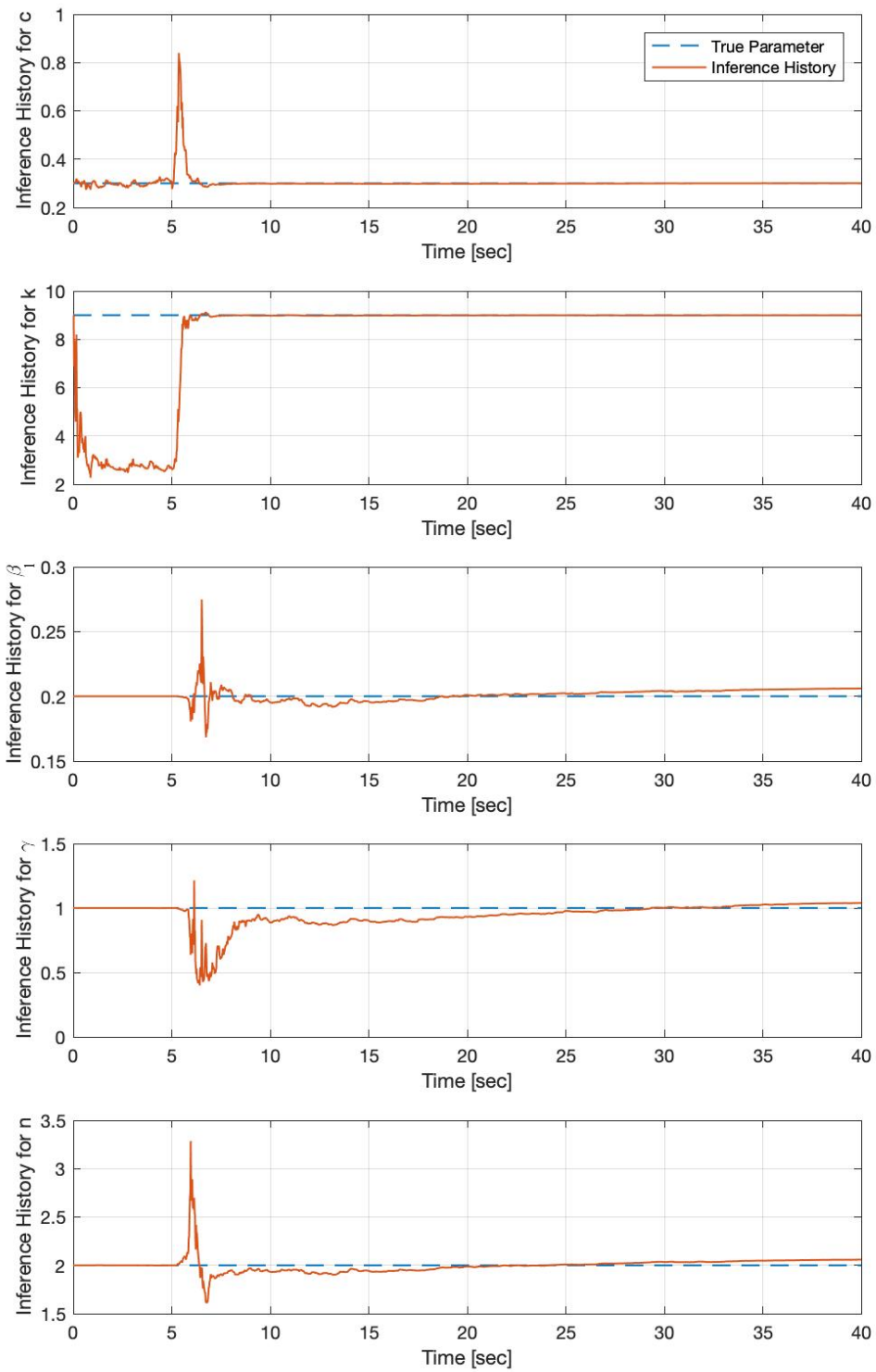
Figure 3.13. Convergence History of Parameters for Non-Physical Model using UKF
at a Noise of 2% RMS
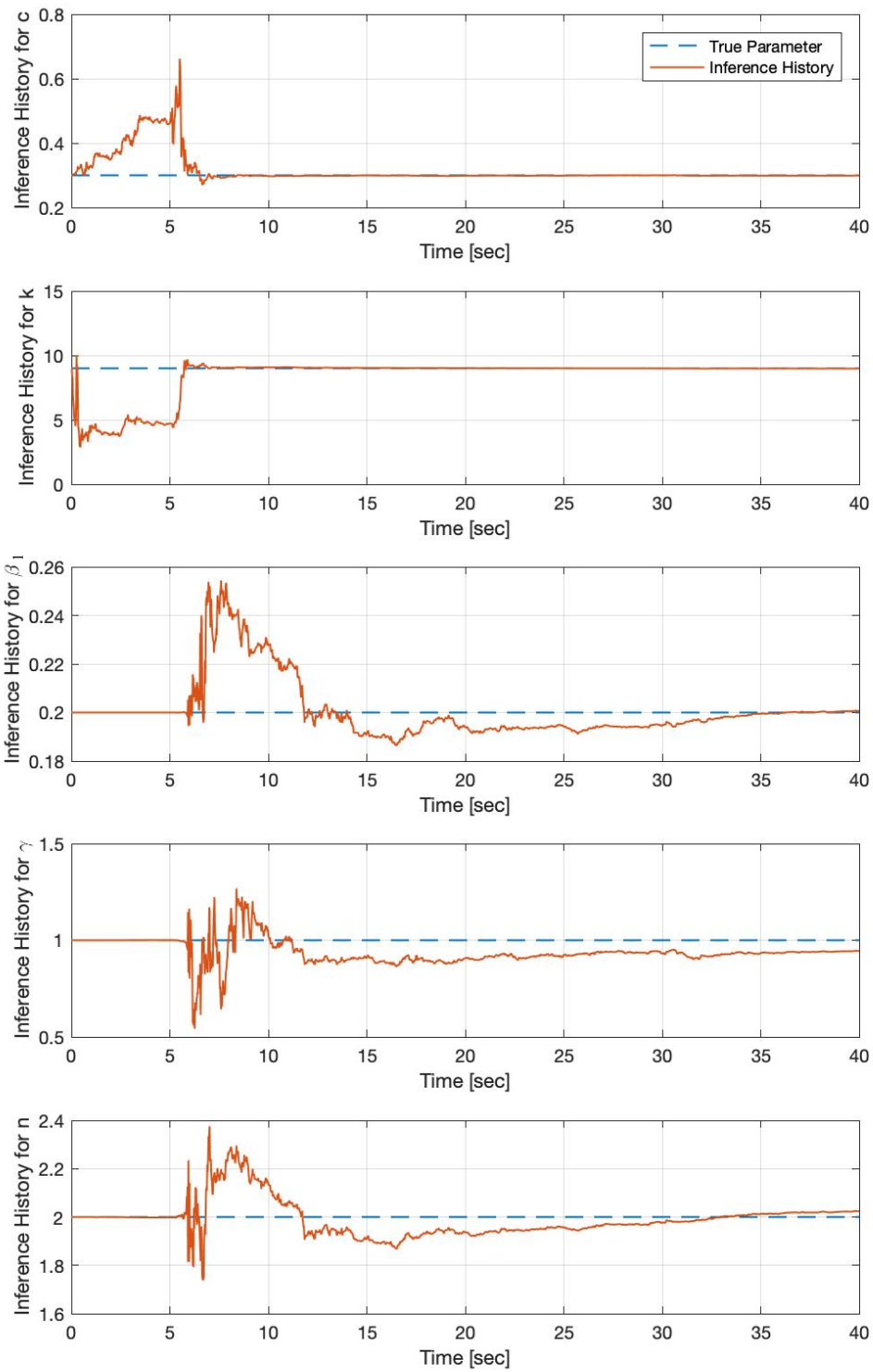
Figure 3.14. Convergence History of Parameters for Non-Physical Model using UKF at a Noise of 5% RMS

Table 3.2. Parameter Estimation for SDOF Bouc-Wen Model using UKF

Process and Measurement Noise		c	k	β_1	γ	n
	Exact value	0.3	9	2	1	2
1%	Estimated Value	0.3008	8.9979	2.0407	1.0423	2.0423
	% Error	0.2637	0.0232	2.0343	4.2285	2.1157
2%	Estimated Value	0.3005	8.9942	2.0623	1.0418	2.0607
	% Error	0.1752	0.0643	3.1143	4.1787	3.0365
5%	Estimated Value	0.2992	8.9831	2.0076	0.9461	2.0250
	% Error	0.2795	0.1880	0.3788	5.3894	1.2523

The stability of the UKF algorithm in estimating the states and parameters also plays a major role in the current model selection study. The UKF algorithm sometimes fails to run due to a lack of convergence of the covariance matrix in the calculation. The stability of the algorithm not only depends on the choice of the UKF parameters (α_h, κ and β_h) but also depends on the level of RMS noise, initial state estimations, input signal and the structural and model parameters. The algorithm is stable for high levels of process and measurement noise, but the stability of the simulation increases as these noise level decrease. The El-Centro input signal used for this example was rich enough at an input excitation of 50 times the original signal. The structural and the Bouc-Wen model parameters seem to converge well for this input signal while performing UKF identification. The algorithm gave higher errors for parameter estimation when an input signal like 'frequency sweep up and down' was used. The algorithm was also tried for an amplitude sweep and sine wave signal and good approximations were achieved for a slight variation in structural properties. The natural frequency of the structure was also varied by changing the value of the stiffness parameter, k. It was found that these signals helped in getting good estimates from the UKF algorithm when the sampling frequency of these signals was set around 2000 Hz.

The initial estimation on parameters should be near the mean. Using initial estimates too far away from the mean can sometimes cause the parameter estimations to diverge from their true values. A good rule of thumb is to keep these initial estimations on parameters within one standard deviation away from the mean. In addition, the UKF considers the parameters to lie in open domain from $-\infty$ to $+\infty$. This consideration might sometimes lead to the final estimation values falling in the negative domain. Since the parameters considered for the current nonlinear identification study lie in the positive domain, negative parameter estimates tend to yield incorrect and illogical output

from the UKF algorithm. The problem of estimations from negative domain can be solved by taking a logarithm (to the base e) on initial parameter estimations (Lund et al., 2020). The parameters are then converted back to the original estimated values by taking an exponent of the final parameters. Thus, a final parameter estimate in positive domain is obtained.

Although the initial logarithms solve the problem of having negative parameter estimations, initial parameter values that are less than 1 or higher than 100 might lead to convergence issues in the UKF algorithm. First, the magnitudes of all parameters are to be set at relatively same level for a quicker convergence to true values. The logarithm for values less than 1 gives a negative value, for a value equal to 1 gives zero and for a value greater than 100 gives a value greater than 2. In all these cases, the UKF fails to converge sometimes. As a result, the initial parameter estimates are first converted to a suitable value between 1 and 100 by dividing or multiplying them by values in the order of 10. In the next step, a logarithm of these values is taken. After the UKF algorithm ends, these values are again converted to the original form by taking an exponent to the power of parameters and then multiplying or dividing by the corresponding values by which the parameters were divided or multiplied before. The approach of dividing or multiplying and taking logarithm is further explained through Equations (3-37) and (3-38). The i in the subscript of parameters represents an initial estimated value, and the f in the subscript of parameters represents the final estimated value of the UKF algorithm.

$$\hat{X}_0 = [x, \dot{x}, r, \log_e(c_i * 10), \log_e(k_i * 1), \log_e(\beta_{1_i} * 1), \log_e(\gamma_i * 10), \log_e(n_i * 1)]^T \quad (3\text{-}37)$$

$$\hat{X}_k = \left[x, \dot{x}, r, \frac{(e^{c_f})}{10}, \frac{(e^{k_f})}{1}, \frac{(e^{\beta_f})}{1}, \frac{(e^{\gamma_f})}{10}, \frac{(e^{n_f})}{1}\right]. \quad (3\text{-}38)$$

The damping coefficient, c and the stiffness, k represent the structural parameters of the system. The UKF estimates for these parameters is very close to their true value. The estimates for the Bouc-Wen parameters, β_1, γ and n do not converge as well as do the structural parameters c and k. This behavior can be attributed to the fact that the Bouc-Wen model parameters are very sensitive to the slightest change in the structural system and its response. Still the Bouc-Wen parameters converge very closely to the true values. This finding confirms the efficacy of the UKF for parameter estimation for highly sensitive models.

3.6   Model Selection, Training and Validation

Model selection for the current nonlinear identification study is performed after the system state and parameter estimation with the UKF as described in Section 3.5. This approach is also known as state augmentation. The computational models of MR damper used for the study contain parameters in the positive domain. Therefore, the UKF estimates for all parameters is restricted to the positive domain by taking a logarithm of each parameter as indicated in Equation 3-37. The multiplication/division constant for each parameter varies depending upon the model. Thus, the transformed parameters will have values between 1 and 100 before taking their logarithms. The transformation still enforces the unconstrained optimization on parameters and the UKF algorithm runs without any errors. The augmented state vector generally consists of the structural damping coefficient, stiffness coefficient, hysteretic component, and the damper parameters. This form of augmented state vector is thus similar to Equation 3.33 and is given as,

$$\hat{X}_0 = [x_1, x_2, x_3, x_4, x_5, x_6, x_7, x_8]^T. \tag{3-39}$$

In the experimental setup discussed later in this thesis, the process noise is quantified using the measurements obtained from both the accelerometer installed on the shake table and the displacement sensor and accelerometer installed on the first floor. It is assumed that the measurement noise from the displacement sensor and accelerometers are independent of each other.

The identification of the states and parameters starts with the selection of an excitation signal that is able to generate a dynamic response in the system. The response should be capable of generating an excitation in all components of the structural system. The UKF algorithm is capable of identifying the states and parameters of the structural system if these conditions are met. The response of the structure and further excitation of the parameters is usually studied by an analytical approach known as identifiability analysis. This analysis helps to study the response of the structure under various input signals and identifies a set of input signals for which the parameters show a moderate to high excitation. Once the excitation signals are determined, the UKF identification algorithm is used to generate a set of models depending upon the prior distribution of the parameters. This step is known as training. The generated models are then used to predict system response under an input signal and the model with least error is selected. This step is known

as validation. Thus, the model selection process comprised of training and validation of models for a set of input signals and the selection of a model with the least error. The training and validation steps are further described in Sections 3.6.1 and 3.6.2.

3.6.1 Model Training

In the model training step, a number of models are generated using an input signal and the UKF algorithm. The UKF identification algorithm starts with a prior assumption on the parameters. The prior distribution on parameters plays a major role in determining the stability of the algorithm. Although the algorithm is stable and yields converging results for a set of prior distribution on parameters, it might be unstable and fail sometimes due to some badly conditioned matrices. While it is relatively easy to set a suitable prior distribution that will produce converging results for the numerical setup, it will be more difficult to predict this distribution for the experimental setup where the response and system states are related to parameters. To avoid difficulties in the experiment, a set of prior distributions is pre-selected and the algorithm is implemented for each sampled distribution in the set. The models are generated for each distribution for which the algorithm is sensitive. The initial mean and covariance matrices are given by,

$$\mu_0 = [\mu_0^{(x)} \ \mu_0^{(\theta)}]^T \tag{3-40}$$

$$P_0 = \begin{bmatrix} P_0^{(x)} & 0 \\ 0 & P_0^{(\theta)} \end{bmatrix}. \tag{3-41}$$

In the above equations, the initial mean on the states is given by $\mu_0^{(x)}$ and the initial mean on the parameters is given by $\mu_0^{(\theta)}$. The covariance matrix is a diagonal matrix consisting of covariance distribution on states and parameters. The states and parameters are assumed to be independent of each other and hence, the resulting covariance matrix contains only non-zero diagonal terms.

The set of prior distributions for the parameters is generated using a Latin hypercube sampling approach (LHS). This approach is useful for generating a set of random values of parameters in a multi-dimension parameter distribution. The LHS samples generally help to converge to the true value of parameters quicker than would normally distributed parameters. The

advantage of the LHS sampling is that each parameter value is selected such that the value is unique in the axis-aligned hyperplane containing it. This method can be further explained by an example selecting 10 random values within the range $0-10$. The LHS samples are generated such that each value will be selected from each of the ten hyperplane axes $(0-1, 1-2, \cdots 9-10)$. In the current study, the LHS samples of the model parameters are generated within a plausible range for each parameter. The plausible range of each parameter for MR damper models is determined by studying the response of the system under different parameter values under a known input signal. The initial covariance estimates on the parameters are assigned in the following way,

$$\sigma_j = \tau(\mu_0)_j, \tag{3-42}$$

$$\tau \in \{0.1, 1, 10, 25, 50, 75, 100, 200, 300, 600\}\%. \tag{3-43}$$

The coefficient j in Equation 3-42 starts from 4 and goes until parameters in the MR damper model are included. The covariance estimate in Equation 3-42 consists of an index of dispersion, τ. The index of dispersion is the ratio of the variance to the mean. The UKF algorithm is implemented for each index of dispersion on covariance samples and converging results are obtained for some indices of dispersion. The covariance level on each parameter is increased simultaneously and thus the algorithm is iterated over all the values. In total, the UKF algorithm is implemented 100 times generating 100 different models in the training step. The 100 iterations are a result of 10 sets of LHSs and 10 samples of the indices of dispersion on covariance samples for each LHS $[10\ (LHS) \times 10\ (\alpha) = 100$ iterations].

3.6.2   Model Validation

In the model validation step, the trained models with all sets of parameter values are used to generate a structural response under an input validation signal that is different than the training signal. The computed system states using the identified model parameters are then compared with the actual structural response for this validation signal. A suitable model is then selected from a set of 100 models by comparing the mean square error (MSE). The MSE is computed using the predicted displacement and accelerations values with the actual structural response for the validation signal. The equation for MSE is given by,

55

$$MSE = \frac{100}{N} \sum_{i=1}^{Z} \left(\frac{(x_i - \hat{x}_i)^2}{\sigma_d^2} + \frac{(\ddot{x}_i - \hat{\ddot{x}}_i)^2}{\sigma_a^2} \right)$$
(3-44)

where the total number of observation values from the actual structural response for the validation signal is given by Z. The value of Z can be calculated by multiplying the total input time of the signal to the sampling frequency. In general, it is the size of the one-dimensional input matrix in MATLAB. The observed actual structural displacement for the validation signal at the ith time step is given by x_i and the computed displacement under same input signal generated by the simulation of the model is given by $\hat{x}_i$. Similarly, the observed actual structural acceleration for the validation signal is given by $\ddot{x}_i$ and the computational acceleration from simulation of the model is given by $\hat{\ddot{x}}_i$. σ_d^2 and σ_a^2 in the above equations are variances in the displacement and acceleration noise, respectively.

In addition to the MSE mentioned above, the relative quality of the trained models can also be assessed using the difference in the error between the predicted and measured value of force (Spencer et al., 1996). These error values are calculated with respect to the time, displacement and velocity of the measured response. The expressions defining the three error values used are given as,

$$E_t = \frac{\varepsilon_t}{\sigma_f}, \qquad E_x = \frac{\varepsilon_x}{\sigma_f}, \qquad E_{\dot{x}} = \frac{\varepsilon_{\dot{x}}}{\sigma_f}$$
(3-45)

where

$$\varepsilon_t^2 = \frac{1}{N} \sum_{i=1}^{N} (f_{exp}^i - f_{pre}^i)^2$$
(3-46)

$$\varepsilon_x^2 = \frac{1}{N} \sum_{i=1}^{N} (f_{exp}^i - f_{pre}^i)^2 |\dot{x}_i|$$
(3-47)

$$\varepsilon_{\dot{x}}^2 = \frac{1}{N} \sum_{i=1}^{N} (f_{exp}^i - f_{pre}^i)^2 |\ddot{x}_i|$$
(3-48)

$$\sigma_f^2 = \frac{1}{N} \sum_{i=1}^{N} (f_{exp}^i - \mu_F^i)^2.$$
(3-49)

The actual observed value of force at i^{th} time step is given by f_{exp}^i and the predicted computational force is given by f_{pre}^i. The measured velocity and acceleration are given by $\dot{x}_i$ and $\ddot{x}_i$. The mean of measured force values at i^{th} time step is given by μ_F^i. The behavior of MR damper models for the current study is compared using only using force-displacement hysteresis loops. Therefore, it is prudent to compare the relative quality of models on the basis of Equations 3-46 and 3-47. The final MR damper is then selected after comparing the MSE and force errors with respect to time and displacement for each model.

3.6.3 Identification and Validation Methods

The model training and validation described in Sections 3.6.1 and 3.6.2 may be implemented using various methods. These methods differ from each other by the type and order of the input signals used in the training and validation. Lund et al., (2020) demonstrated three different methods to perform model training and validation. The first step before the implementation of these methods is to select an appropriate input signal that excites the parameters of the model. The authors identified two such input signals that excited the parameters of the NES model. Method 1 for identification and validation consists of using each of the two input signals individually and training models with prior distribution on the parameters. This step is then followed by a validation step where the trained parameters of the model are validated using the same input signal that was used in training. In method 2, the models are trained using one of the two signals and the trained parameters of the model are then validated using the other signal as an input. This method is also known as cross-validation. In method 3, the models are trained simultaneously with two input signals and the trained parameters of the candidate models are validated simultaneously using both input signals. In order to use both signals simultaneously in the training and validation steps, the state space vector, the base function for the transition function and the observation equation are updated to take inputs from both signals. The MSE and force error is calculated for each of the candidate models after the validation step in each of the three methods and the model with the least MSE is selected.

The training and validation approach followed in method 1 sometimes overfits the candidate models due to high sensitivity of input signals on a small variation in parameters (Lund et al., 2020). In order to get best estimation of the model used in the experimental response, it is

important to avoid overfitting. Overfitted models tend to give good response for the input signal that was used for training. However, the response of these models with other input signals usually generates high errors. It was predicted that the implementation of using two signals simultaneously in method 3 can tackle this issue. However, the authors found that simultaneously using two signals in method 3 overfitted the model towards the signal that was more sensitive to a small variation in parameters. The cross-validation in method 2 prevented the overfitting of models and the final validated models comprised of the lowest MSE. Therefore, the current nonlinear identification study will demonstrate model selection using methods 1 and 2. It is believed that the results of method 3 will overfit models towards one signal like in method 1 and will not provide better results when compared to methods 1 and 2 (Lund et al., 2020).

Methods 1 and 2 are selected for the nonlinear identification study here, and are further explained in Figure 3.15. A particular mechanical model form for the MR damper is chosen and the training and validation is performed using both methods. The model training phase starts with the UKF identification algorithm with 100 prior distribution on the parameters. The trained models are then validated with the same signal as used in training phase in method 1 and with the other signal in method 2. It should be noted that the number of potential MR damper models after the training phase can be fewer than 100. The UKF algorithm is sometimes unstable for some values of the index of dispersion on covariance samples and thus leads to poorly conditioned matrices. As a result, the parameter estimates on some of these models are returned as zero and such models are not used for the validation step. Methods 1 and 2 described in Figure 3.15 are performed for a particular mechanical model of MR damper. This mechanical model is denoted by the subscript 'x' in the figure. Model training and validation, and thereby model selection based on lowest error, can be performed for different forms of the mechanical models of the MR damper. The current study considers three different model forms for the MR damper, and performs the identification and selection using methods 1 and 2 for each of these models. Finally, the model with the lowest MSE out of three models is selected. Figure 3.16 shows this error comparison method for each of the three models labelled as 'x', 'y' and 'z'.
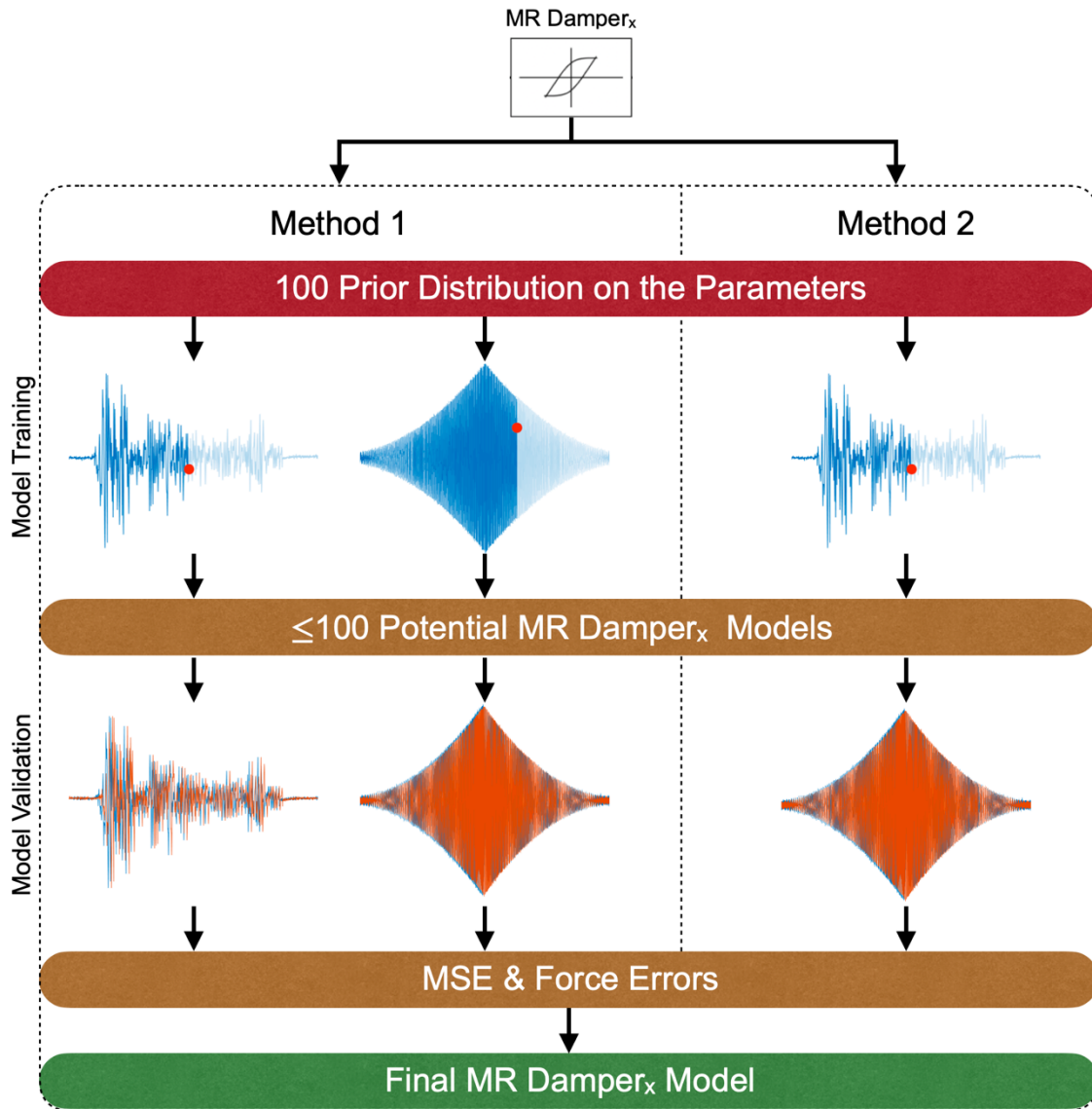
Figure 3.15. UKF Identification and Model Selection
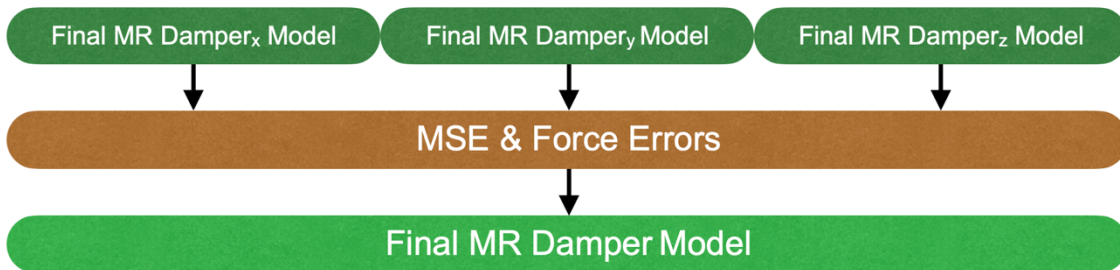
Figure 3.16. Error Comparison and Final Model Selection

3.7　MR Damper Models

The various computational models for MR damper available in the literature are based on several different modelling techniques used. Bouc-Wen, Bingham, Sigmoid, Dahl and LuGre are some of the phenomenological modelling techniques usually adopted for MR damper models. Several researchers have proposed modifications on the primary versions of these models depending on the behavior of these models under certain parameters. Some of these models consider the varying input voltage and current values in their formulation while the rest assume them as constant. Here, a set of such models for MR damper are selected that have the potential to replicate the structural response with a fair accuracy and at the same time are computationally efficient. These models generate a hysteresis response aligned with the experimental results observed and are able to generate responses in the structure that are similar to the experimental structural response. These models primarily differ in the formulation of the hysteretic component, z. The UKF implementation for the training and validation steps remains stable and provides good estimates for states and parameters using these models. Models x, y and z indicated in the previous section are described here.

3.7.1　Normalized Bouc-Wen Model

The Bouc-Wen model defined in Section 3.5.2 contains some parameters that are redundant (Ma et al., 2004). The identification algorithms could fail to converge on values of these parameters. These redundant parameters are therefore usually assigned particular values for state and parameter estimation. A modified version of this model known as normalized Bouc-Wen model has been proposed by Ikhouane and Rodellar (2005) and used by several researchers (Chang et al., 2016; Ismail et al., 2009; Zhu & Lu, 2011). The normalized Bouc-Wen model removes any redundant parameters from the model and helps in proper state and parameter estimation using UKF. The original Bouc-Wen model has the restoring force, f and hysteretic component, r that are given as follows,

$$f = \alpha_1 kx + (1 - \alpha_1)kr \tag{3-50}$$

$$\dot{r} = A\dot{x} - \beta_1|\dot{x}||r|^{n-1}r - \gamma\dot{x}|r|^n \tag{3-51}$$

where the ratio of post-yield to pre-yield stiffness is given by α_1, the stiffness coefficient is given by k and A, n, β_1, γ are the model parameters determining the shape of the hysteresis curve. The normalized form of the Bouc-Wen model is proposed of the following form,

$$f = k_s x + k_z z \tag{3-52}$$

$$\dot{z} = \rho(\dot{x} - \sigma|\dot{x}||z|^{n-1}z + (\sigma - 1)\dot{x}|z|^n) \tag{3-53}$$

where,

$$r_0 = \sqrt[n]{\frac{A}{\beta_1 + \gamma}}, \qquad \rho = \frac{A}{r_0}, \qquad \sigma = \frac{\beta_1}{\beta_1 + \gamma}$$

$$k_s = \alpha_1 k, \qquad k_z = (1 - \alpha_1)kr_0, \qquad z = \frac{r}{r_0}. \tag{3-54}$$

The normalization constant in the above equations is given by r_0. The internal hysteresis variable is given by z. k_s and k_z are the post-yield stiffness and initial stiffness, respectively. The initial stiffness of z is given by ρ and the shape of the hysteresis loop is determined by σ. The parameters r_0, z and σ are non-dimensional in the above equation. The dimensions of k_z and ρ are 'N' and 'm^{-1}', respectively. k_s has the dimension of 'N/m' and is similar as the structural stiffness, k. Since k_s only depends on the structural displacement, it is kept common by combining both the structural and Bouc-Wen parameter values. The UKF algorithm might sometimes give improper estimations for parameters values that depend on similar structural properties, but are considered as different. The approach of combining k_s and k makes the UKF algorithm more stable. Thus, for the UKF system state and parameter estimation, the normalized Bouc-Wen model consists of four parameters (k_z, ρ, n, σ) in addition to two structural parameters (c, k). The equation of motion for the SDOF system with normalized Bouc-Wen model is given by,

$$m\ddot{x} + c\dot{x} + kx + k_z z = -m\ddot{x}_g. \tag{3-55}$$

The augmented state vector of the resulting system, its base function and the observation equation are given by,

$$X = [x, \dot{x}, z, c, k, k_z, \rho, n, \sigma]^T \qquad (3\text{-}56)$$

$$f(X(t), u(t)) = \begin{bmatrix} \dot{x} \\ -\ddot{x}_g - (c\dot{x} + kx + k_z z)/m \\ \rho(\dot{x} - \sigma|\dot{x}||z|^{n-1}z + (\sigma - 1)\dot{x}|z|^n) \\ 0 \\ 0 \\ 0 \\ 0 \\ 0 \\ 0 \end{bmatrix} \qquad (3\text{-}57)$$

$$H(X(t), v(t)) = \begin{bmatrix} x \\ -(c\dot{x} + kx + k_z z)/m \end{bmatrix} + v. \qquad (3\text{-}58)$$

3.7.2   Modified Dahl Model

A Dahl model consists of Dahl hysteresis component and was proposed by Dahl (1976). The Coulomb force in the model is estimated using a smaller number of parameters when compared to the Bouc-Wen model. A modified version of the Dahl model has been developed primarily to represent better relationship between the force and velocity at lower velocity values (Xu et al., 2019). This model is shown is Figure 3.17. The damper force and the hysteresis component of the modified Dahl model is given by,

$$f = kx + c\dot{x} + F_d z - f_0 \qquad (3\text{-}59)$$

$$\dot{z} = \sigma\dot{x}(1 - z\text{sgn}(\dot{x})) \qquad (3\text{-}60)$$

where the Coulomb frictional force is given by F_d (in 'N'), the initial force in the MR damper is given by f_0 (in 'N'). The shape of the hysteresis loop is determined by the dimensionless parameter σ. Thus, for the UKF implementation, a total of five parameters are used, three parameters from the modified Dahl model (F_d, σ, f_0) and two from the structural system (c, k). The resulting equation of motion of the SDOF system with the modified Dahl model is given by,

$$m\ddot{x} + c\dot{x} + kx + F_d z - f_0 = -m\ddot{x}_g. \tag{3-61}$$

The augmented state vector, base function and the observation equation for the system with modified Dahl model are given by,

$$X = [x, \dot{x}, z, c, k, F_d, \sigma, f_0]^T \tag{3-62}$$

$$f\big(X(t), u(t)\big) = \begin{bmatrix} \dot{x} \\ -\ddot{x}_g - (c\dot{x} + kx + F_d z - f_0)/m \\ \sigma\dot{x}(1 - z\,\mathrm{sgn}(\dot{x})) \\ 0 \\ 0 \\ 0 \\ 0 \\ 0 \end{bmatrix} \tag{3-63}$$

$$\mathrm{H}\big(X(t), v(t)\big) = \begin{bmatrix} x \\ -(c\dot{x} + kx + F_d z - f_0)/m \end{bmatrix} + v. \tag{3-64}$$
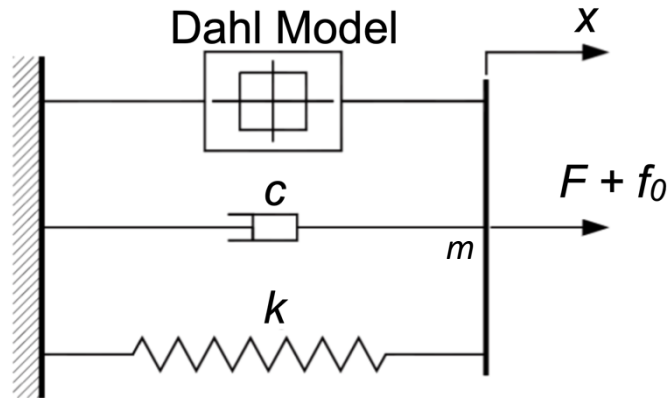
Figure 3.17. Modified Dahl Model

3.7.3 Modified LuGre Model

The LuGre model is an extension of the Dahl model and was proposed by Canudas De Wit & Lischinsky (1995). It is evident from this study that the model is simple and yet provides highly accurate hysteretic response of the MR damper. The modified version of the LuGre MR damper

63

model has been developed by Jiménez & Álvarez-Icaza (2005). The mechanical model for a SDOF structure with modified LuGre looks similar as with the modified Dahl model and has been shown in Figure 3.18. The damper force and the hysteretic component are given by,

$$f = kx + c\dot{x} + \beta z + \varepsilon\dot{z} + f_0 \tag{3-65}$$

$$\dot{z} = \dot{x} - \alpha|\dot{x}|z \tag{3-66}$$

where, β and α are the generalized stiffness parameters and have dimensions of 'N/m' and 'm^{-1}', respectively. ε is the generalized damping parameter of the model and has dimensions of 'Ns/m'. The parameters β and α depend on the electric current in the damper, but for the current study, the electric current is assumed to be constant. Thus, a total of six parameters are required for UKF implementation of a SDOF system with modified LuGre model. The modified LuGre model requires four parameters $(\beta, \varepsilon, \alpha, f_0)$ and the structural system is defined by two parameters (c, k). The equation of motion of the resulting system is given by,

$$m\ddot{x} + c\dot{x} + kx + \beta z + \varepsilon\dot{z} + f_0 = -m\ddot{x}_g. \tag{3-67}$$

The augmented state vector, base function and the observation equation for the system with modified LuGre model are given by,

$$X = [x, \dot{x}, z, c, k, \beta, \varepsilon, \alpha, f_0]^T \tag{3-68}$$

$$f\big(X(t), u(t)\big) = \begin{bmatrix} \dot{x} \\ -\ddot{x}_g - (c\dot{x} + kx + \beta z + \varepsilon\dot{z} + f_0)/m \\ \dot{x} - \alpha|\dot{x}|z \\ 0 \\ 0 \\ 0 \\ 0 \\ 0 \\ 0 \end{bmatrix} \tag{3-69}$$

$$\text{H}(X(t), v(t)) = \left[-(c\dot{x} + kx + \beta z + \varepsilon\dot{z} + f_0)/m \right] + v. \qquad (3\text{-}70)$$
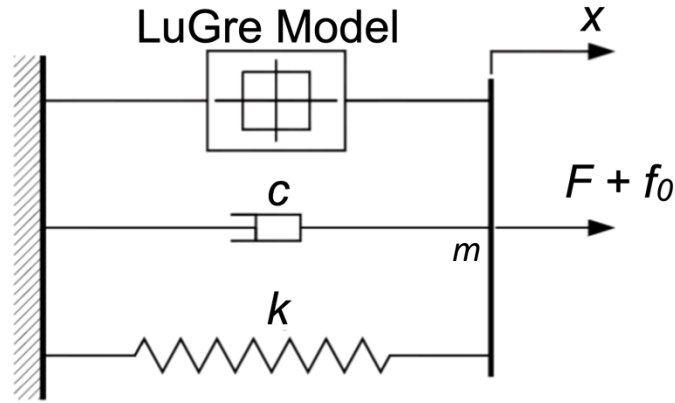
Figure 3.18. Modified LuGre Model

3.8 Numerical Model Selection Example

The three MR damper models described in Section 3.7 are used in this section to demonstrate the model selection process using the UKF. The UKF identification algorithm requires actual structural response for training and validation steps. In addition, two sets of actual structural response are needed to perform the model selection process for methods showcased in Figure 3.15 and 3.16. In this section, the model selection procedure is demonstrated using simulated sets of data generated for training and validation. These sets of data are generated using a mechanical model of the modified Dahl model on a SDOF structure excited with two different input signals. The response of this SDOF structure is then used to train and validate the normalized Bouc-Wen and modified LuGre model described in Sections 3.7.1 and 3.7.3.

For the numerical model selection example described in this section and the experimental model selection performed in Chapter 5, it is assumed that the initial force f_0 in the MR damper remains negligible. Therefore, this term is removed from the equations of the MR damper models described in the previous section. The model selection process is demonstrated with zero initial force in all MR damper models. The removal of this term also lowers the computational time required for training and validation by a small amount.

3.8.1 Data Generation for Training and Validation

The numerical setup for the generation of actual structural response consists of a SDOF structure with a modified Dahl model. The SDOF structure has a mass, $m = 50$ kg, damping coefficient, $c = 100$ Ns/m and stiffness, $k = 20$ kN/m. The Coulomb frictional force, F_d and the hysteresis shape parameter, σ for the modified Dahl model are set as 25 N and 2500, respectively. This setup is subjected to excitation signals from a frequency sweep up and down and an El-Centro earthquake. The structural response for displacement, acceleration and force is recorded in MATLAB and these responses are then used for training and validation for other two mechanical models. The frequency sweep up and down signal is referred to as signal I and the El-Centro earthquake input is referred as signal II in the remaining part of this section.

Signal I is generated in MATLAB using sampling frequency of the data at 4096 Hz. Figure 3.19 shows acceleration of signal I with respect to time. The maximum frequency, f_{max} of acceleration is 10 Hz and the amplitude, A_{max} is set at 0.8 mm. The length of the signal, T is 40 seconds. The equation for the input displacement for this signal is given by,

$$x_g = \begin{cases} A_{max}\sin\left(\pi t^2 f_{max}/T\right) \\ A_{max}\sin\left(\pi t f_{max}[2T - t]/T\right) \end{cases} \tag{3-71}$$

The true system behavior is replicated by introducing a 1% RMS random, band-limited white noise as the process noise and measurement noise. Thus, the input excitation signal and the displacement and acceleration data are prepared for real experimental conditions. The presence of hysteretic behavior in the system is confirmed by the contribution of MR damper hysteretic force towards total force in Figure 3.20. Figure 3.21 shows the displacement, velocity and acceleration response of the system when excited with the input signal I. The maximum displacement of the structure is around 4.4 mm and the maximum acceleration is around 2.31 m/s². The MR damper hysteresis loop is plotted in Figure 3.22.
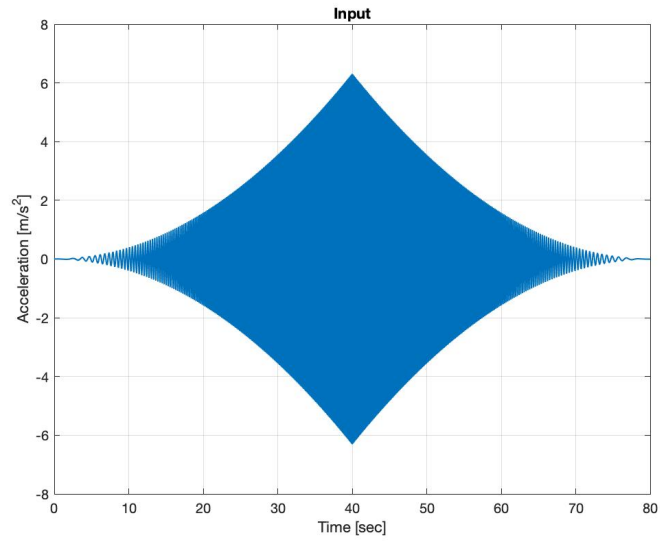
Figure 3.19. Input Signal I – Frequency Sweep Up and Down

Figure 3.20. Input Signal I – Modified Dahl Model Force Contribution
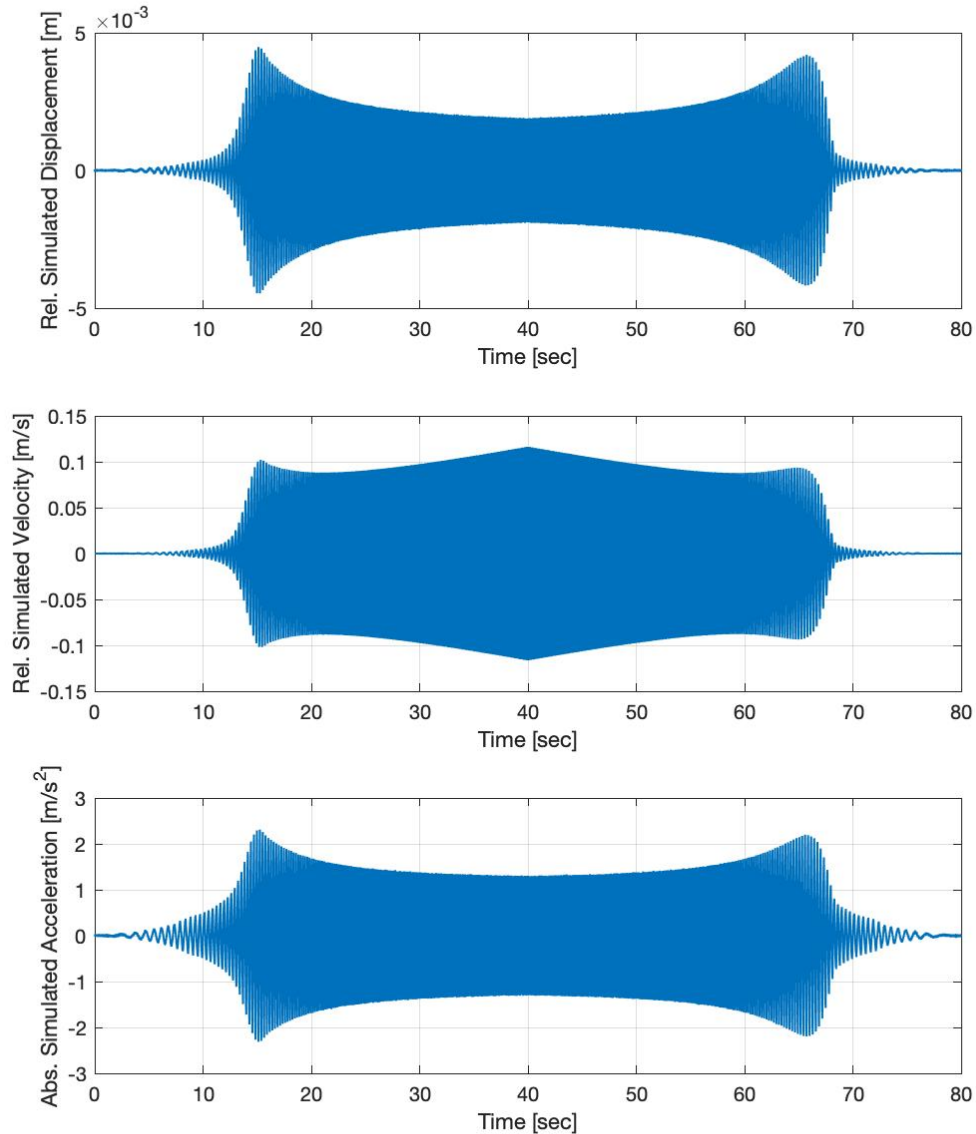
Figure 3.21. Input Signal I – Modified Dahl Model Displacement, Velocity and
Acceleration Response

Signal II is a scaled El-Centro earthquake input measured in the north-south (NS) direction. This input is set at 50% of the original earthquake acceleration. The sampling frequency of the original data was available at 50 Hz. This sampling frequency of the input data is increased to 4000 Hz in MATLAB by using 'interp1' command on the original data. The higher sampling frequency ensures better UKF convergence and estimates. The input acceleration data is shown in Figure 3.23. The process and measurement noise are again set at 1% RMS. The displacement, velocity and acceleration response to this signal is shown in Figure 3.24. The presence of MR damper

hysteretic force towards the total force in the system is confirmed in Figure 3.25 and the MR damper hysteresis loop is shown in Figure 3.26.

Figure 3.22. Input Signal I – Modified Dahl Model Hysteresis Loop

Figure 3.23. Input Signal II – El-Centro Earthquake NS Direction

Figure 3.24. Input Signal II – Modified Dahl Model Displacement, Velocity and Acceleration Response
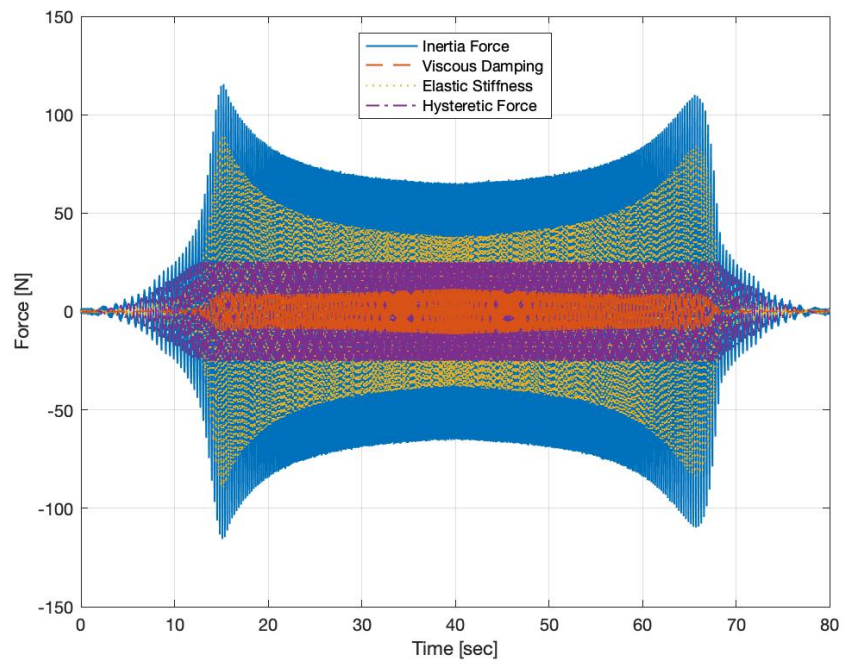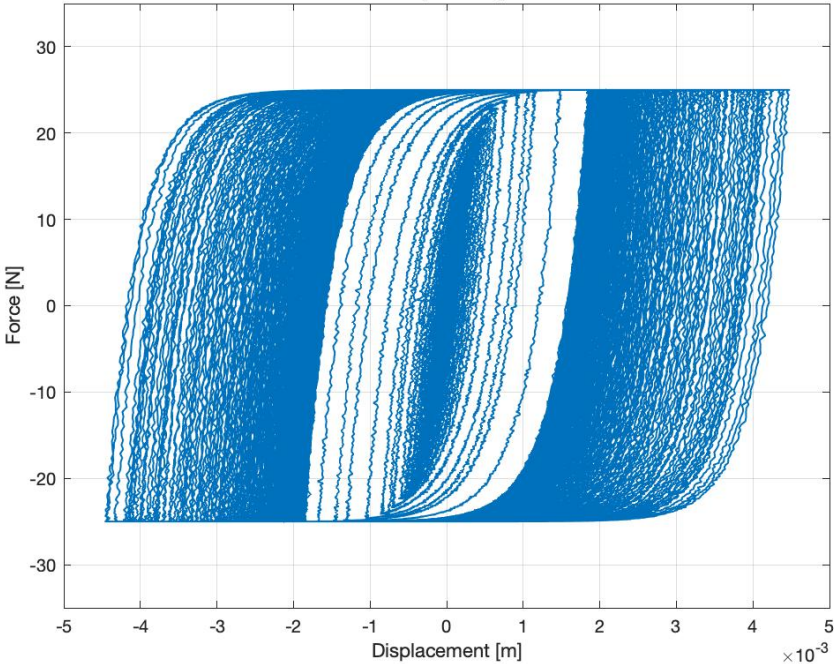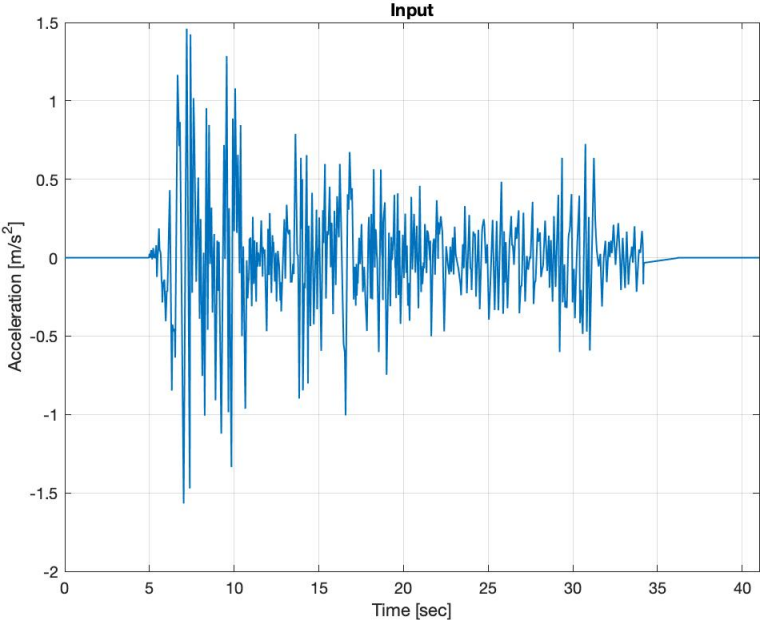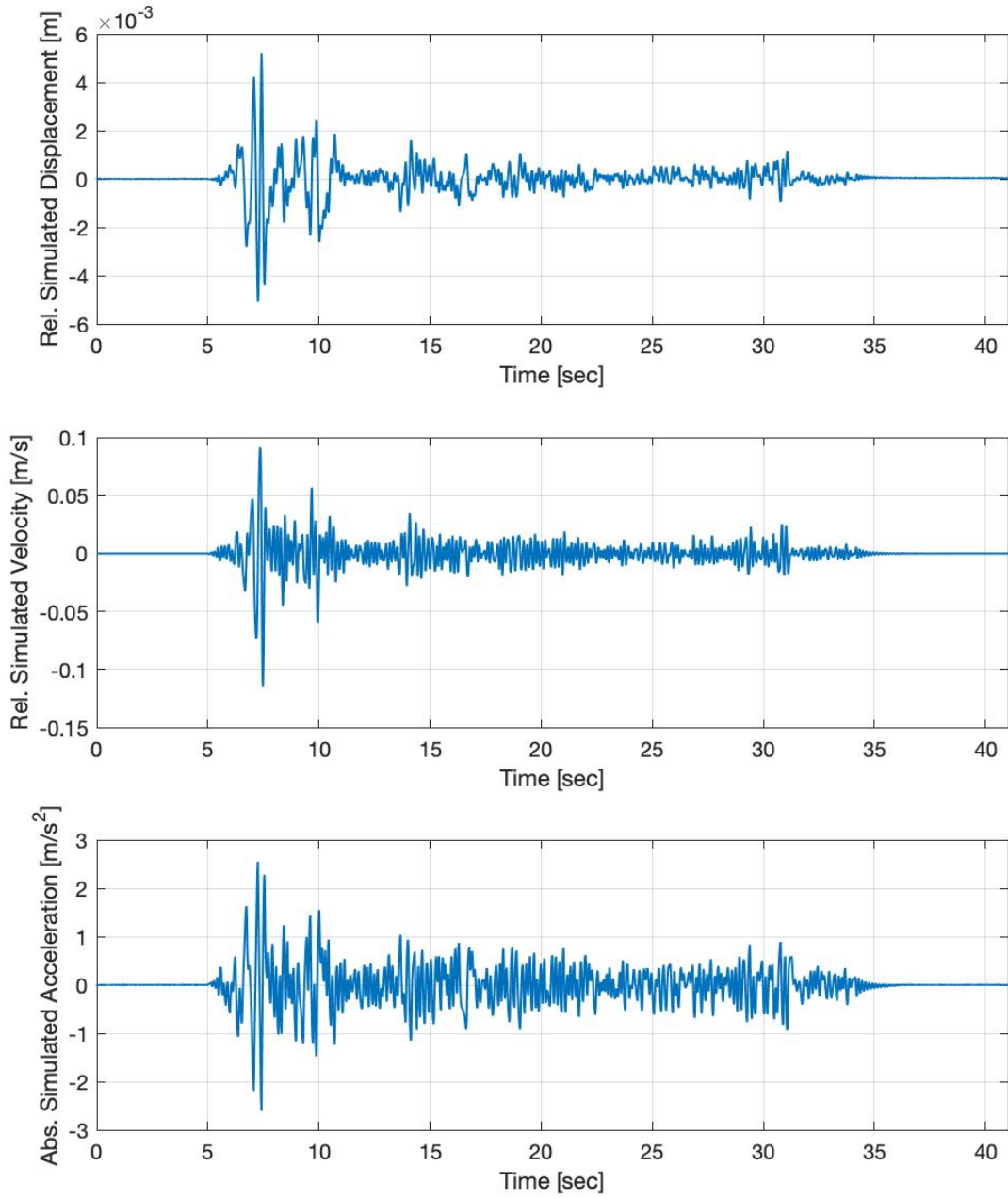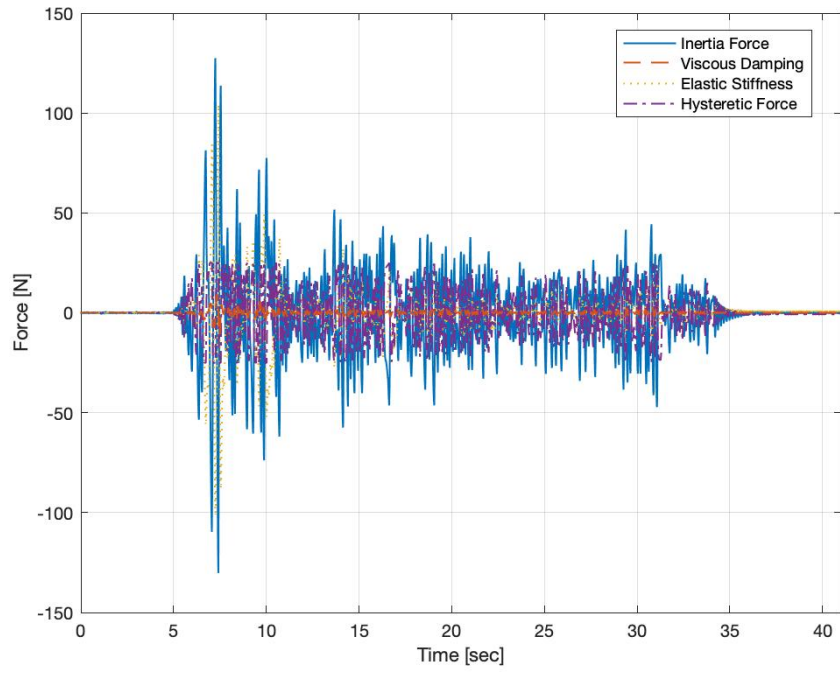
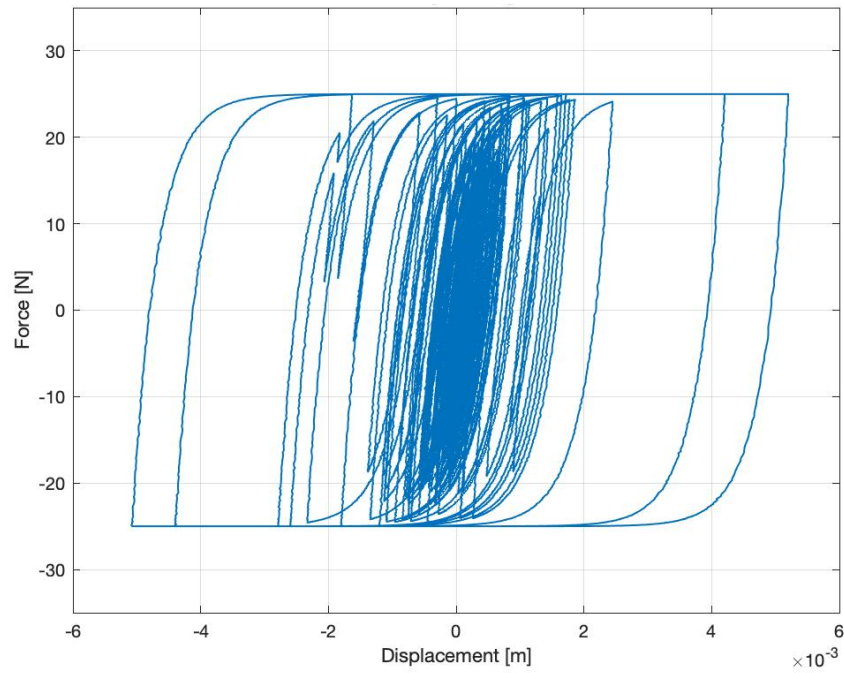Figure 3.25. Input Signal II – Modified Dahl Model Force Contribution

Figure 3.26. Input Signal II – Modified Dahl Model Hysteresis Loop

3.8.2 Normalized Bouc-Wen Model Training and Validation

The training and validation of the normalized Bouc-Wen model using the response of SDOF modified Dahl model under excitation signals I and II is demonstrated here. As indicated in Figure 3.15, the model is trained and validated by the same signal in method 1 and is validated from the other signal in method 2. Therefore, to perform method 1, the normalized Bouc-Wen model is trained using signals I and II and validated using the same signal used for training. The signal I training and validation approach is referred as trial 1 and the signal II approach is referred as trial 2 here. In method 2, the model is trained by signal I and then validated by signal II. This approach is referred as trial 3. The final results for all three trials are compared and a best candidate normalized Bouc-Wen model is selected to compare with the best candidate modified LuGre model from Section 3.8.3.

The normalized Bouc-Wen model in this section is referred to as '*MR Damper$_x$*' from Figure 3.15. 100 prior distribution on parameters with 10 sets of LHSs and 10 samples of the indices of dispersion on covariance samples are taken for training the '*MR Damper$_x$*' with signals I and II. The potential '*MR Damper$_x$*' models are then validated with the various methods used. The number of trained models reduces from 100 due to poor convergence in the UKF implementation. A total of 35 potential '*MR Damper$_x$*' models are generated by training using signal I and 32 '*MR Damper$_x$*' models are generated by training using signal II. The distribution of the parameters of these potential '*MR Damper$_x$*' models for signals I and II is shown in Figures 3.27 and 3.28, respectively. The UKF algorithm identifies the structural and damper properties well for both signals. The maximum number of values for each of these parameters remain in a suitable range for both signals. Although several potential '*MR Damper$_x$*' models failed to converge (only 30-35% trained models for both signals), it is evident that the UKF algorithm is clearly is able to provide quite consistent parameter estimates.

The next step after training is the validation of these models. The displacement, velocity and acceleration response of the potential candidate '*MR Damper$_x$*' model with lowest MSE for trial 1 is shown in Figure 3.30. The candidate model estimates the states of modified Dahl model well. The comparison for force-displacement hysteresis loops is shown in Figure 3.29. Similarly, the potential candidate model with the lowest MSE for trials 2 and 3 is shown in Figures 3.31 and 3.32, respectively. Figures 3.33 and 3.34 compare the hysteresis loops of this model for trials 2 and 3, respectively. A better understanding of these hysteresis loops is obtained from Figures 3.35

and 3.36 for trials 2 and 3, respectively. In these figures, the force-displacement hysteresis loops are plotted for the time interval from 7 to 7.65 seconds.
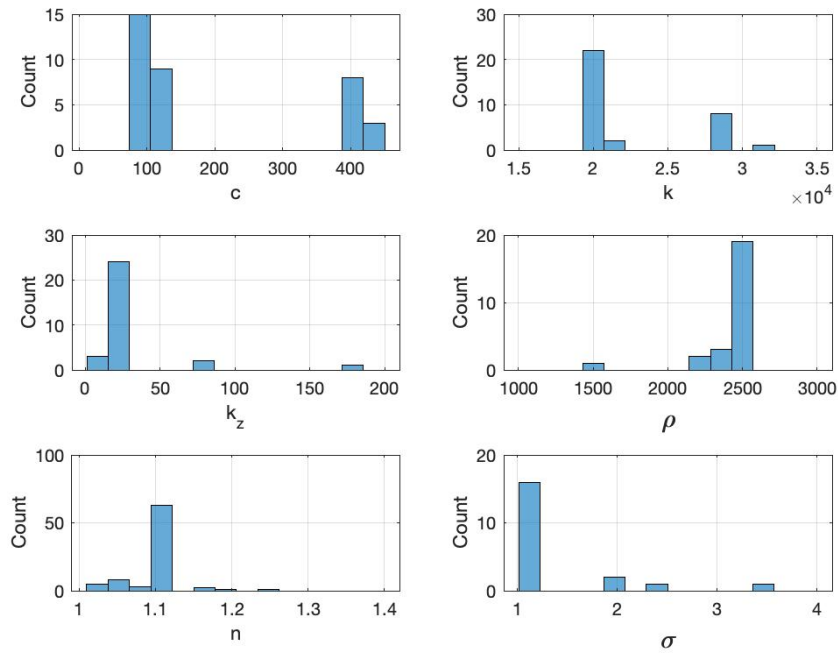
Figure 3.27. Distribution of Normalized Bouc-Wen Candidate Models for training with Signal I
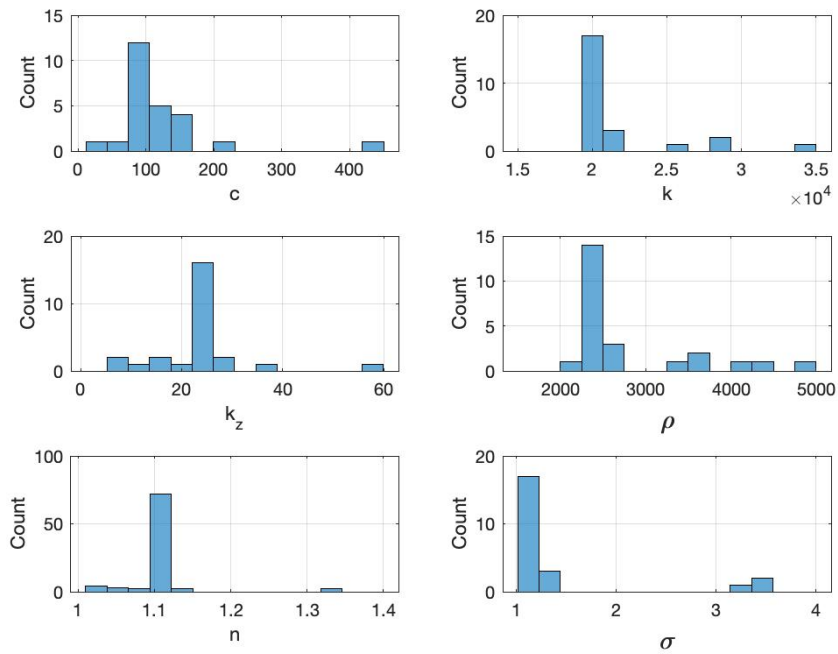
Figure 3.28. Distribution of Normalized Bouc-Wen Candidate Models for training with Signal II

73
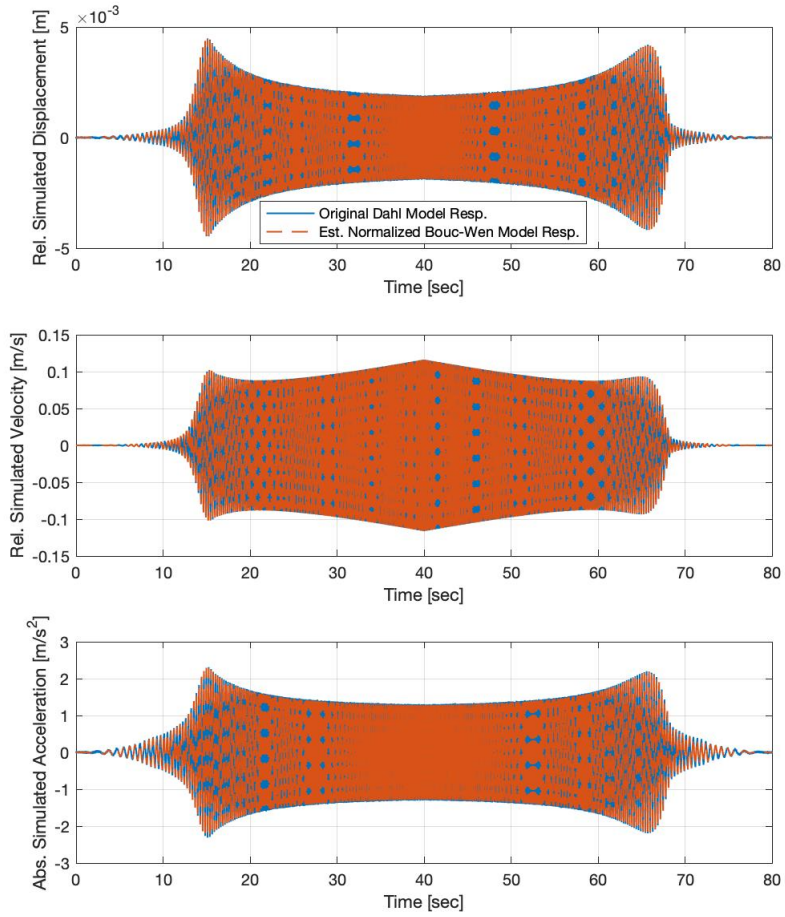
Figure 3.29. Comparison of State Estimates for Normalized Bouc-Wen
model with Lowest MSE in Trial 1
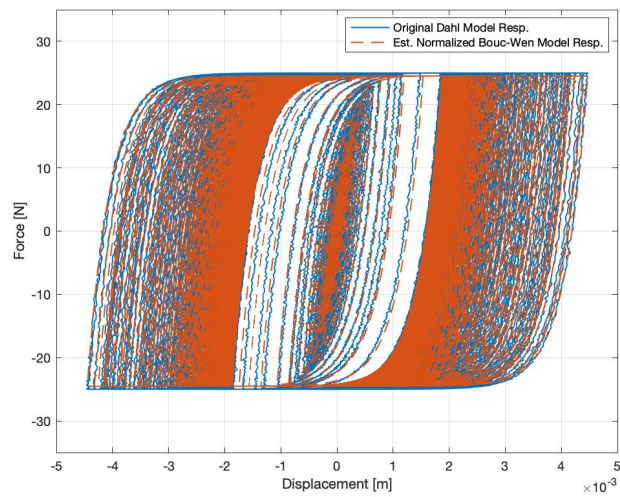
Figure 3.30. Comparison of Hysteresis Loops for Normalized
Bouc-Wen model with Lowest MSE in Trial 1
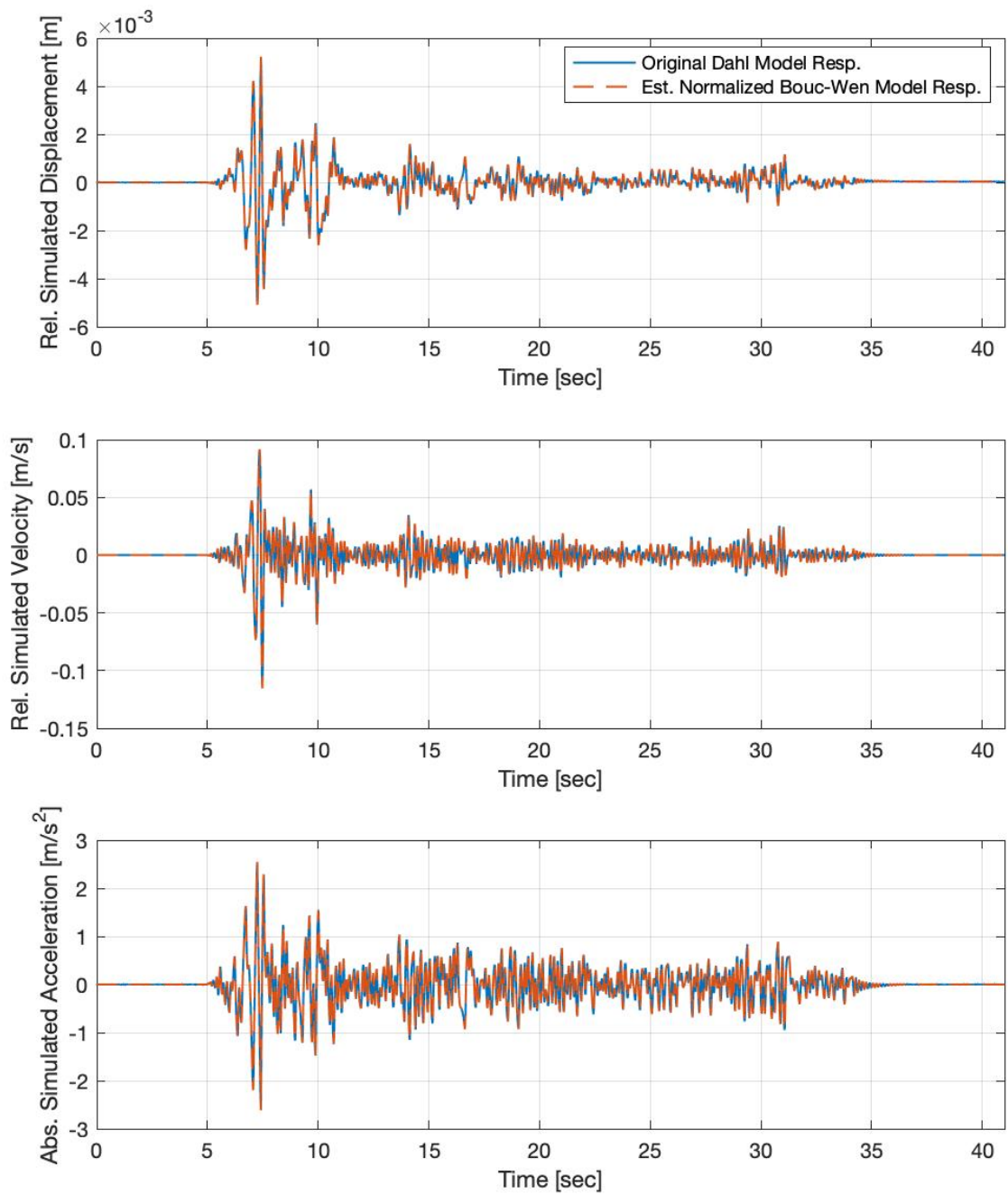
Figure 3.31. Comparison of State Estimates for Normalized Bouc-Wen model with Lowest MSE in Trial 2

Figure 3.32. Comparison of State Estimates for Normalized Bouc-Wen model with Lowest MSE in Trial 3
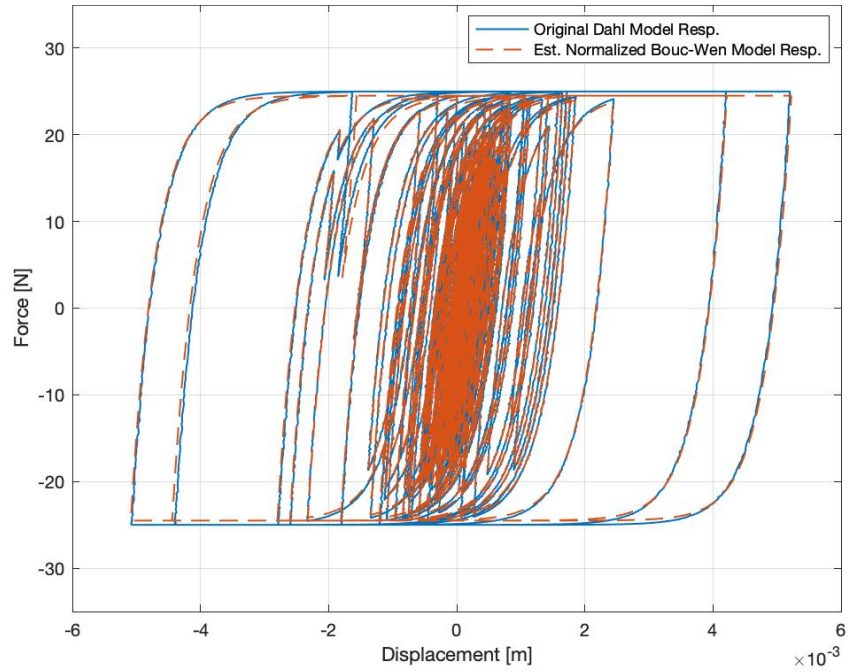
Figure 3.33. Comparison of Hysteresis Loops for Normalized Bouc-Wen
model with Lowest MSE in Trial 2
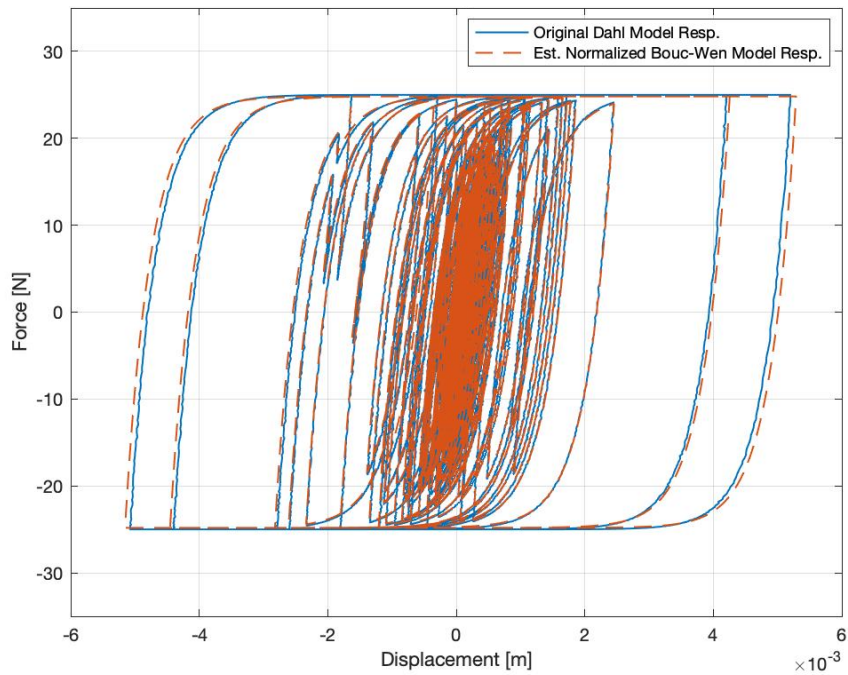
Figure 3.34. Comparison of Hysteresis Loops for Normalized Bouc-Wen
model with Lowest MSE in Trial 3
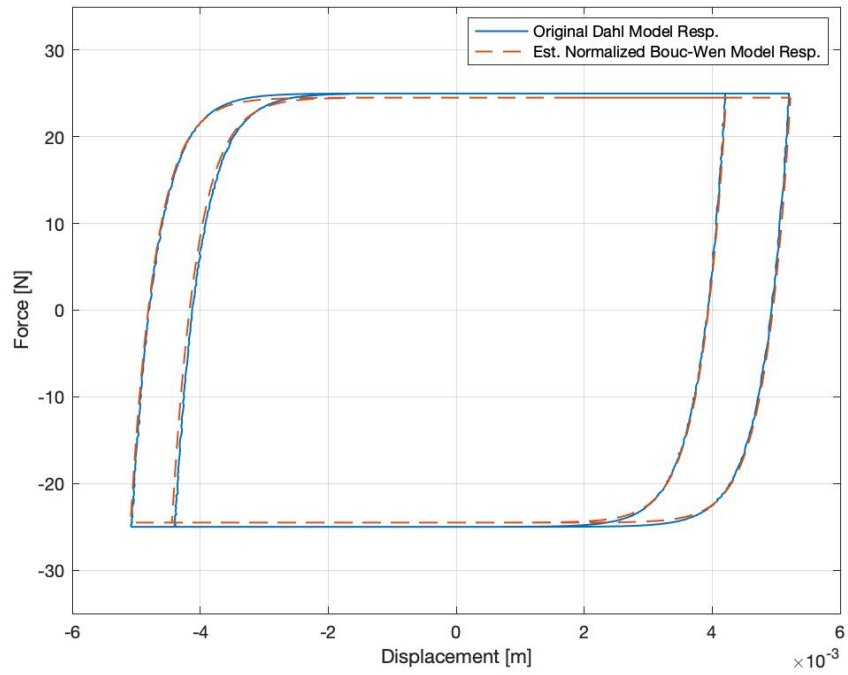
Figure 3.35. Comparison of Hysteresis Loops between 7 and 7.65 seconds
for Normalized Bouc-Wen model with Lowest MSE in Trial 2
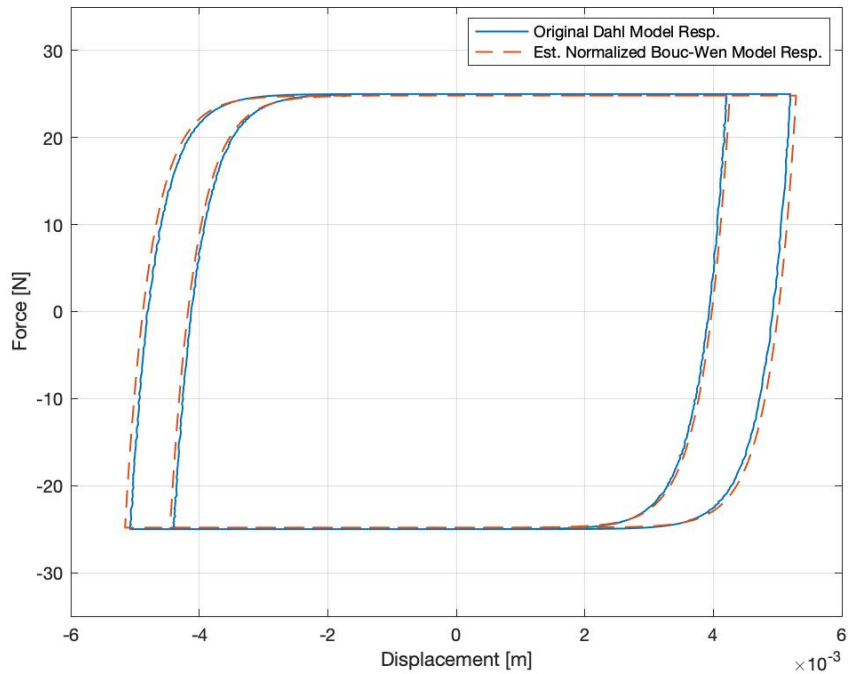
Figure 3.36. Comparison of Hysteresis Loops between 7 and 7.65 seconds
for Normalized Bouc-Wen model with Lowest MSE in Trial 3

The above figures indicate that the UKF algorithm estimates system states and parameters well for the normalized Bouc-Wen model in all trials. A comparison of parameters of the best candidate model from each trial is made in Table 3.3. The structural damping and stiffness coefficients, c and k, are close to the original values from the modified Dahl model. The parameters of the normalized Bouc-Wen model are very close to each other for all trials. A comparison of MSE and error in force with respect to time and displacement for each of these models is made in Table 3.4. A very close relation for error in force of each of these models is visible. The models are accurate and the error lies in the range of second decimal. A high value of MSE is observed for each of these models because of the low values of displacement and acceleration variance in the denominator of the MSE equation. The best candidate normalized Bouc-Wen model on the basis of MSE is thus obtained from Trial 2. This model also has a lowest error in force with respect to time and is very close to the lowest error in force with respect to displacement. This model will be further compared with the best candidate modified LuGre model obtained from next section.

Table 3.3. Normalized Bouc-Wen Best Candidate Model for each Trial

Trial	Method	Training Signal	Validation Signal	c	k (x 10^4)	k_z	ρ (x 10^3)	n	σ
1	1	I	I	103.47	2.0007	24.53	2.485	1.06	1.02
2	1	II	II	103.13	2.0148	24.51	2.508	1.06	1.03
3	2	I	II	99.64	1.9919	24.81	2.482	1.03	1.02

Table 3.4. Normalized Bouc-Wen Model Error Comparison

Trial	Method	Training Signal	Validation Signal	MSE	E_t (x 10^{-2})	E_x (x 10^{-2})
1	1	I	I	168.17	1.84	0.43
2	1	II	II	25.89	1.42	0.18
3	2	I	II	57.37	1.95	0.19

3.8.3   Modified LuGre Model Training and Validation

In this section, the modified LuGre model is trained and validated using the response generated from modified Dahl model excited with signals I and II. Trials 1, 2 and 3 are conducted similar to Section 3.8.2 and modified LuGre model is treated as '*MR Damper$_z$*' from Figure 3.15. The best candidate modified LuGre model is compared to the best candidate normalized Bouc-Wen model in the next section. 100 prior distributions on parameters are trained using signals I and II and the potential number of models available for training reduced due to poor convergence in the UKF algorithm. Thus, a total of 42 potential models are obtained by training from signal I and a total of 41 potential models are obtained by training from signal II. The distribution of parameters of trained models using signals I and II is shown Figures 3.37 and 3.38, respectively. The parameters lie in a suitable range for training done with both signals I and II. The UKF algorithm identifies a majority of the parameters in this range well.

It is evident that only 40-45% of total models are available after training using both signals. These models are further validated for trials 1, 2 and 3. Figures 3.39, 3.40 and 3.41 show the estimates of states for potential modified LuGre models with lowest MSE validated in trials 1, 2 and 3, respectively. An initial observation from these figures suggests that the model response is quite similar to the original response of modified Dahl model. The hysteresis loops for force-displacement relationship of these models for trials 1, 2 and 3 is further compared in Figures 3.42, 3.43 and 3.44, respectively. These figures are followed by the comparison of the force-displacement hysteresis loops for the time interval from 7 to 7.65 seconds. The figures are shown in Figures 3.45 and 3.46 for trials 2 and 3, respectively. The high accuracy of the UKF estimation algorithm for the modified LuGre model is evident in these figures. All models seem to perform fairly well and therefore, it is imperative to compare these models on the basis of the MSE and force errors.
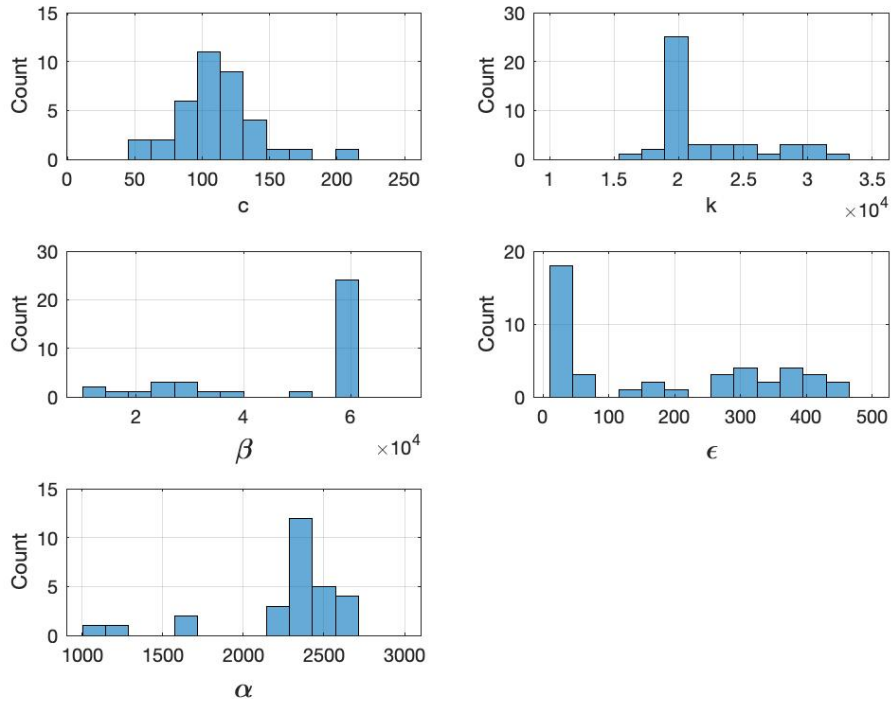
Figure 3.37. Distribution of Modified LuGre Candidate Models for training with Signal I
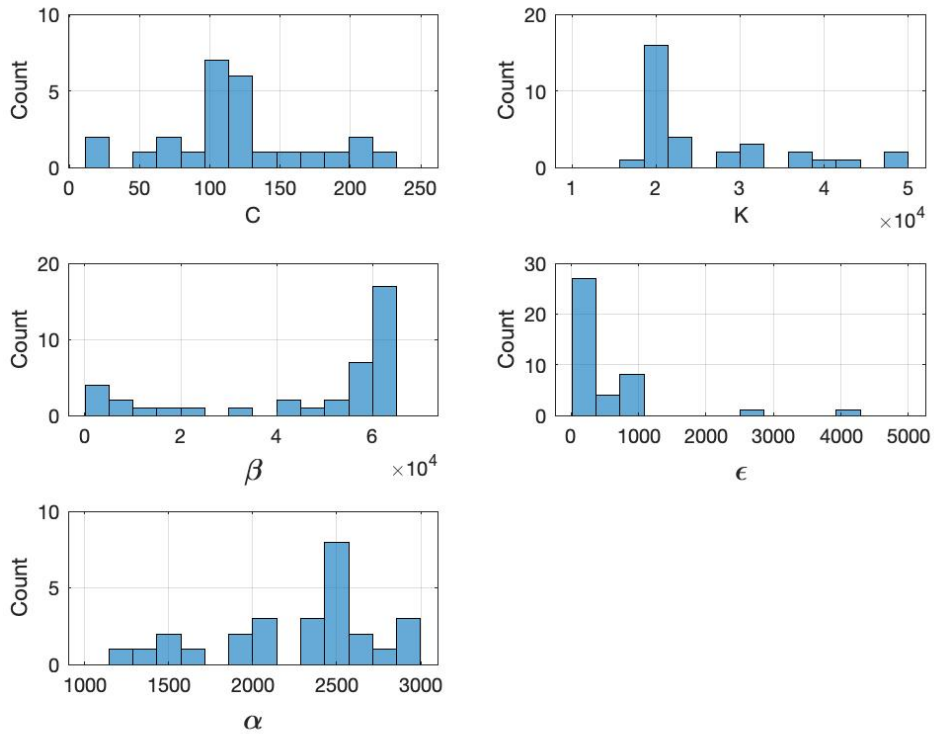
Figure 3.38. Distribution of Modified LuGre Candidate Models for training with Signal II
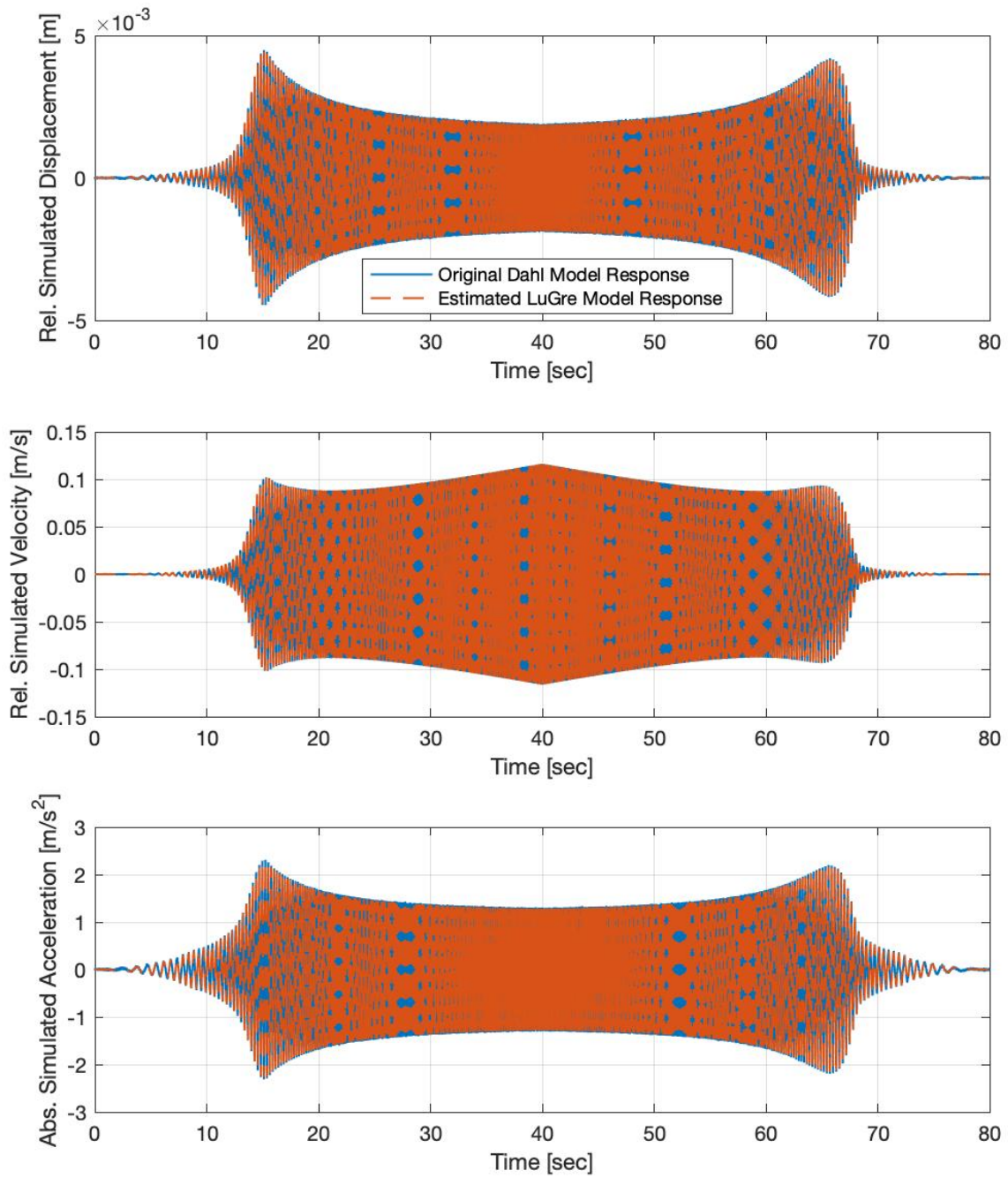
Figure 3.39. Comparison of State Estimates for Modified LuGre model with Lowest MSE in Trial 1
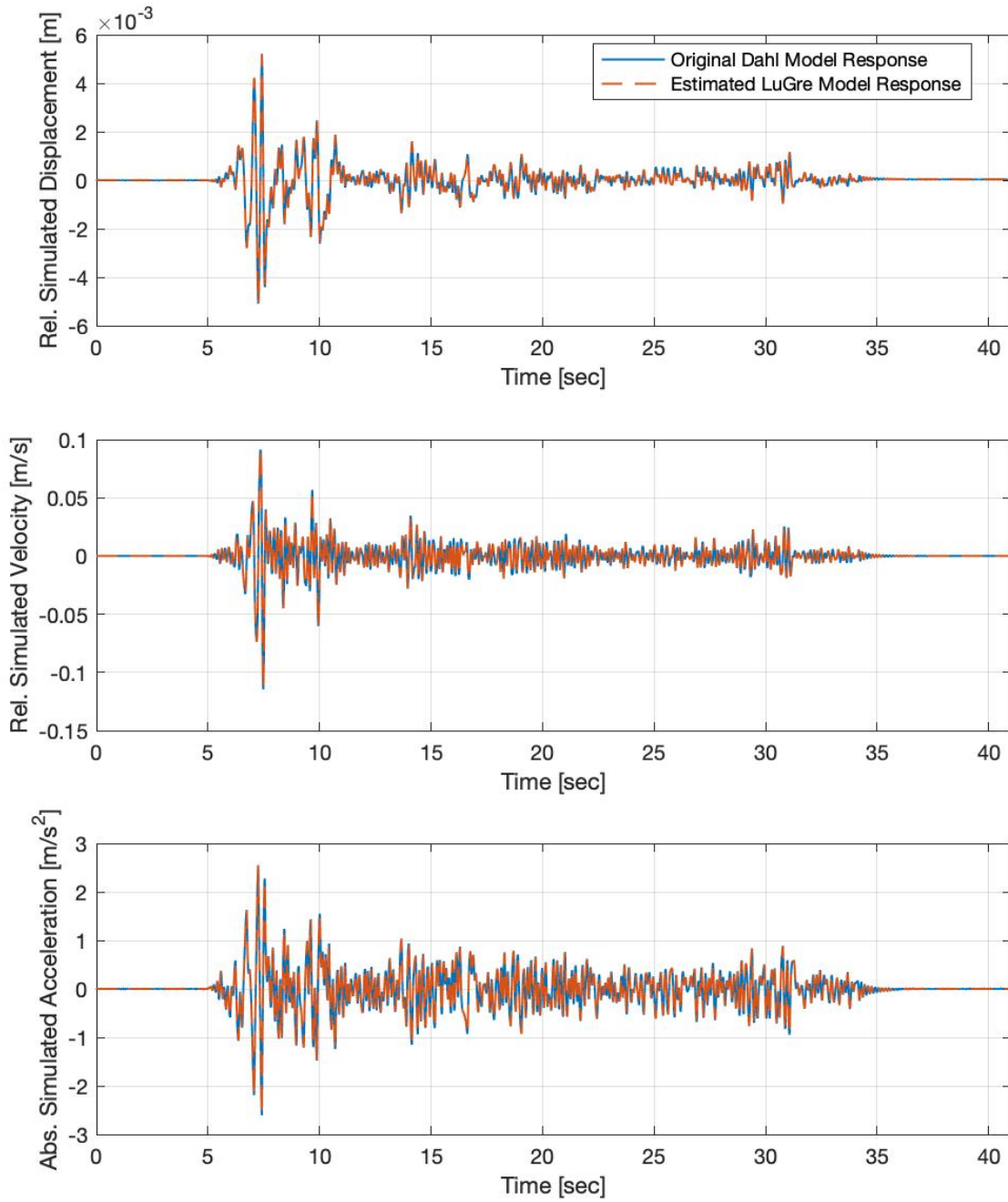
Figure 3.40. Comparison of State Estimates for Modified LuGre model with Lowest MSE in Trial 2
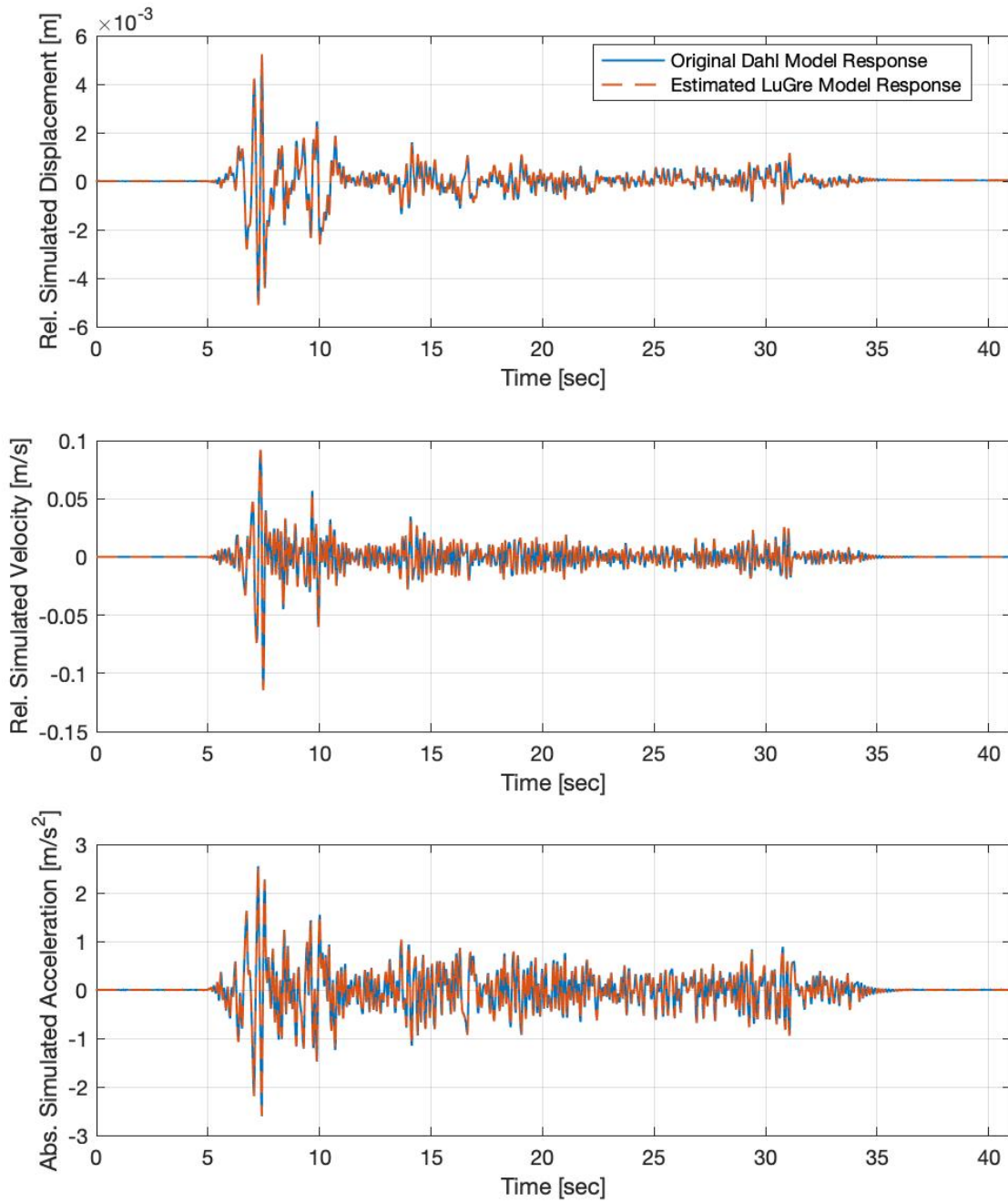
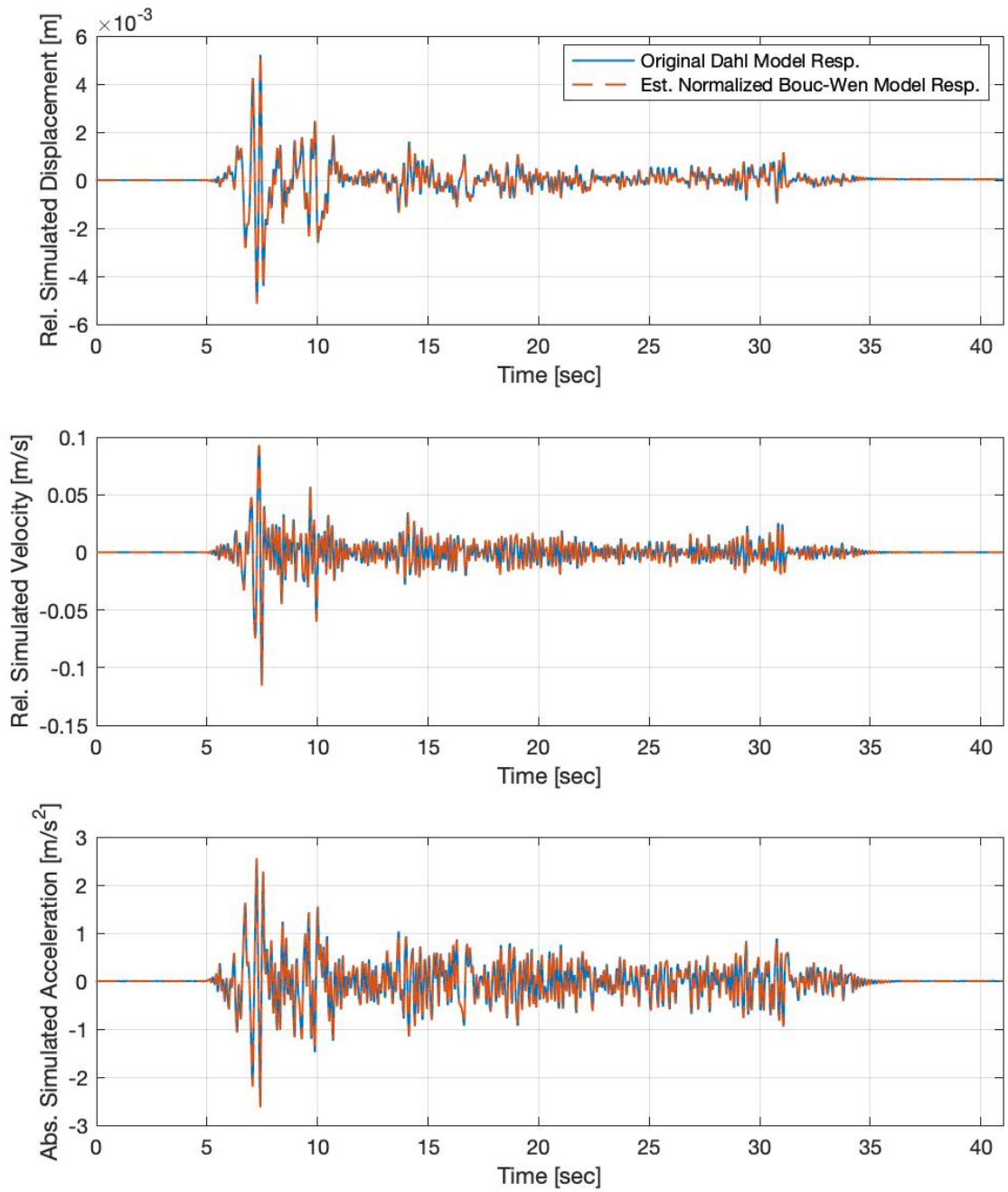Figure 3.41. Comparison of State Estimates for Modified LuGre model with Lowest MSE in Trial 3
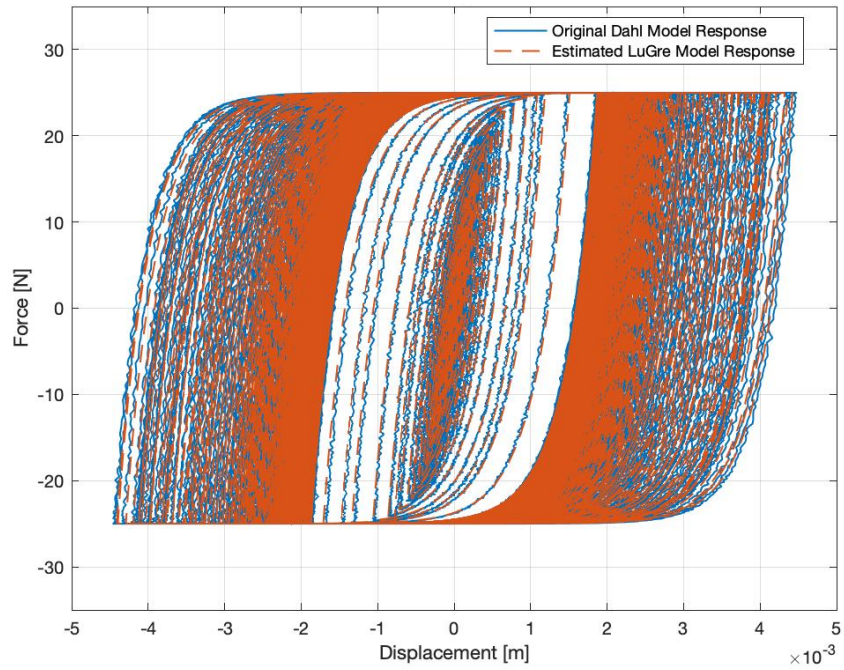
Figure 3.42. Comparison of Hysteresis Loops for Modified LuGre model
with Lowest MSE in Trial 1
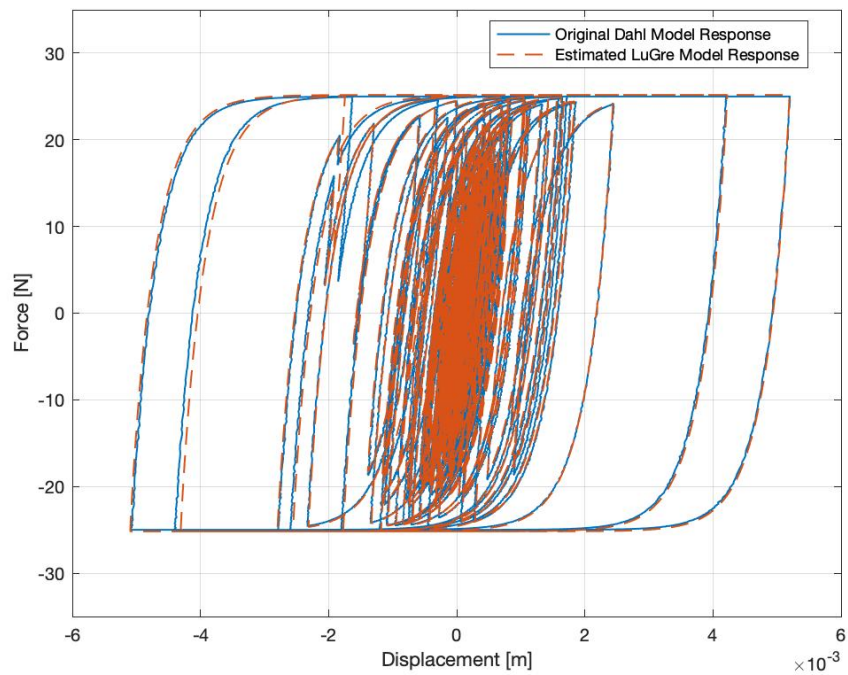
Figure 3.43. Comparison of Hysteresis Loops for Modified LuGre model
with Lowest MSE in Trial 2
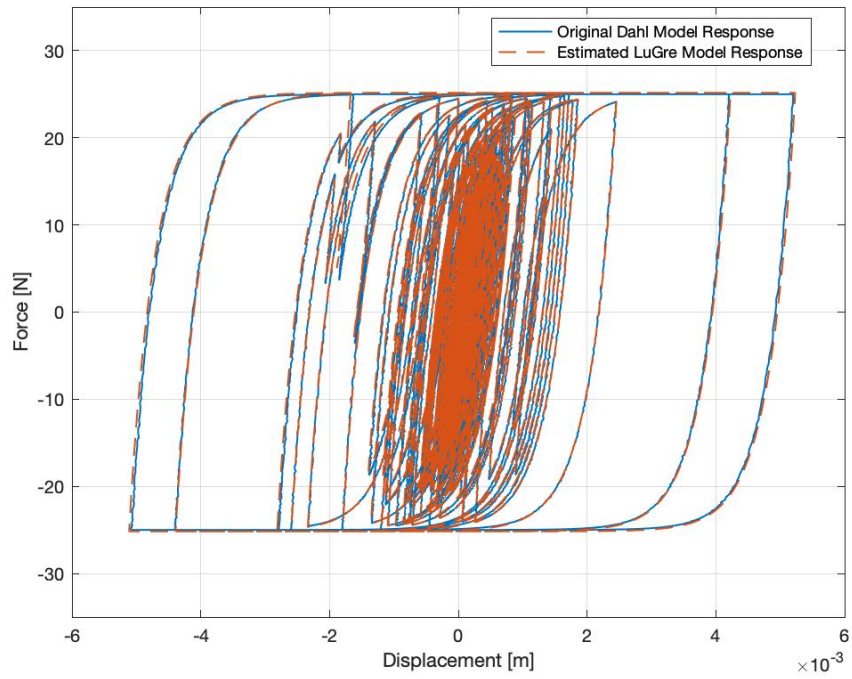
Figure 3.44. Comparison of Hysteresis Loops for Modified LuGre model
with Lowest MSE in Trial 3
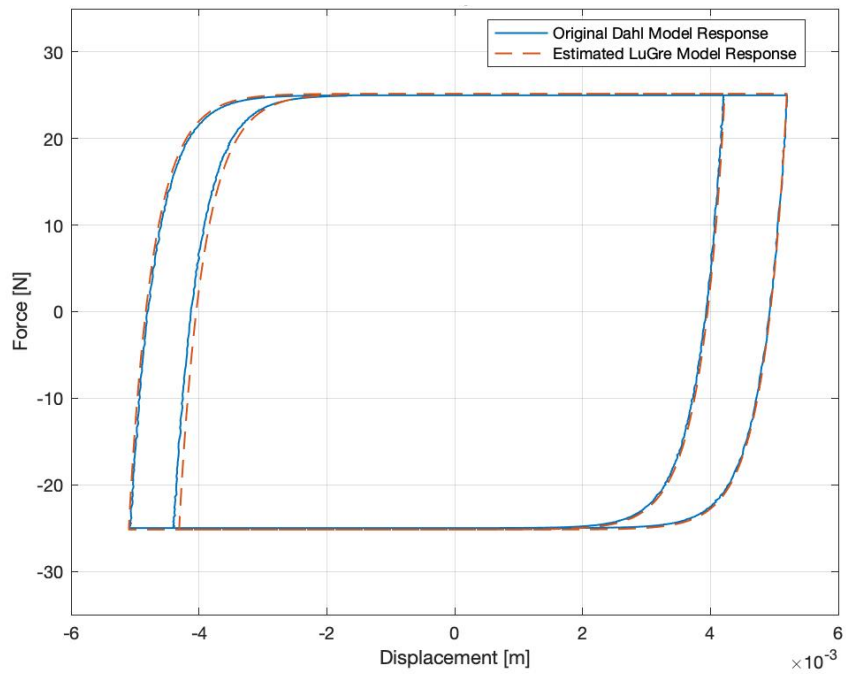
Figure 3.45. Comparison of Hysteresis Loops between 7 and 7.65 seconds
for Modified LuGre model with Lowest MSE in Trial 2
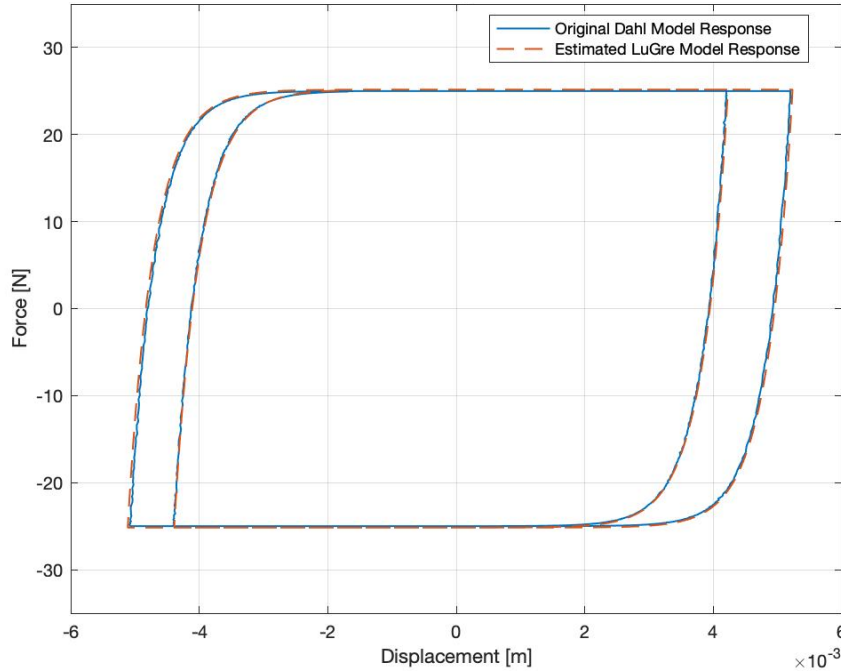
Figure 3.46. Comparison of Hysteresis Loops between 7 and 7.65 seconds
for Modified LuGre model with Lowest MSE in Trial 3

The parameters of the best candidate model for each trial are shown in Table 3.5. The structural damping and stiffness coefficients, c and k, remain close to the original value in the SDOF modified Dahl model system. The generalized stiffness parameters β and α of the modified LuGre model do not show high variation between trials. A slight variation is observed in the generalized damping parameter, ε and it ranges from 9 to 39 in these trials. Table 3.6. compares the MSE and force error with respect to time and displacement for each of the best candidate model from all trials. The lowest MSE is recorded for the model in trial 2. Although the error in force with respect to time and displacement is not the least for the model in trial 2, these values are still in an acceptable range. The error in force for all these models remains close to 0 and is only visible in the second decimal. Therefore, the model in trial 2 is selected as the best of candidate modified LuGre models and has been taken to the next section for comparison with the best candidate normalized Bouc-Wen model.

Table 3.5. Modified LuGre Best Candidate Model for each Trial

Trial	Method	Training Signal	Validation Signal	c	k $(\times 10^4)$	β $(\times 10^4)$	ε	α $(\times 10^3)$
1	1	I	I	101.20	1.9916	6.0827	9.15	2.436
2	1	II	II	102.35	1.9843	6.1484	38.39	2.442
3	2	I	II	99.04	1.9870	6.0827	12.84	2.417

Table 3.6. Modified LuGre Model Error Comparison

Trial	Method	Training Signal	Validation Signal	MSE	E_t $(\times 10^{-2})$	E_x $(\times 10^{-2})$
1	1	I	I	116.76	0.81	0.13
2	1	II	II	99.40	3.00	0.24
3	2	I	II	135.45	3.58	0.31

3.8.4 Model Form Selection

The UKF algorithm used in Sections 3.8.3 and 3.8.4 estimated true modified Dahl model states well. The parameters of the identified normalized Bouc-Wen and modified LuGre model remained in an acceptable range for all trials. The best candidate model from each of these sections is compared in Table 3.7. The force error for each of these models remains close to zero and the MSE remains high due to small covariance in the denominator of its equation. On the basis of MSE, it is evident that the normalized Bouc-Wen model obtained from trial 2 is the best of all models. The convergence history of parameters for this model is shown in Figure 3.47. The parameters seem to converge during the initial 5 seconds of the excitation and then remain stable throughout the remaining time of the input signal. This behavior is evidence of the robustness of the UKF identification algorithm. The algorithm is able to quickly converge to obtain good parameter estimates.

Table 3.7. Numerical Model Selection

Trial	Model	Method	Training Signal	Validation Signal	MSE	E_t (x 10^{-2})	E_x (x 10^{-2})
2	Normalized Bouc-Wen	1	II	II	25.89	1.42	0.18
2	Modified LuGre	1	II	II	99.40	3.00	0.24

In this numerical study, the model with the lowest MSE is the normalized Bouc-Wen. The parameters of the model were determined using method 1 and the training and validation was performed using signal II. This model closely represents the modified Dahl model response in Section 3.8.1 and is therefore selected as the best model. The model selection process demonstrated for this numerical example indicates that the best model is obtained using method 1. However, this result does not demonstrate that the method 1 is better than the method 2 in model validation. The best model can be obtained from either of the methods and will depend on experimental conditions and data availability. The process of obtaining the best model for each of the methods will be further discussed with the experimental model selection performed in Chapter 5.
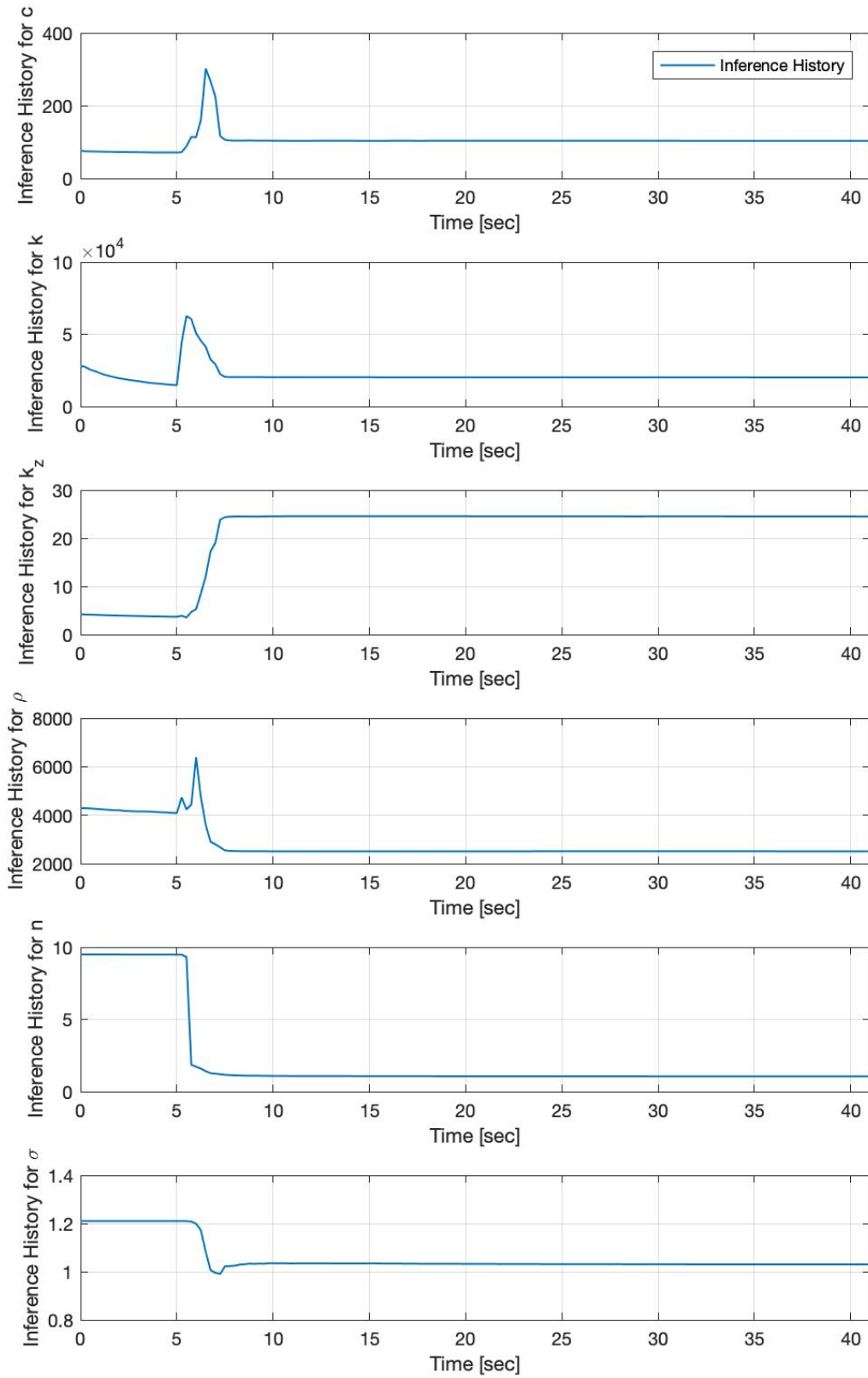
Figure 3.47. Convergence History of Parameters for the Selected Model

3.9 Summary

The chapter on the numerical study of model selection can be summarized as:

- The UKF uses an Unscented Transform and provides good approximation of system states and parameters for the hysteretic systems considered herein. (Section 3.5)
- The model selection process consists of training and validation of the model and selecting the most appropriate model on the basis of MSE. (Section 3.6)
- The training and validation steps can be performed using several methods and these methods vary depending upon the validation signal used. (Section 3.6)
- The normalized Bouc-Wen, modified Dahl and modified LuGre are the mechanical models that estimate structural response with a fair accuracy and are computationally efficient. (Section 3.7)

3.10 Findings

The critical findings from this chapter are as follows:

- The UKF is accurate to third order Taylor series expansion and minor variation in process and measurement noise does not change the accuracy of the estimates. (Section 3.5)
- The UKF algorithm fails to converge sometimes due to poorly conditioned matrices. (Section 3.5)
- The estimation of structural displacement, velocity and acceleration response for all mechanical models is very close to the original response in all trials. (Section 3.8)
- The UKF algorithm converges parameters to the true value in the first five seconds of the input excitation signal for the numerical example. (Section 3.8)

4. EXPERIMENTAL SETUP

4.1   Introduction

An experiment is conducted to obtain high quality data for use in demonstrating the proposed model selection method with experimental data of a nonlinear device in a structure. A small-scale version of the MR damper is installed between the base and first story of the structure. Various constant current inputs are used, resulting in different passive-on systems each with nonlinear behavior. A hydraulic shake table is used at the Intelligent Infrastructure Systems Laboratory (IISL) at Purdue University. This chapter provides a full description of the experiment conducted, including the MR damper used. A SDOF is defined later and the setup of the MR damper on the structure is explained. The steps to operate the MR damper with necessary safety precautions have been provided to get best results from the damper.

4.2   MR Damper Setup

A magnetorheological (MR) damper is a semi-active controllable device used for energy dissipation in a structural system. The damper has nonlinear responses during the energy dissipation and is therefore chosen for this nonlinear identification study using Bayesian approach. The passive damping provided by the MR damper can be controlled to a certain extent by using various constant current inputs to the damper. Figure 4.1 shows a typical MR damper used for this study.
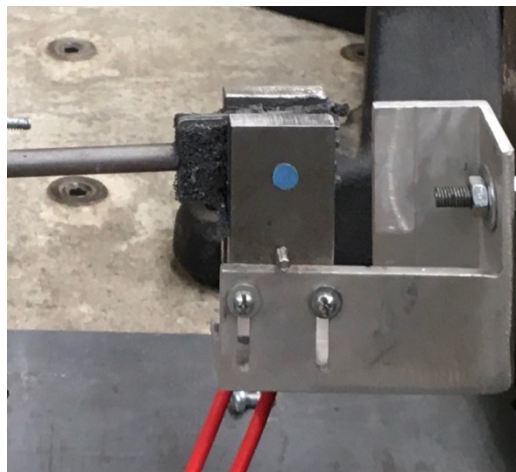
Figure 4.1. MR Damper

4.2.1 Components

The components for the MR damper can be divided into primary and secondary components. The primary components control the behavior of the damper while the secondary components provide proper functioning of the damper.

a. Primary Components

i. *Paddle –*

A paddle along with foam and damping fluid moves horizontally between parallel plates and produces necessary damping force. Paddles are available in different dimensions and thicknesses. The thicknesses of paddle available in the lab are 0.135 in, 0.222 in and 0.238 in. The average dimensions for these paddles are 1.502 in x 0.754 in, 1.496 in x 0.685 in and 1.747 in x 0.703 in respectively.

ii. *Foam –*

A foam padding is applied over the paddle and serves as a seat for the damper fluid. The foam used for the MR dampers is the open-cell camera foam. The foam absorbs the damper fluid and is the only component other than damper fluid touching parallel plates. The two thicknesses of the foam available are 0.037 in and 0.090 in.

iii. *Electromagnet -*

An electromagnet situated between parallel plates produces a magnetic field between the plates when an electric current is applied.

iv. *Parallel Plates –*

The parallel plates work as a housing for the electromagnet and provides a direction for the paddle and foam to move during motion. The plates attract damper fluid particles in motion and thus provide damping to the structure. The widths of the three available parallel plates are 0.302 in, 0.252 in and 0.248 in. The portion of the MR damper paddle inside this width of parallel plates is responsible for energy dissipation. The parallel plate with width 0.302 in is used for story 1 on SDOF tests.

v. *Wonder Box –*

A Wonder Box takes a voltage input and supplies an output current to the electromagnet. A rotating knob on the Wonder Box changes the output voltage supply and thereby the effective output current. The dimensions of the Lord Rheonetic Wonder Box used for existing set of tests are 3.5 in x 2.5 in x 1.1 in. The box is also be referred to herein as

'Device Controller' and its model number is RD-3002-1. The external input rated voltage is 0-5 V and its rated output is 0.4 A/V. The recommended power supply specifications for the Wonder Box is 12 V 2 A.

vi. *Damper Fluid* –

The damper fluid is evenly applied over both sides of the foam using a paint brush. The magnetic behavior of the fluid is the primary reason for the damping behavior of the MR damper. The MR damper fluid used for these tests is labelled as MRF-140N.

b. **Secondary Components**

i. *Shaft* –

The shaft is circular rod of small diameter connecting paddle on one end and the load cell on the other. The shaft has threaded rod of dimension 3-48 to go into the paddle. The other end of the shaft is connected to the load cell using a shaft adapter. The diameter of the shaft is 0.286 in.

ii. *Shaft Adapter* –

A shaft adapter is a small bolt with variable threads and diameters on two sides. The adapter is the interface for variable diameters of the load cell and the shaft. The portion of the adapter that goes into the load cell has 10-32 size while the other side going into the shaft has 3-48 size.

iii. *Load Cell* –

A load cell with a suitable capacity is used to dynamically record the tension and compression force generated from the damper. The load cell is situated between the shaft and the threaded rod. The specification of the load cell is given in the next section.

iv. *Threaded Rod* –

A threaded rod connects load cell on one end and reaction plate and stability spring with its plate on the other. The size of the threaded rod is 10-32.

v. *Mounting Tower* –

A mounting tower is used to raise the paddle assembly to a certain height to reach the level of damper parallel plates and electromagnet. The height of the mounting tower used for experiments is 10.65 in. The tower is used for the base story for the SDOF test.

vi. *Reaction Plate* –

A reaction plate provides the necessary horizontal reaction force during damper compression and tension. The threaded rod is tightened with a nut near the reaction plate. It should be noted that the size of the reaction plate should be greater than the width of the opening of the mounting tower. The dimensions of the reaction plate used for the experiments are 1.721 in x 0.937 in x 0.111 in. The reaction plate with smaller width than the mounting tower will sink inside the tower and would not provide necessary reaction.

vii. *Stability Spring –*

A stability spring ensures vertical stability of the entire paddle to rod system. The stability spring consists of a stability plate on one end and the back of mounting tower on the other.

viii. *Stability Plate –*

A stability plate supports the other side of the wall of mounting tower and takes the incoming rod coming from the reaction plate. The stability plate works in conjunction with stability spring to provide vertical stability. The stability plate contains grooves parallel to the shorter side and they help to fasten the plate along with the spring to the mounting tower. The width of the plate is smaller than the outer dimensions of the mounting tower but greater than the width of the opening of mounting tower. The dimensions of the plate used for the experiments are 0.240 in x 1.336 in x 0.719 in.

ix. *Mounting Angle –*

A mounting angle is used to connect the parallel plates to the story above. The parallel plates are fastened to one leg of the mounting angle using small bolts. Loctite thread locker Blue 242 is applied to the threads to prevent bolts from loosening up due to the force generated from the paddle movement. Thus, mounting tower connects paddle from the story below and a mounting angle connects parallel plates from the story above. In addition, a mounting angle also provides an option for adjustment in the direction perpendicular to the shaft. The leg width and thickness of legs of the mounting angle is 1.5 in and 0.4 in. The length of the angle is 2.5 in. The slotted hole on the mounting angle has an average length of 1 in and diameter of 0.14 in.

x. *Mounting Angle Stability Plate –*

A mounting angle stability plate is situated on the hanging leg of mounting angle and prevents the electromagnet and parallel plates from rotating due to the torque created from

the damper. The average dimensions of the plate used for the experiments is 1.70 in x 1.0 in x 0.111 in.

xi. *Nut –*

Nuts are used to tighten the interface between shaft, threaded rod and the load cell and also between threaded rod and reaction plates. The nuts are accompanied by suitable washers for proper force distribution.

xii. *Power Adapter –*

A 12 V 2 A power adapter is used to power up the Wonder Box. An adapter with a current range between 1 A and 1.5 A with 12 V can also be used provided the output current from the Wonder Box remains at 1 A.

xiii. *Connecting Wires –*

Connecting wires are used to connect the Wonder Box to the electromagnet. Current is measured using a Tektronix A622 AC/DC current probe placed around one of the two wires.

Figures 4.2 and 4.3 show the primary and secondary components of the MR damper. The component names in the figure can be identified with the definitions above by numbers indicated in the bracket.
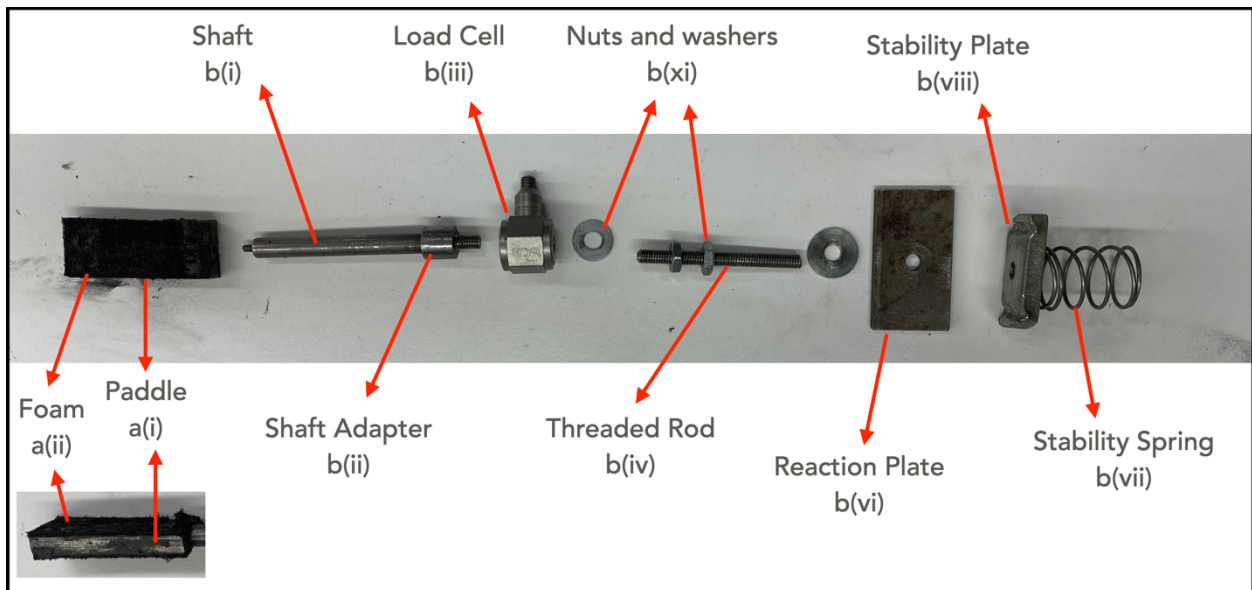
Figure 4.2. Primary and Secondary Components
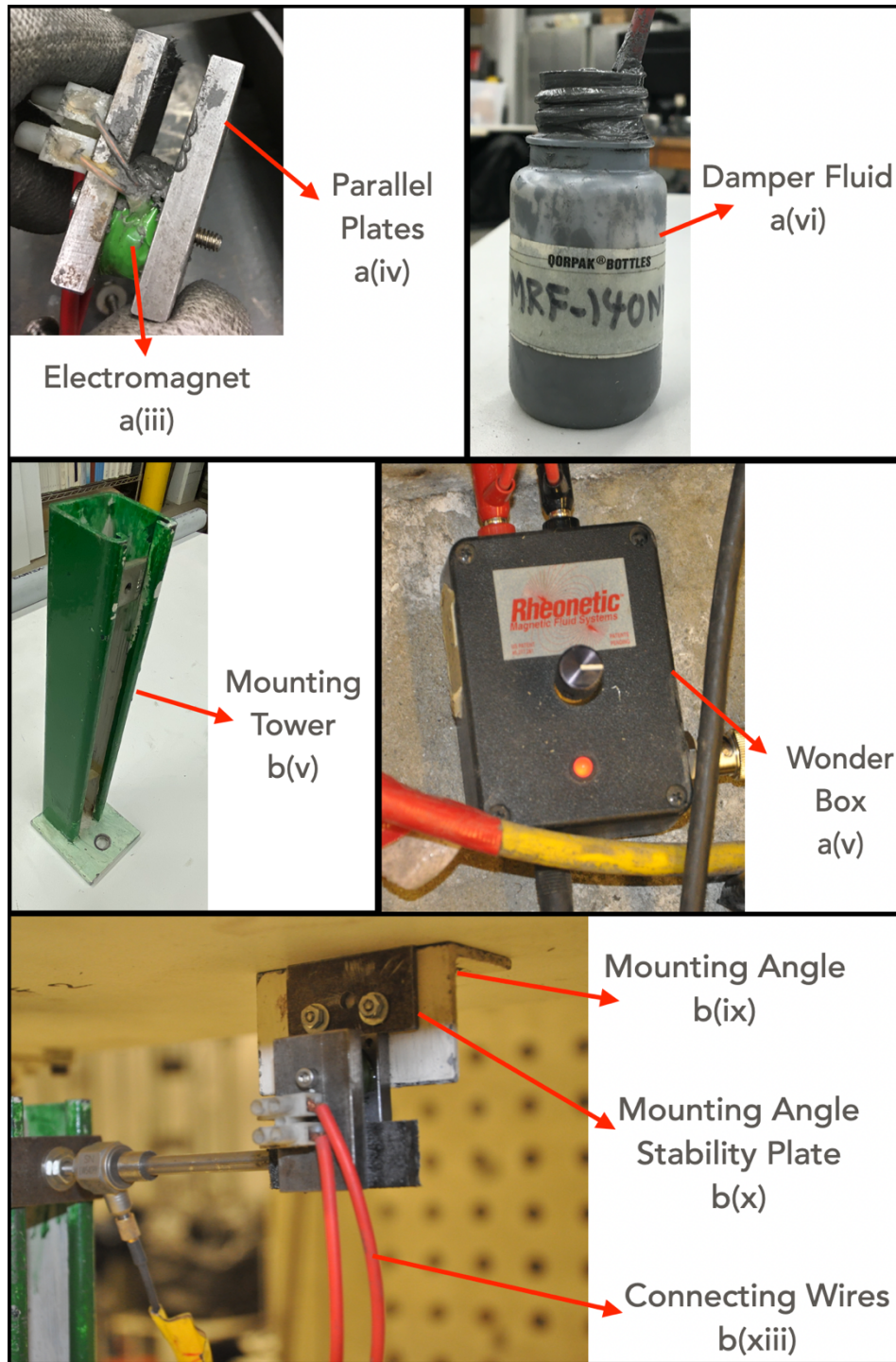
Figure 4.3. Primary and Secondary Components

Figure 4.4 shows the assembled part of the damper shaft components. Figure 4.5 shows the entire MR damper assembly mounted on the structure.
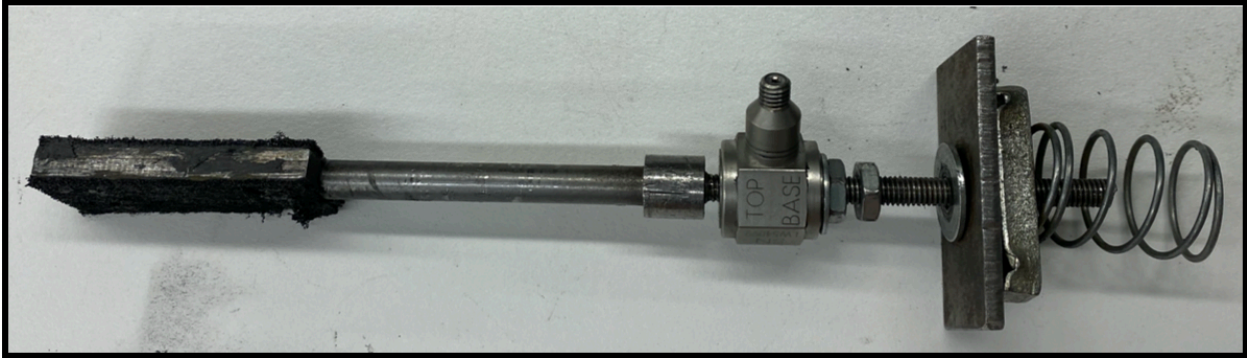
Figure 4.4. Damper Shaft Components
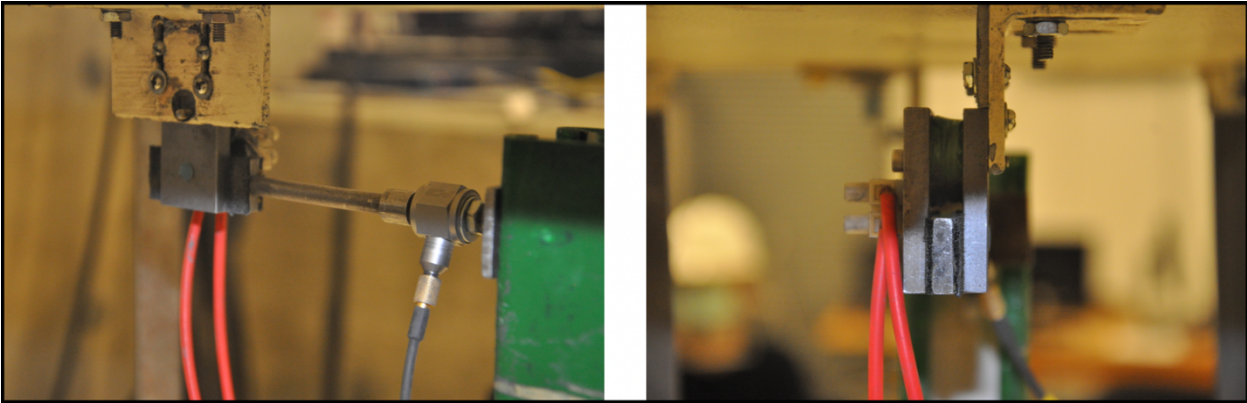
Figure 4.5. MR Damper Assembly on a Structure

4.2.2   Alignment

In order to obtain a proper force-displacement curve from the MR damper, it is important to align the paddle and foam properly with respect to parallel plates and electromagnet. A properly aligned MR damper requires three levels of alignment, they are horizontal, vertical and twisting alignment. The steps for three levels of alignment and their significance are described in this section. A comparison between the force-displacement curves for a poorly and properly aligned MR damper is shown in Figure 4.6.
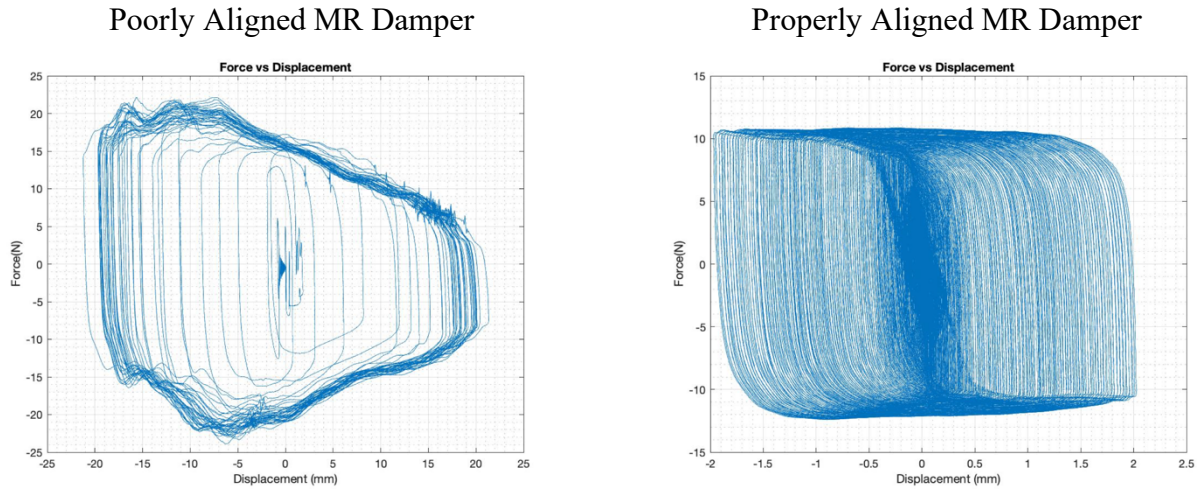
Figure 4.6. Comparison of Force-Displacement Curve

a. ***Horizontal Alignment*** –

Horizontal alignment of the paddle is necessary to ensure that the paddle does not interfere with the parallel plates. The paddle should be placed at center position and the paddle foam should line parallel with the parallel plates. In the case when the paddle does not lie at the center, the mounting angle can be adjusted in one direction to ensure that the incoming paddle lies exactly between the parallel plates. In addition to this, the portion of the paddle outside the parallel plates on both sides should be equal. This procedure will ensure a proper force-displacement diagram during compression and tension (in and out) cycles.

b. ***Vertical Alignment*** –

The paddle with its foam should not project vertically out of the parallel plates. The paddle and foam should project out only in the direction of the shaft and not in the direction perpendicular to the shaft. Additionally, it should be ensured that the paddle does not touch the electromagnet between parallel plates. The mounting angle stability plate can be cut if needed to provide an extra adjustment in the vertical direction for parallel plates and electromagnet.

The horizontal and vertical alignment for the MR damper is schematically shown in Figure 4.7.

c. ***Twisting Alignment*** –

The MR damper paddle may be able to rotate in the plane as shown in Figure 4.8. The rotation of the paddle in this plane or in other directions will lead to the generation of a twisting force and result in improper force-displacement curve. Therefore, the orientation of the paddle

should be checked thoroughly at the start and between tests. Figure 4.9 shows a proper aligned damper paddle in horizontal and vertical directions.
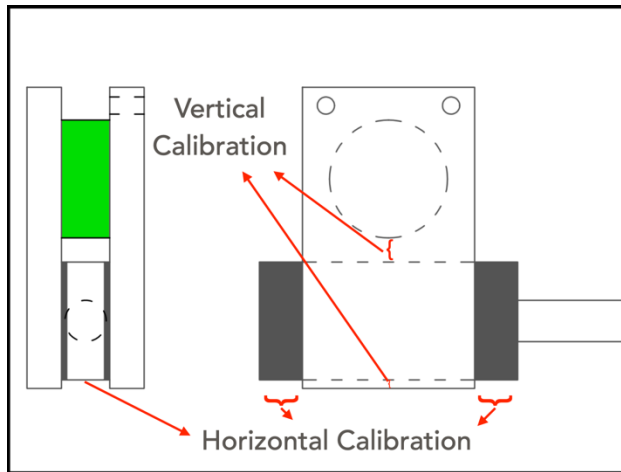
Figure 4.7. Horizontal and Vertical Alignment
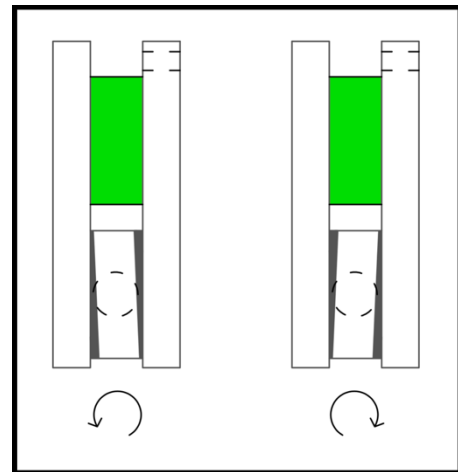
Figure 4.8. Twisted Paddle
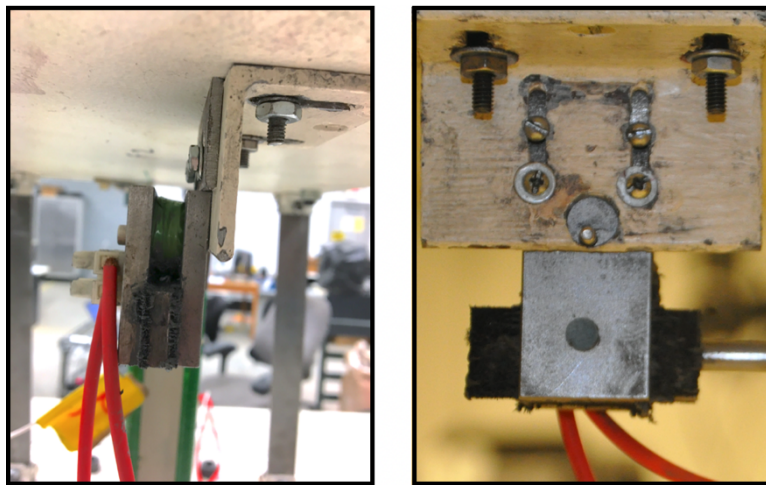
Figure 4.9. MR Damper Paddle Alignment

4.2.3   Variables

a. *Damper Fluid* –

The amount of the applied damper fluid plays a major role in the behavior of the MR damper. The fluid should be applied uniformly over both sides of the paddle and should be applied only once before the start of a series of tests. Applying fluid again after the start of the test will lead to a slightly different behavior for the damper.

b. *Electric Current* –

The current output from the Lord Rheonetic Wonder Box is kept at 1 A for all of the tests discussed here. The damper is current-controlled, and thus any change in output current from the Wonder Box will lead to different behavior for the damper.

c. *Paddle Displacement* –

The effective paddle displacement should be kept at or below 5 mm (+/in and -/out) to obtain a proper force-displacement loop of the damper. An increase in the displacement at either or both sides will lead to varying force-displacement behavior of the damper. The variation of force-displacement curve with different maximum displacement values is shown in Figure 4.10. The behavior of the curve is properly observed for displacements of less than 5 mm.
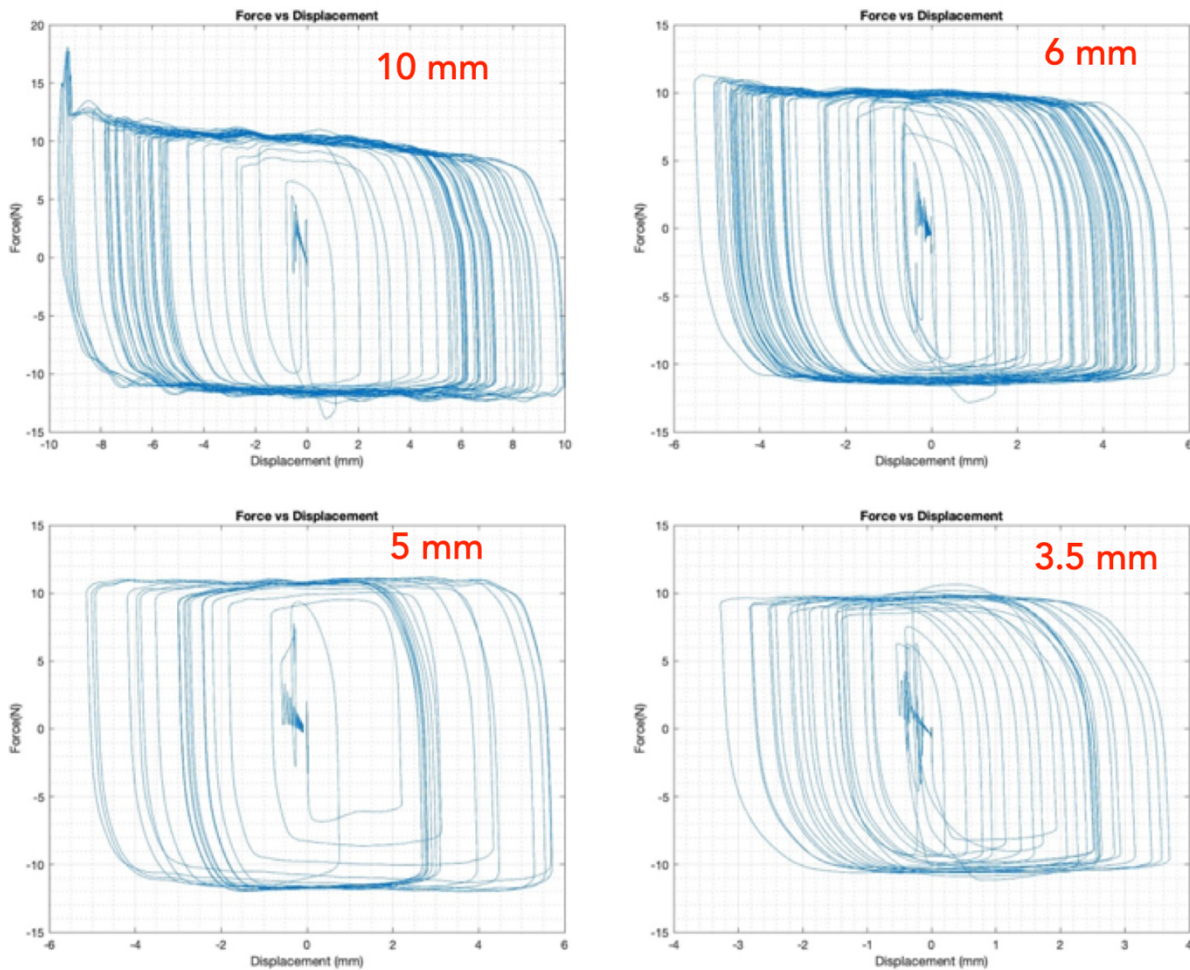
Figure 4.10. Variation in the Force-Displacement Loop with Displacement

d. *Temperature* –

The temperature of the electromagnet does not play a major role in the behavior of the damper. However, the temperature for the electromagnet and parallel plates should be kept low to ensure proper functioning of the MR damper. The passage of current when offered a resistance from the electromagnet results in heating of the electromagnet and thereby of parallel plates. Overheating of electromagnet would make it difficult to align the damper between tests and might also damage the electromagnet in long run. As a result, the temperature is kept under check by turning the damper off and on between specific set of tests.

e. *Foam and Paddle Thickness* –

The foam and paddle thickness should be varied depending on the distance between the parallel plates. There are three versions of varying thickness of paddles and two versions of foam available. These dimensions are described in Section 4.2.1. The damper paddle and foam should not restrict the movement of the shaft between the parallel plates when the damper is switched off.

4.2.4   Instructions for Setting up MR Damper on an Experimental Setup

Figure 4.11 shows a MR damper installed on the structure. The general instructions to set the MR damper on a structure are as follows:

a. Scrape old foam over the paddle if signs of deterioration or peeling off are visible. Apply new foam using a gasket glue. The gasket glue takes 4 hours to completely set and stick the paddle and foam.

b. Apply damper fluid over the paddle.

c. Connect paddle with its shaft, rod and load cell. Pass threaded rod through reaction plate and then by stability plate. The top wire from
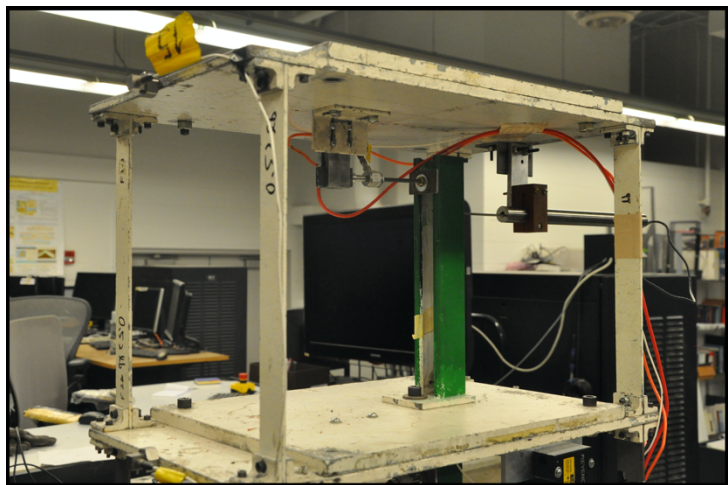
Figure 4.11. Aligned MR Damper on the Structure

the electromagnet goes into the black outlet of the Wonder Box and the bottom wire goes into the red outlet of the Wonder Box. The red wires in Figure 4.18 are the electromagnet wires.

d. Place paddle between parallel plates and tighten nuts on one side of the load cell and on one side of the reaction plate.

e. Follow alignment instructions as indicated in Section 4.2.2.

f. Connect electromagnet wires and Wonder Box and connect adapter to the Wonder Box input.

g. Turn Wonder Box knob to its full position (clockwise extreme) to ensure a constant output of around 11.6 V and 1 A. In the event when a variable current is desired from the Wonder Box, the Wonder Box should be connected to an external DC power supply using a BNC cable and the knob on the Wonder Box should be set to zero position (anticlockwise extreme). The external DC power supply thus can be used to vary the current passing through the Wonder Box.

h. Provide necessary displacement to the structure to limit damper displacement to 5 mm.

4.2.5   Safety Precautions

The following safety precautions are recommended to protect the MR damper from unexpected failures:

a. The Lord Rheonetic Wonder Box should not be left switched on for extended periods of time. The current supply and temperature of parallel plates and electromagnet might damage the components in the electromagnet. Ideally the Wonder Box should be switched off between sets of tests. Each set can be of around 10-15 minutes.

b. In the event of a variable current requirement, the Wonder Box can be supplied input current through a DC power supply in addition to the input from the power adapter. A DC power supply (as shown in Figure 4.12) available in the IISL is GW Instek GPR-30600. The current in

Figure 4.12. DC Power Supply

the Wonder Box can be varied using the DC power supply when the knob on the Wonder Box is set to zero (anticlockwise extreme).

4.3   Experimental Setup

A SDOF shear frame structure is constructed for the current study. The main components in the structure are composed of steel plates acting as lumped mass on each floor, steel plates of small thickness acting as columns, connector angles and nuts and bolts for joining columns to connector angles and thereby to steel plates. The experimental structure is modified to accommodate MR damper within the story. The sensors used for measurement of structural properties are accelerometers, force sensor (load cell), laser sensor and linear variable differential transformer (LVDT). The supporting equipment used for the experiments consists of a SO Analyzer System with a m+p VibPilot data acquisition system, power supplies and hydraulic actuators. The details on this supporting equipment along with the structural information and the sensors used are discussed in this section.

4.3.1   Structural Properties

The components of the experimental setup are described as follows,

a. ***Floor Lumped Mass*** –

A combination of steel plates is used as a lumped mass for each floor. A 15 in x 12 in plate has been placed over a 20 in x 12 in plate and is connected with nuts and bolts on four corners of the small plate. The thickness of the smaller plate is 0.52 in and that of larger plate is 0.36 in The average total combined mass of both small and large plate along with connector angles is 52 lb. In order to connect columns and angles to the shake table a base plate of dimensions 24 in x 12 in x 0.36 in is used. The remaining components are then connected above this base plate.

b. ***Connector angles*** –

Connector angles act as a medium to connect columns to steel plates on each floor. One leg of the connector angle is connected to the base plate and the other leg is connected to the column plate. The leg dimensions of the angle connecting columns are 1.32 in x 0.75 in while the dimensions for the leg connecting to the floor plate are 1.32 in x 1.03 in. The thickness of the

connector angle is 0.2 in. A total of two connector angles have been used to connect one end of each column on the floor. Therefore, a total of eight connector angles are used on one side of the floor mass to connect four ends of columns from the story opposite to that face. Thus, sixteen connector angles are required for the SDOF structure. Bolts with appropriate lock nuts are used for the interface between connector angles and other components. Each connector angle requires two sets of nuts and bolts to pass through the story mass. One set of nut and bolt is common between two connector angles to pass through the column between them. This set passes through the angle on one side, a column plate in between and then through the angle on the other side. The lock nuts are useful to prevent nuts from loosening up due to structural vibration.

c. *Column Plates* –

Column plates of dimensions 12 in x 1.25 in x 0.13 in are used between the story. The mass of each column plate is 0.52 lb. The effective unrestrained length of these columns after installing connector angles is 10.5 in A total of four plates are used as a column between each story. These columns are installed at four corners of the floor mass. Each column is connected to the connector angle with one set of nut and bolt on each end.

A SDOF drawing of the experimental setup is shown in Figure 4.13.

4.3.2   Sensors and Additional Mass

The sensors and additional mass associated with them are described in this section.

a. *Accelerometer* –

A PCB Model 333B40 piezoelectric accelerometer is used to measure vibrations resulting from structural response. A total of two accelerometers have been used for the SDOF experimental setup. The average sensitivity of accelerometer is ($\pm$ 10%) 500 mV/g. The peak measurement range of the accelerometer is $\pm$10g and each accelerometer weighs 0.26 oz (7.5 gm). The frequency range for operation of the accelerometer is ($\pm$ 5%) 0.5 to 3000 Hz. The sensing element used in the accelerometer is ceramic and a mounting magnet is used to install accelerometer on the structure. The mounting magnet has grooves on one side for the accelerometer and has a magnet on the other side to stick to the structure.
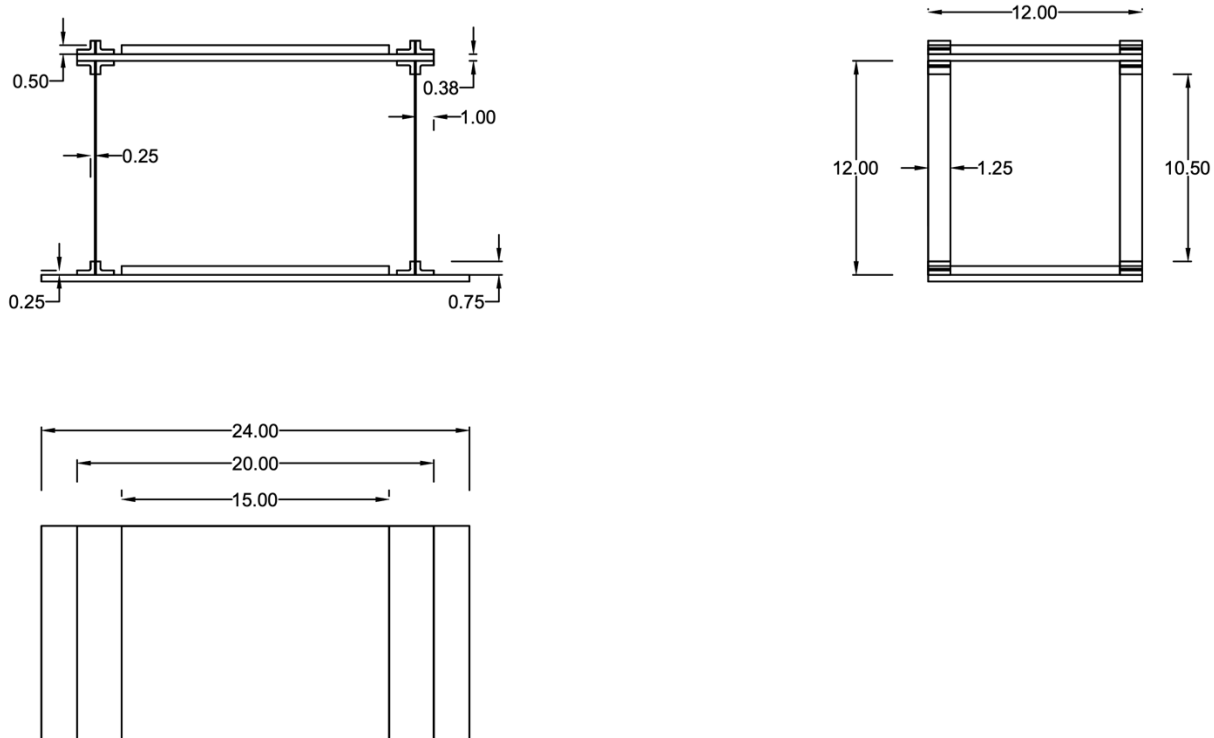
Figure 4.13. SDOF Setup

(All dimensions are in inches)

b. ***Force Sensor*** –

PCB ICP Model 208C02 and 208B01 are used as force sensors for the experiments. The measurement range for model 208C02 is 100 lb and the sensitivity is $\pm$ 50 mV/lb. The lower and upper frequency response limit for the force sensor are (-5%) 0.001 Hz and 36000 Hz respectively. The measurement range for model 208B01 sensor is 10 lb. and the average sensitivity is $\pm$ 500 mV/lb. Both sensors have a 10-32 female mounting thread. The model 208C02 sensor is used for the SDOF experimental structure. Figures 4.14 and 4.15 show accelerometer and force sensor installed on the structure.

c. ***LVDT*** –

Lucas-Schaevitz LVDT of range $\pm$ 1 in is used for the initial MR damper alignment experiments. The model number of the LVDT is DC-EC 1000 and the sensitivity is 10.381 V/in. The measurement range is $\pm$ 10 V. The LVDT is powered from an appropriate power

supply. The power supply has been described in Section 4.3.4. The LVDT is calibrated using a calibration tower by changing the LVDT displacement in increments of 1 in throughout its range.

Figure 4.14. PCB Accelerometer

Figure 4.15. PCB Force Sensor

d. *Laser Sensor* –

Keyence Laser Sensor model LK-G157 is used for displacement measurement on the structure. The measurement range for the sensor is $\pm$ 40 mm. The sensitivity of sensor is 2.494 V/cm and the internal sampling is set at 20kHz (50μs). The reference point for the sensor is set at 150 mm. The sensor is driven by a power supply and a control box, this is described further in Section 4.3.4. The Keyence laser sensor installed on the structure is shown in Figure 4.16.

Figure 4.16. Keyence Laser Sensor

4.3.3   MR Damper on Experimental Structure

The MR damper setup consisting of parallel plates, paddle, shaft, Wonder Box, tower, mounting angles etc. has been described in Section 4.2. The MR damper setup is installed between stories 0 and 1 for the experimental setup. The components of the MR damper consist of a thick paddle (1.496 in x 0.685 in x 0.222 in) and thin foam (0.037 in) The parallel plates are set at widest gap (0.302 in). The power adapter is 12 V/2 A (as shown in Figure 4.17) and the Wonder Box is numbered 1. In addition to this, it should be noted that the Wonder Box is supplied with input from a power adapter as well as a DC power supply for all set of tests. Figure 4.18 shows the setup for 1 MR damper SDOF. The total mass of the experimental setup with sensors and MR damper setup is tabulated in table 4.1.
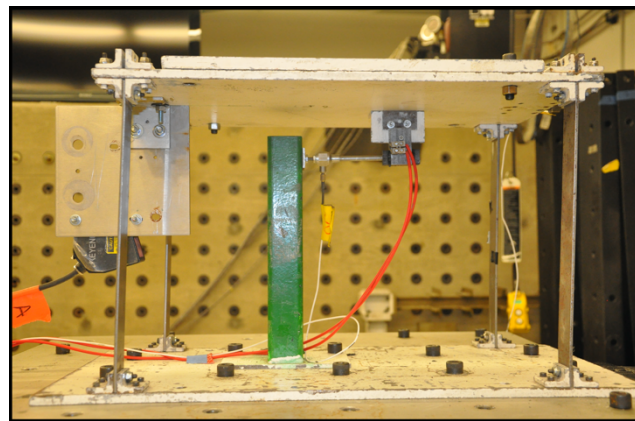

Figure 4.17. Power Adapter 1
(12V 2A)

Figure 4.18. 1 MR Damper SDOF Setup

Table 4.1. SDOF Total Mass

Story	Material	Mass (lb.)	Total Mass (lb.)
1	Columns (x 4)	2.08	59.71
	Floor Mass	52.29	
	Laser Sensor	0.62	
	Accelerometer (with Magnet)	0.07	
	Laser Plate	1.32	
	Laser Angle (with bolts)	0.28	
	Connector Angle Bolts (x 8)	0.08	
	MR Damper Parallel Plates	0.28	
	MR Damper Shaft (from plate to paddle)	0.19	
	MR Damper Angle	0.24	
	Mounting Tower	3.14	

4.3.4 Supporting Equipment

a. *SO Analyzer System with VibPilot acquisition state* –

A Smart Office (SO) Analyzer system consisting of 24-bit sigma-delta A/D converters uses analog anti-aliasing filters at 80 kHz. The digital anti-aliasing filters in the system are determined based on the sampling rate. An AC ground setting is set for piezo (PCB) sensors and a DC ground setting is set for DC sensors. The sampling rate is set at 4096 Hz for existing set of experiments. In addition to the output from sensors, the system also takes inputs from actuator displacement (internal LVDT of the actuator) and the command signal (Command voltage from the Shore-Western system).

b. *Hydraulic Actuator* –

The 6 DOF shake table consists of six Shore Western 1.1 kip 91-series double-ended hydraulic actuators. Figure 4.19 shows hydraulic actuators situated on one side of the shake table.

Figure 4.19. Hydraulic Actuators

c. *Keyence Power Supply* –

A Keyence Model MS2-H50 is used as a power supply for the laser sensor. The output current for the power supply is 2.1 A and the voltage is 24 V. The rated power is 50 W for this model.

d. *Keyence Control Box* –

A Keyence control box model LK-G3001 is used in conjunction with the power supply and the laser sensor. This separate controller is used to take raw input data from the sensor and give output voltage into the acquisition system. The data from the control box is analyzed in the VibPilot system. The Keyence power supply and control box are housed together using a flat plate at the back.

Figure 4.20 shows a m+p VibPilot data acquisition system for the test setup with inputs from different sensors and Figure 4.21 shows the Keyence Power Supply and Control Box.

Figure 4.20. VibPilot Acquisition System

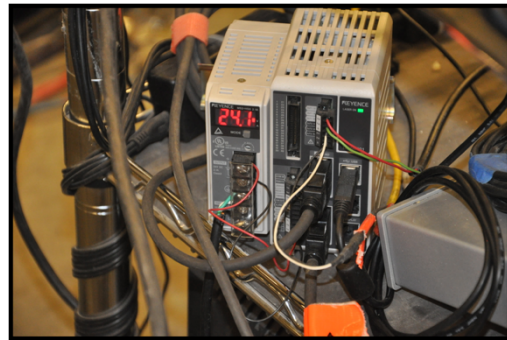Figure 4.21. Keyence Power Supply (Left) and Control Box (Right)

e. *LVDT Power Supply* –

The power supply used for the nonlinear device identification experiments is Measurement Technologies PSD-40-15. Two PSD-40-15 power supplies are encased in the hard-shell box and the input and output terminals are kept on the hard-shell box. The power supply setup enclosed in a hard case is shown in Figure 4.22.

f. ***Battery Backup and Surge Protector*** –

An appropriate extension box to power up the acquisition system and power supplies is used for the experiments. The extension box is equipped with a fuse to protect the equipment from unwanted surge in main current supply.

g. ***BNC Cable and Coaxial Cable*** –

A Bayonet Neill–Concelman (BNC) cable is used for DC ground setting equipment and sensors and
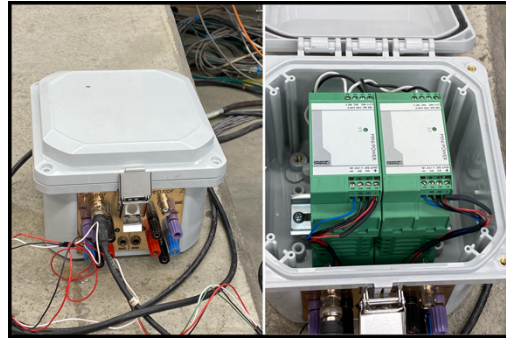
Figure 4.22. New LVDT Power Supply

a coaxial cable is used for AC ground setting equipment and sensors. The cables are connected to equipment and sensors on one end and the VibPilot system on the other. A BNC female splice adapter is used to extend short BNC cables.

4.3.5 Test Sets

A set of experiments are conducted for the SDOF structure with 1 MR damper between the story. The setup for these set of experiments along with the associated sensors are tabulated in Table 4.2. The SDOF structure with 1 MR damper is shown in Figure 4.23.

Table 4.2. SDOF Test Set with Sensors

Set	1
Setup	SDOF
Mode (without damper)	6 Hz
MR Damper	1 (Between base and story 1)
Accelerometers	PCB 333B40 (x 2)
Force Sensor	PCB 208C02
Displacement	Keyence LK-G157

111
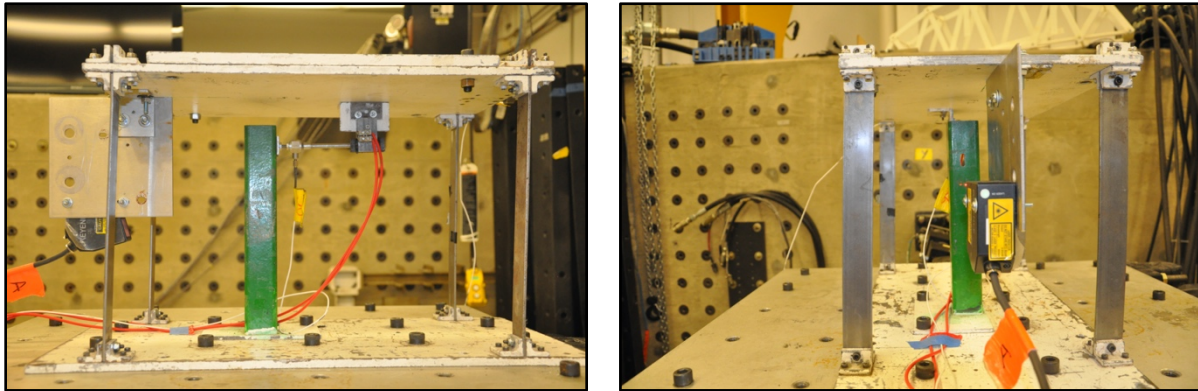
Figure 4.23. SDOF, 1 MR Damper

In addition to the above tests, two more sets of tests are performed initially. One set of tests is performed to assess functioning of the MR damper. The second set of tests are performed to make comparisons between the LVDT and the Keyence laser sensor. These comparison tests are performed on the SDOF setup with both laser sensor and a LVDT between the base and story 1. A MR damper nonlinear device identification experiment is shown in Figure 4.24. The setup for LVDT-Keyence tests is shown in Figure 4.25.

Figure 4.24. MR Damper Identification
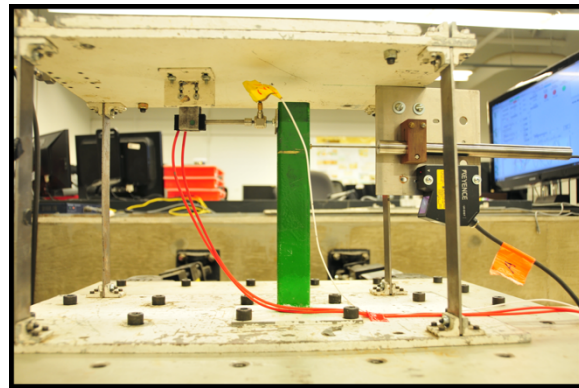
Figure 4.25. LVDT-Keyence Test Setup

4.4 Summary

The chapter on the experimental setup can be summarized as:

- A small-scale MR damper consists of primary and secondary components. The damper should be properly aligned (horizontal, vertical and twisting alignment) to get good results. (Section 4.2)

- The behavior of the MR damper depends on a set of variables (fluid, current, paddle displacement, foam and paddle thickness). The hysteresis loop of the damper is affected drastically if the variables are too high or too low. (Section 4.2)

- It is important to follow safety precautions for the MR damper due to its sensitive parts. (Section 4.2)

- A shear frame experimental setup of SDOF is constructed for identification tests with MR damper. (Section 4.3)

- The MR damper is installed between stories 0 and 1 for SDOF experimental tests. (Section 4.3)

5. MODEL SELECTION AND COMPARISON

5.1   Introduction

The experimental setup described in Chapter 4 is subjected to different input excitation signals. In this chapter, the model selection process and the state and parameter estimation is performed on the experimental data with the UKF identification algorithm using measurements from displacement and acceleration sensors. The training and validation for this process are identified in Sections 5.3 and 5.4. The MSE with respect to displacement and acceleration is calculated for the validated signals in Section 5.4. The candidate model with the lowest MSE for each validation signal is identified and the parameters of the most appropriate model are identified in Section 5.5. As in the numerical implementation in Chapter 3, a comparison of error in force with respect to time and displacement is made for the models with the lowest MSE.

5.2   Input Signals

The input excitation signals selected for the experimental structure are such that they produce sufficient excitation for all parameters in the SDOF MR damper setup. These set of input signals are shown in Table 5.1. For each of the input signals mentioned in Table 5.1., the signals were varied with respect to amplitude A_{max}, frequency f_{max} and the scale S in the first set of preliminary experimental tests. These variations in signal properties helped to find the most appropriate values of the signal that give a substantial structural response for the UKF identification. These variations also help to observe structural response and discard any input signal that either does not produce a good hysteresis response, or is too large to permanently damage the current shear frame experimental structure. In addition, any problems arising from initial MR damper alignment are averted due to the preliminary observation performed for the signal and structural response. Finally, the experimental structure is subjected to the input excitations for signals with properties in Table 5.1. Two sets of structural response are recorded for each input signal to account for any problems arising from error in data acquisition system or the shake table input.
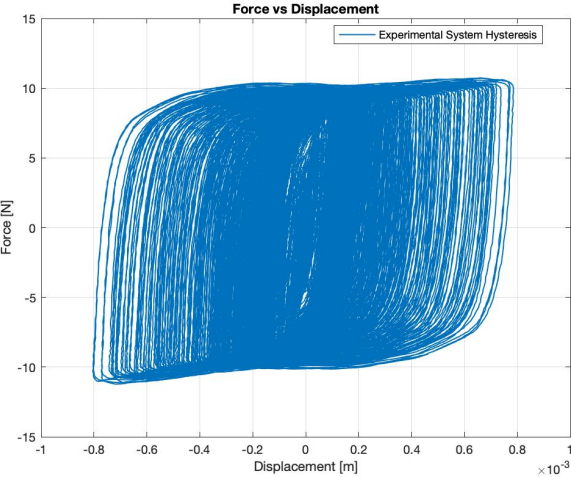
Table 5.1. Experiment Input Signals

| Input Signal Type	Mathematical Description of Input Displacement		Signal #	A_{max} [mm]	f_{max} [Hz]	T [sec]	S [--]
BLWN	$x_g = \text{lowPassFilter}(r, F)$	$r_{1xT} \sim N(0, A^2)$	I	3	20	40	--
Amp Sweep Up-Down	$x_g = \begin{cases} A\sin(\pi t^2 F/T) \\ A\sin(\pi t\, F[2T - t]/T) \end{cases}$	$\begin{array}{l} t < T \\ T \leq t < 2T \end{array}$	II	2	4	40	--
Earth-quake	$x_g = A \cdot ElCentro(Sk \cdot \Delta t)$	$k = 1,2,\dots,T$	III	0.1	--	42	0.4
	$x_g = A \cdot Kobe(Sk \cdot \Delta t)$	$k = 1,2,\dots,T$	IV	0.1	--	51	0.4
Step	$x_g = \begin{cases} (A/T)t, & t < T \\ A, & T \leq t \end{cases}$	$\begin{array}{l} t < T \\ T \leq t \end{array}$	V	10	--	0.1	--
Amp Sweep Up	$x_g = A\sin(\pi t^2 F/T)$	$t \leq T$	VI	2	4	40	--
Freq Sweep Up	$x_g = A\sin(\pi t^2 F/T)$	$t \leq T$	VII	0.75	20	40	--
Freq Sweep Up-Down	$x_g = \begin{cases} A\sin(\pi t^2 F/T) \\ A\sin(\pi t\, F[2T - t]/T) \end{cases}$	$\begin{array}{l} t < T \\ T \leq t < 2T \end{array}$	VIII	0.5	20	40	--

The initial observations made from the MR damper hysteresis loops revealed that the damper shows two very different behaviors. For structural displacements that are less than 2 mm one behavior is observed, and for displacements more than 2 mm another behavior is observed. Here the focus is on the tractable behavior of the MR damper observed for structural displacements of more than 2 mm. A comparison of the behavior of MR damper for displacements of less than 2 mm and more than 2 mm is made in Figure 5.1. The MR damper exhibits a displacement of less than 2 mm for input signal VIII and a displacement of more than 2 mm for input signal II.

The change in behavior of this shear mode MR damper for displacements less than 2 mm can be mainly attributed to properties of the paddle and the damper fluid. For small displacements ($\leq 2\ mm$), the point of contact of fluid particles with the paddle and parallel plates remains same. The displacement is only observed due to a small relative drift of these particles between the two contact surfaces. This behavior is in contrast to the behavior of the damper for large displacements

($\geq 2\,mm$) where the higher displacement is the result of overall paddle movement between parallel plates. Therefore, the properties of mechanical models of the MR damper would change for this behavior at small displacements. The models defined earlier in Chapter 3 do not account for these small variations in MR damper properties. Hence, the current study only focuses on the model selection process for MR damper with large displacements. Figure 5.2 shows the acceleration time history measured from the accelerometer installed on the shake table. The time histories are plotted only for input signals producing displacement of more than 2 mm in the experimental structure. These signals will further be discussed for training and validation in the Sections 5.3 and 5.4.
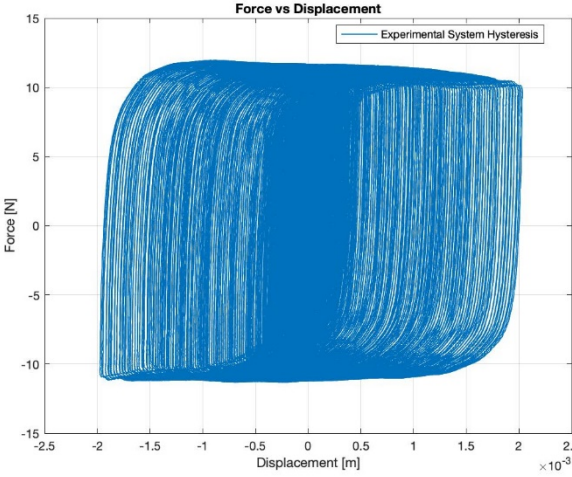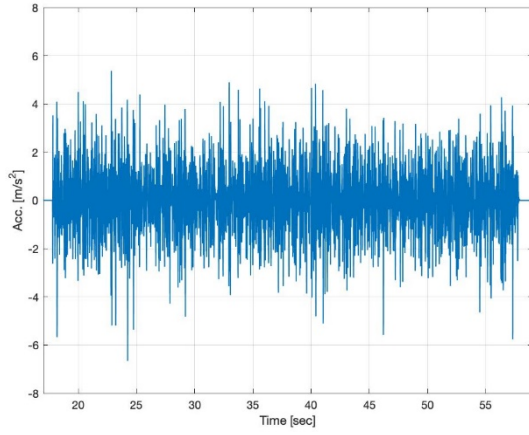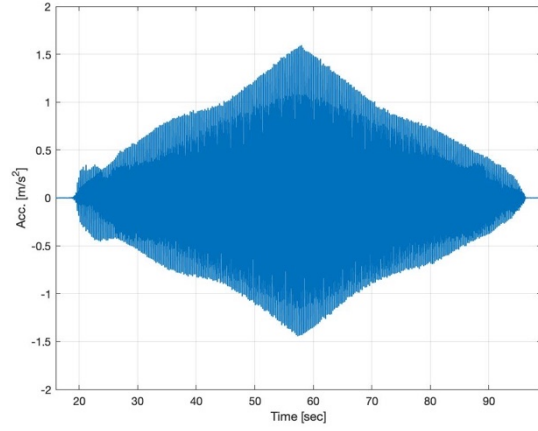

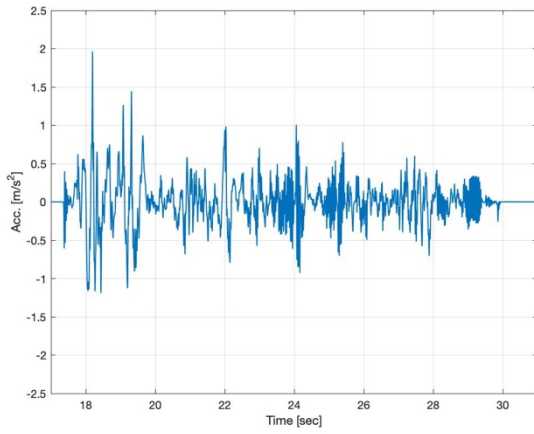Input Signal VIII   Input Signal II

Figure 5.1. Comparison of MR Damper Behavior for Different Displacements
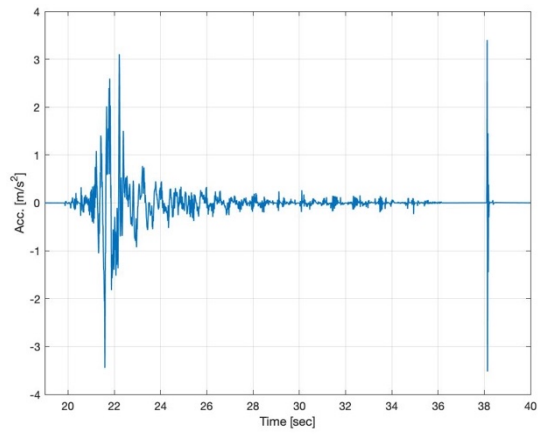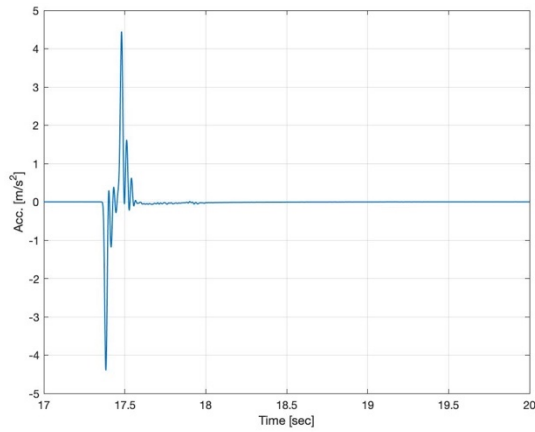
Input Signal I

Input Signal II

Input Signal III

Input Signal IV

Input Signal V

Figure 5.2. Experimental Input Signals

5.3 Model Training

The training of MR damper models is performed in a similar way as performed in Chapter 3. 100 prior distributions on MR damper parameters are taken by taking 10 sets of LHSs and 10 samples of the indices of dispersion on covariances for each LHS. The indices of dispersion from Equation 3-43 are used for model training using experimental signals in this section. 10 sets of LHSs for each mechanical model are prepared by first finding an approximate set of parameters of the model for which the computational model produces results similar to the experiments. The LHS samples are then prepared in a range close to these approximate values. This preliminary work of first finding the approximate range of parameters and then preparing the LHS helps to keep the UKF estimation closer to the true values and gets estimation results quicker. The LHS samples can also be prepared without finding the initial range but, the UKF estimates might diverge from true values if the initial distribution is too far from true values (in orders higher than those of true values). The number of LHS samples can also be increased from 10 to get higher number of trained candidate models. A preliminary study with a higher number of LHS samples indicated that only slight improvement in the accuracy of the results was obtained with a very high computational time in training and validation for each model. It was found that the UKF estimates for 10 LHS samples remain very close to the results obtained with a higher number of LHS samples. This behavior can be mostly attributed to the convergence property of LHS. Fewer LHS samples still produce a good distribution of candidate models and help in convergence to the final estimated values quicker. Thus, in this work the mechanical models are trained using 10 LHS samples at a high computational efficiency without compromising the accuracy of results.

The UKF identification in the current study is performed using measurements from displacement and acceleration sensors. Therefore, the UKF estimation for displacement and acceleration is expected to be close to the true experimental states. However, the algorithm might sometimes underestimate or overestimate the force response. These estimations can be further refined by including the true force response in the training process. For the current study, the model training is only performed using displacement and acceleration measurements. The results from this study help to assess the quality of UKF estimations in the absence of measurements from one of the states. Thus, this study can be further extrapolated to the real-life scenarios where measurements are missing for some of the states.

The preliminary analysis using UKF revealed that good UKF estimates may be obtained for training performed using either signals I or III. Furthermore, the displacement and acceleration estimations remain consistent with all models for training performed using signal I. Therefore, UKF model selection algorithm is performed using displacement and acceleration measurements from this signal. Realistic process and measurement noise covariance values are incorporated into the identification algorithm by taking standard deviation of measurements recorded for a 'NoInput-Hydraulic' test. In this test, the sensors and hydraulic actuators are kept running for 60 seconds without sending any input to the actuators. The inherent sensor measurement noise and actuator process noise is thus recorded and used for the UKF estimation algorithm. To reduce computational time for training, the input signals for training and validation are trimmed and only the portion of the signal with the acceleration input is used. This trimming of signals also helps to start UKF estimation only when the actual input signal is present. The part of the signal before or after the input signal (where there is no excitation, merely noise) is not used for the estimation and hence, quicker convergence to final estimated values is expected from the algorithm. Table 5.2 shows the number of trained candidate models obtained for each mechanical model of the MR damper after training with signal I. It is observed that the modified Dahl model has the highest number of trained candidate models and has lower convergence issues with the UKF algorithm. The modified LuGre model seems to have the highest number of candidate models discarded due to converge problems and badly conditioned matrices.

Figures 5.3, 5.4 and 5.5 show the distribution of parameters for the trained candidate normalized Bouc-Wen, modified Dahl and modified LuGre models, respectively. It is observed that a majority of the parameter values of these trained candidate models remain close to each other in a narrow range. These distributions are a good indication to find the range of structural and individual mechanical damper properties. It is observed that the structural damping, c, remains close to $100\ N.s/m$ and the stiffness coefficient, k, remains close to $25000\ N/m$. It should be noted that the trained models shown in Tables 5.2 and in Figures 5.3, 5.4 and 5.5 are for candidate models with values of damping coefficient, c, ranging between 10 and $1000\ N.s/m$. The damping coefficient, c, for the current structure remains between these values and hence, any candidate models with c out of this range should be discarded. For the current mechanical models, it is observed that this filter does not remove any of the potential trained candidate models. Only the

119

models with convergence issues that failed in training are removed with this filter of keeping c between the limits.

Table 5.2. Trained MR Damper Models

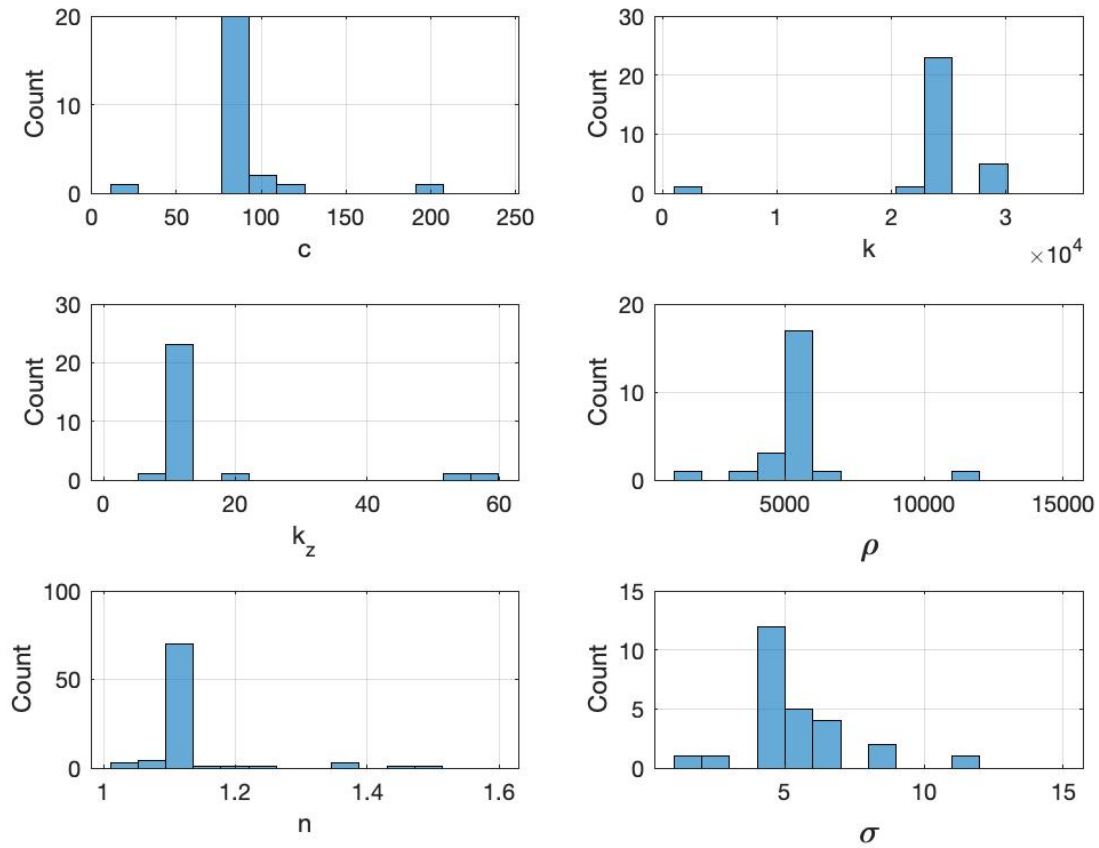| Model	Total Trained Models (out of 100)
Normalized Bouc-Wen	31
Modified Dahl	64
Modified LuGre	12

Figure 5.3. Distribution of Normalized Bouc-Wen Candidate Models for Training with Signal I
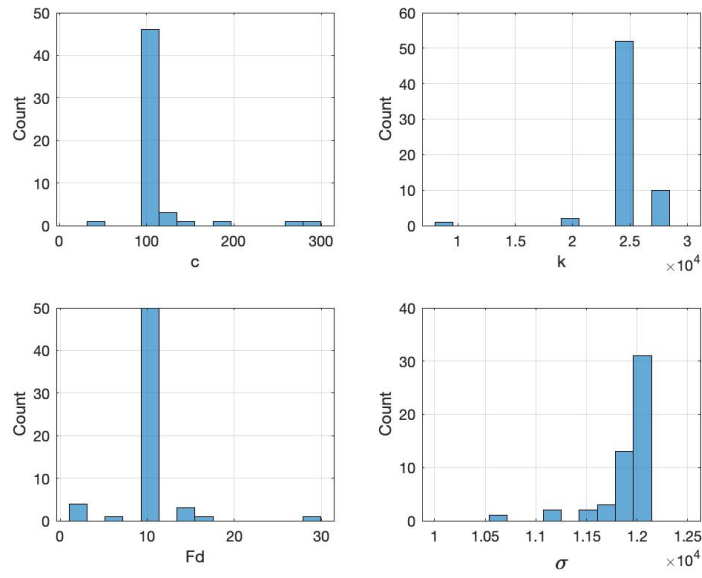
Figure 5.4. Distribution of Modified Dahl Candidate Models for
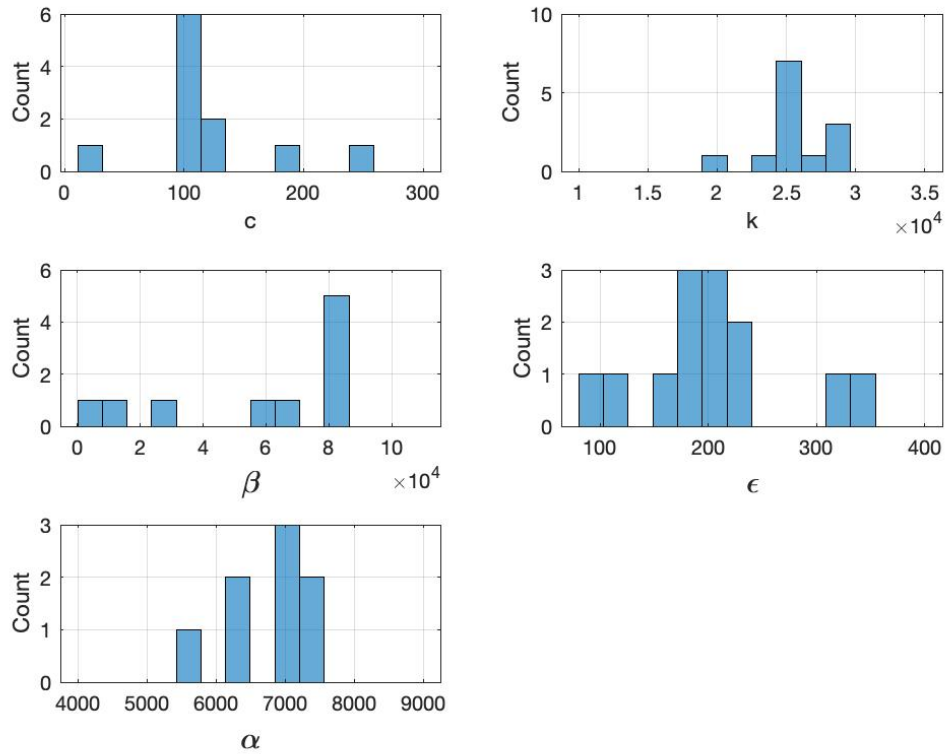Training with Signal I

Figure 5.5. Distribution of Modified LuGre Candidate Models for Training with Signal I

5.4   Model Validation

In this section, the trained candidate MR damper models are validated using both methods 1 and 2 as performed in Chapter 3. The results from method 1 will be useful for scenarios with limited availability of data and the results from method 2 will be useful for scenarios where data is available for multiple forms of input signal. The validation is performed using signal I for method 1 in Section 5.4.1. This step is followed by a validation performed by other signals in Section 5.4.2. The best candidate MR damper model is chosen in each section based on the lowest MSE. The force errors with respect to time and displacement for models with the lowest MSE are also compared in each subsection.

5.4.1   Method 1

The method 1 of model selection comprises of training and validating the model with the same signal. Thus, in this section, the model trained with response from signal I in Section 5.3 is validated using the same structural response. The best candidate model obtained for each mechanical form of the model is given as follows.

a.   *Normalized Bouc-Wen Model*

The best candidate normalized Bouc-Wen model is obtained by validating 31 trained candidate models with signal I from the previous section. The results of this best model are shown in Figures 5.6, 5.7 and 5.8. The contribution of different components of the force towards total force in the system is shown in Figure 5.6. The contribution of maximum hysteretic force remains constant throughout the length of the signal. Figure 5.7 shows the estimated force-displacement hysteresis loop of this model. It is observed that the model underestimates the actual maximum force in the system. A difference of around 2 N for the maximum force in compression and tension is observed for this model. The displacement response however, remains close to the actual structural response. Figure 5.8 shows the estimated displacement, velocity and acceleration response when compared to the original response. Windows a, b and c for each of these responses are provided on the side to compare the displacement, velocity and acceleration response from 35 to 37 seconds. The experimental velocity in these plots is calculated by differentiating the experimental displacement with respect to time using Newton's forward difference formula. The UKF algorithm estimates the

displacement, velocity and acceleration response well. The underestimated force from this model is still under acceptable limits as only displacement and acceleration responses were used for training of the model.
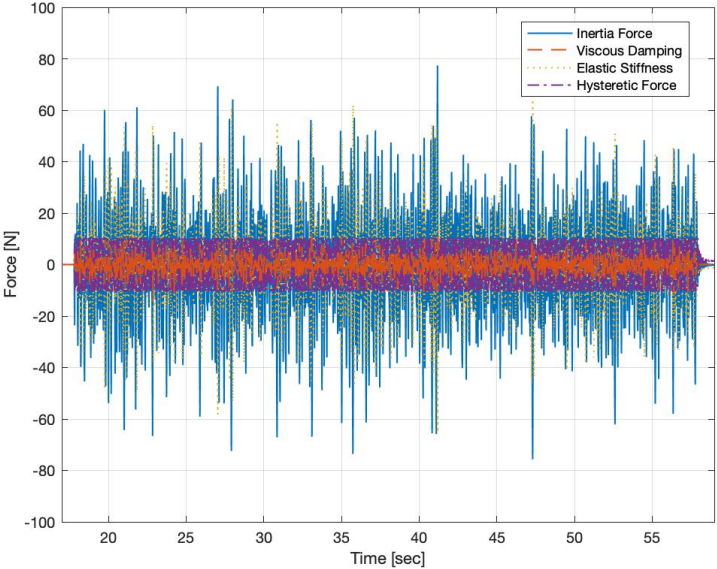

Figure 5.6. Force Contribution in Method 1 for Normalized Bouc-Wen Model with the Lowest MSE Trained using Signal I
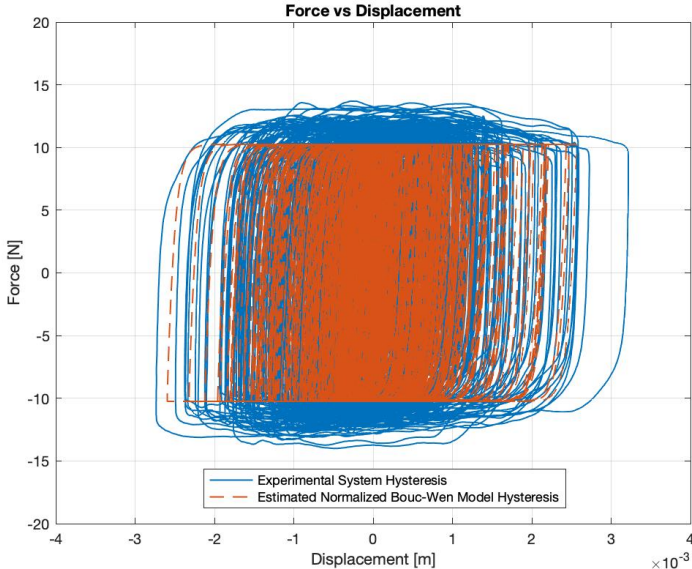

Figure 5.7. Comparison of Hysteresis Loops in Method 1 for Normalized Bouc-Wen Model with the Lowest MSE Trained using Signal I
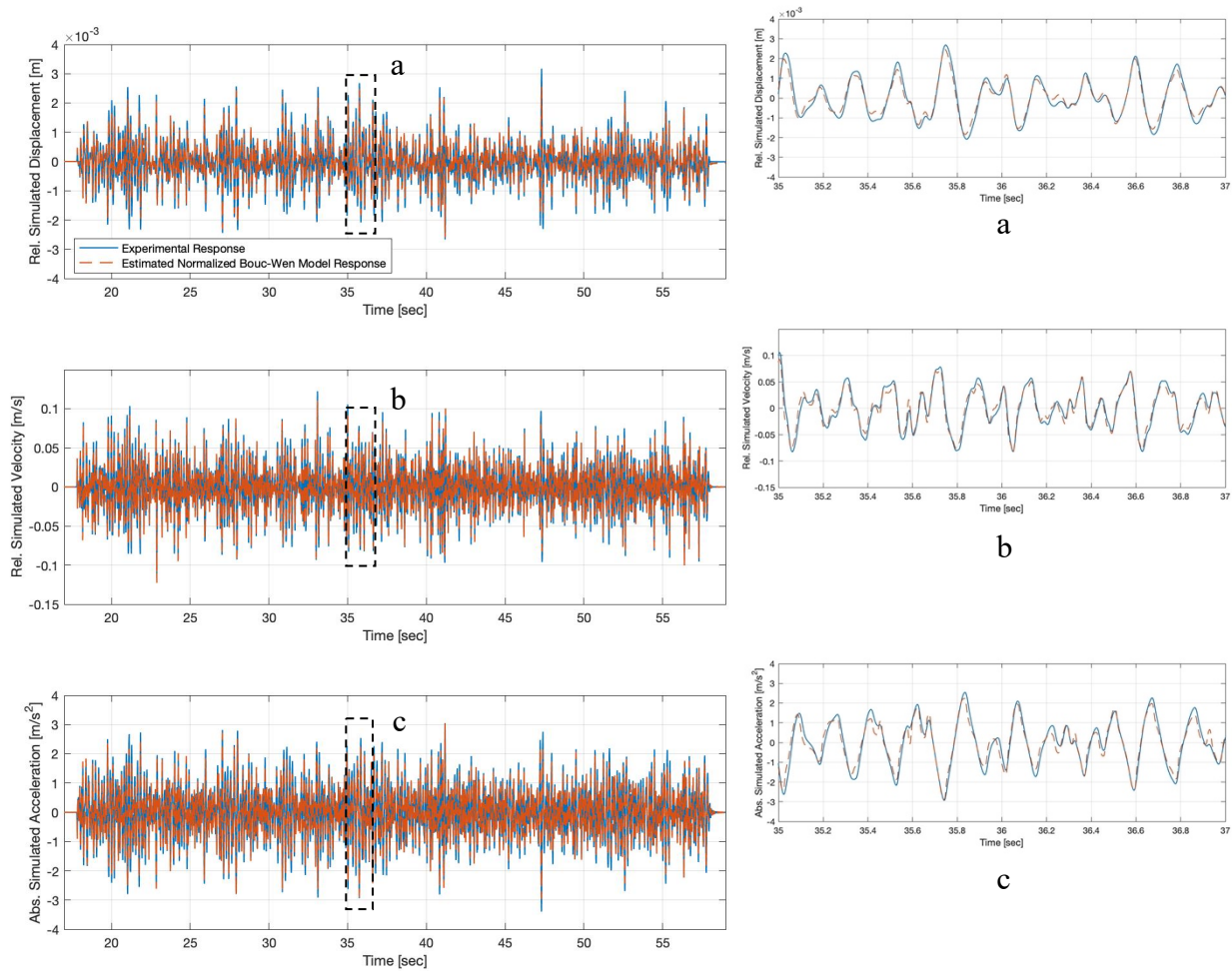
Figure 5.8. Comparison of State Estimates in Method 1 for Normalized Bouc-Wen Model with the Lowest MSE Trained using Signal I

b. *Modified Dahl Model*

Figures 5.9, 5.10 and 5.11 show the response of the modified Dahl model with the lowest MSE. The contribution of force towards total force in the system is shown in Figure 5.9. A constant maximum contribution towards the total force in the system is observed. This model also underestimates the maximum experimental force in the system by around 2 N. This is shown in the force-displacement hysteresis response in Figure 5.10. Windows a, b and c of Figure 5.11 indicate that the model does a great job in estimating the actual structural displacement, velocity and acceleration response.
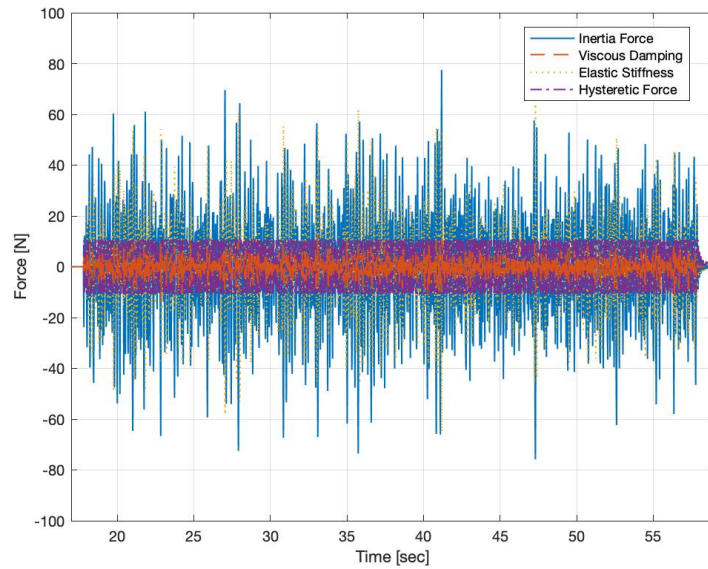
Figure 5.9. Force Contribution in Method 1 for Modified Dahl
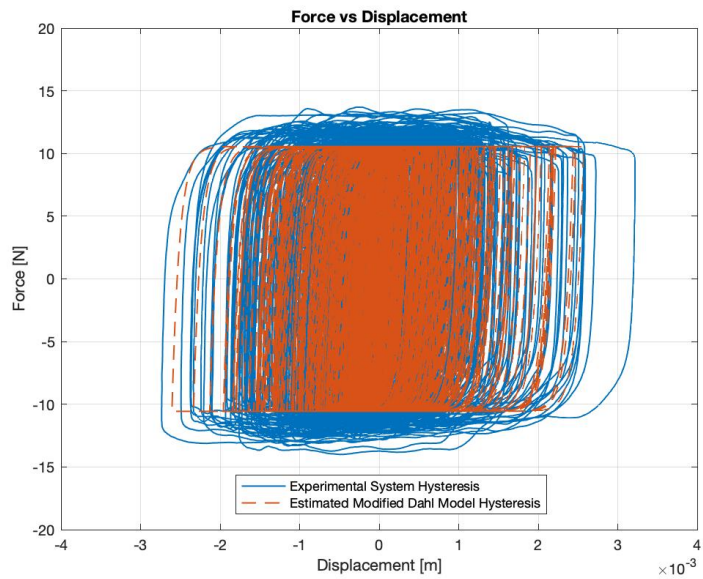Model with the Lowest MSE Trained using Signal I

Figure 5.10. Comparison of Hysteresis Loops in Method 1 for
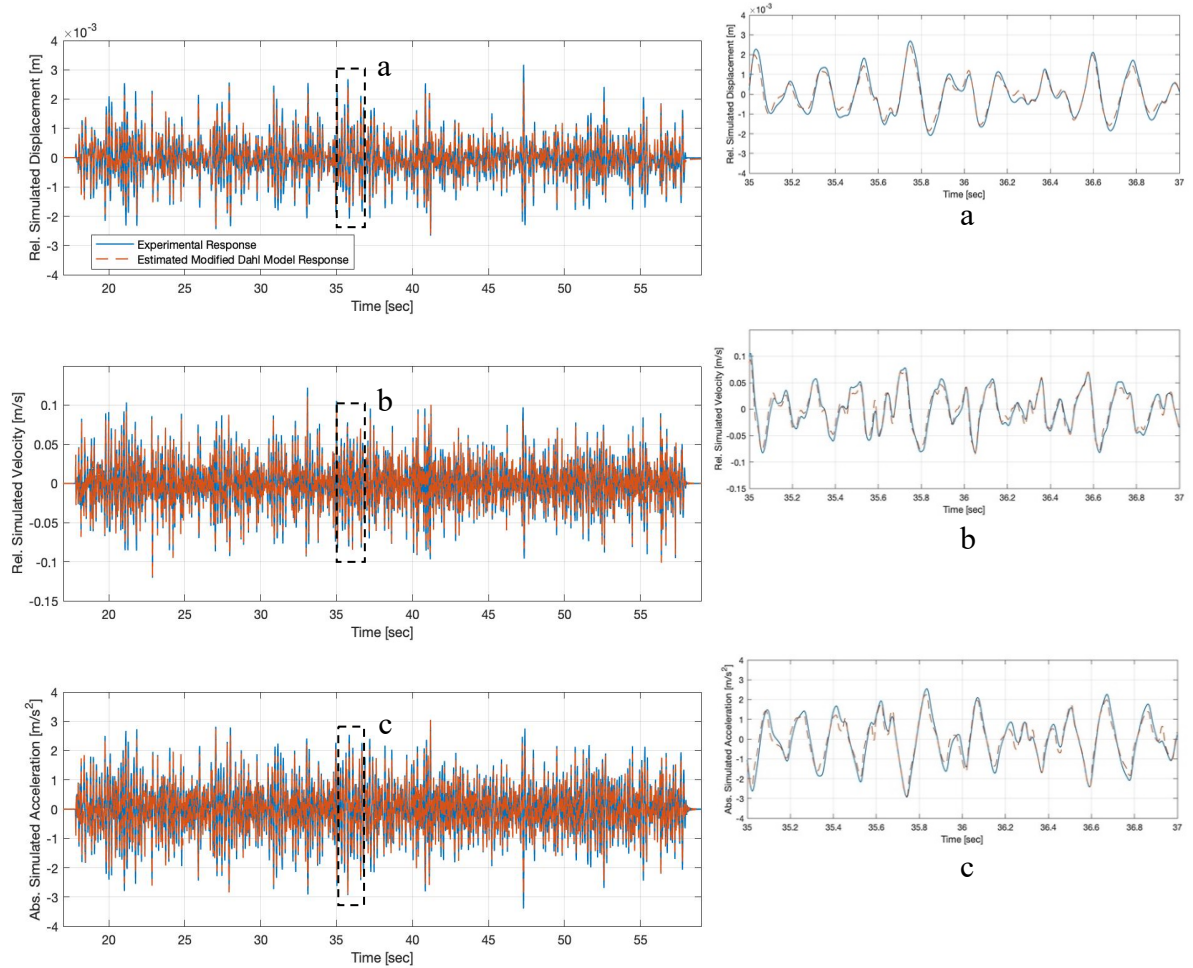Modified Dahl Model with the Lowest MSE Trained using Signal I

Figure 5.11. Comparison of State Estimates in Method 1 for Modified Dahl Model
with the Lowest MSE Trained using Signal I

c. *Modified LuGre Model*

The contribution of hysteretic force towards total force in the system is shown in Figure 5.12. The initial observation on force-displacement hysteresis estimate in Figure 5.13 shows that the modified LuGre model with the lowest MSE is closer to the actual force in the system. The difference in this estimated force from the maximum experimental force remains lower than 2 N for most part of the response. The displacement, velocity and acceleration response of this model in windows a, b and c of Figure 5.14 for time interval from 35 to 37 seconds reveal that the UKF estimates are close to the true value of these responses.
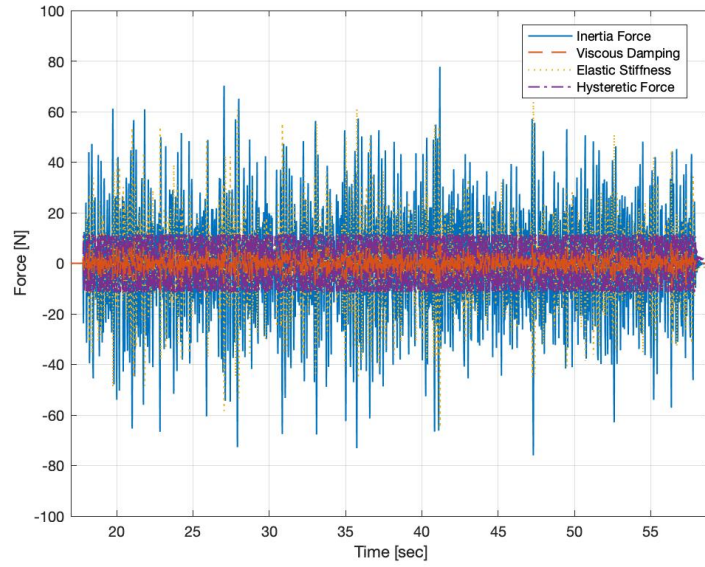
Figure 5.12. Force Contribution in Method 1 for Modified LuGre
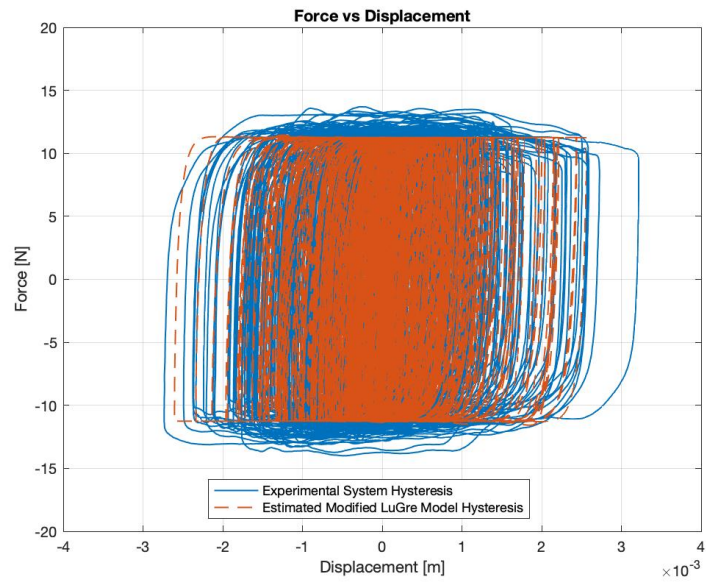Model with the Lowest MSE Trained using Signal I

Figure 5.13. Comparison of Hysteresis Loops in Method 1 for
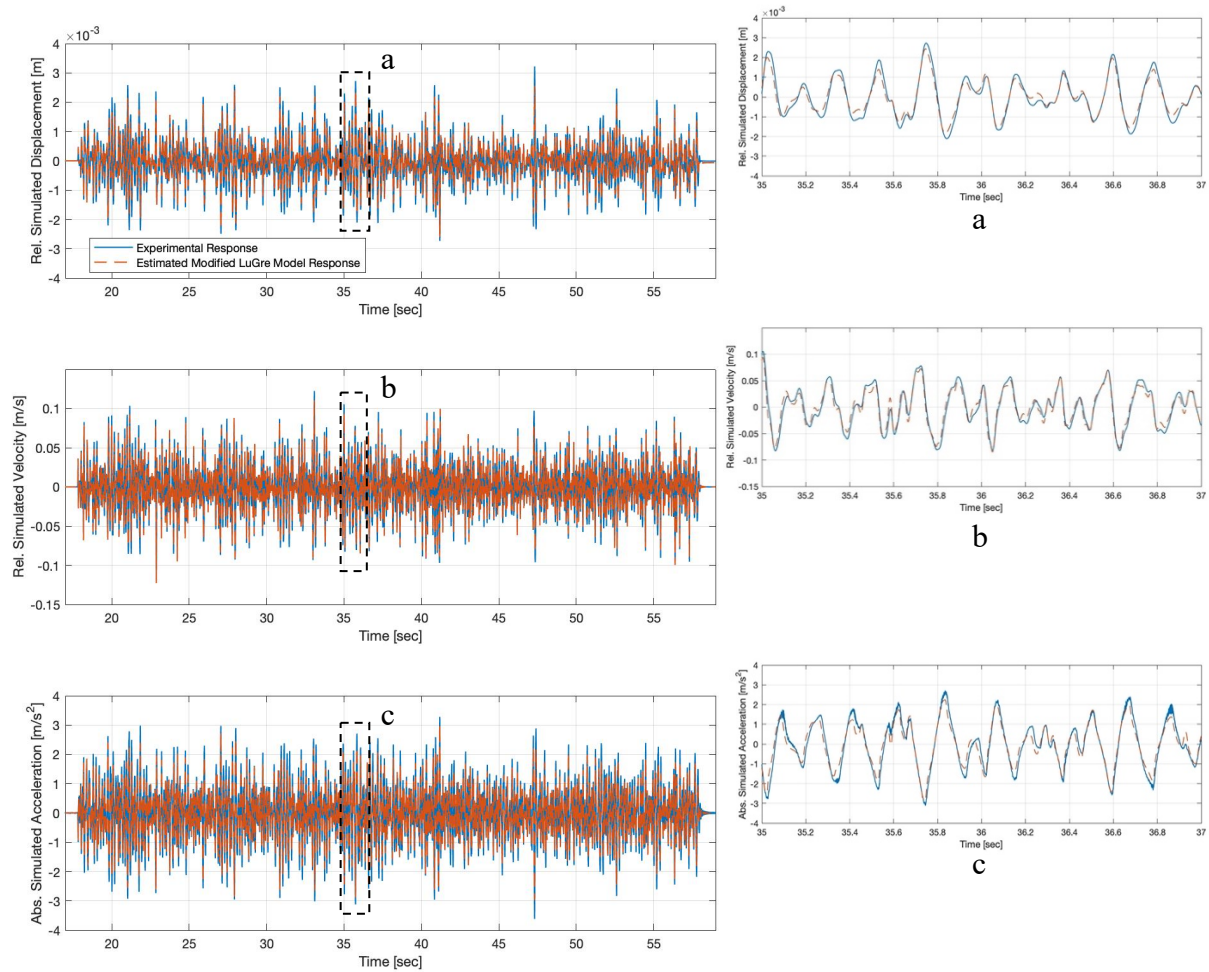Modified LuGre Model with the Lowest MSE Trained using Signal I

Figure 5.14. Comparison of State Estimates in Method 1 for Modified LuGre Model with the Lowest MSE Trained using Signal I

5.4.2 Method 2

For method 2, the candidate models trained using signal I can be validated by using any of the other signals mentioned in Table 5.1. The validation performed by each of these signals gives the required lowest MSE and force errors for model comparison and selection. Thus, each validation signal can lead to a model with the lowest MSE. The most appropriate model based on the lowest MSE can be same or different between these validation signals. The selection of the overall best model in the present study becomes difficult if the best model is different between the validation signals. Therefore, the validation process for method 2 is only performed using one signal from Table 5.1. The parameters of the model with the lowest MSE for each mechanical form of the model are then used to predict the displacement, velocity and acceleration response for other

signals. An initial preliminary study indicated that a good force-displacement hysteresis response was observed for models validated using signal II. Therefore, the candidate models trained using signal I are validated with signal II in this section. The model with the lowest MSE is then selected for each mechanical form of the model and is shown next. In addition, these parameters of the best model are then used to estimate displacement, velocity, acceleration and force response for excitation signals III, IV and V. These figures are added in the Appendix of the thesis.

a. *Normalized Bouc-Wen Model*

The response of the normalized Bouc-Wen model with the lowest MSE for training with signal I and validation with signal II is shown in Figures 5.15, 5.16 and 5.17. The contribution of force from the model towards total force in the system is shown in Figure 5.15. The contribution of maximum hysteresis force remains constant for the major part of the input signal. The estimation of force-displacement hysteresis loop in Figure 5.16 shows that the model again underestimates the actual maximum force in the system by a small value. Figure 5.17 shows the displacement, velocity and acceleration estimates of the model. A small deviation from these responses is observed for 5-6 seconds near 40 and 75 seconds in the time history. The overall estimates however, remain close to the actual structural response.
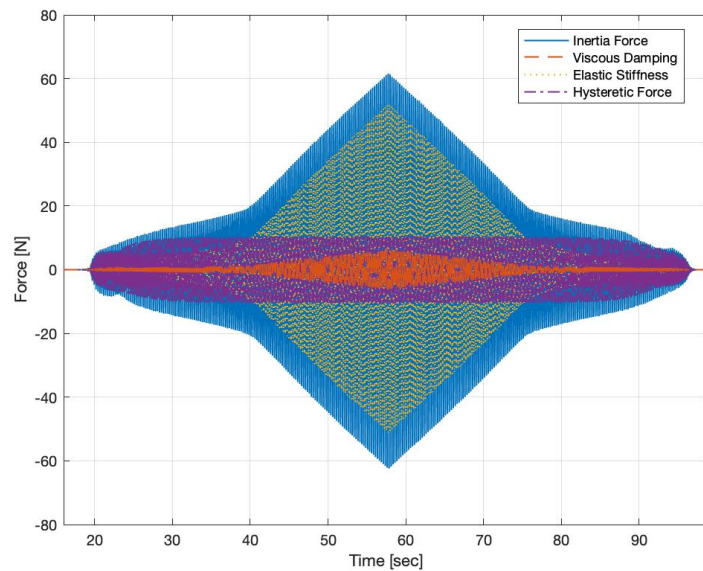

Figure 5.15. Force Contribution in Method 2 for Normalized
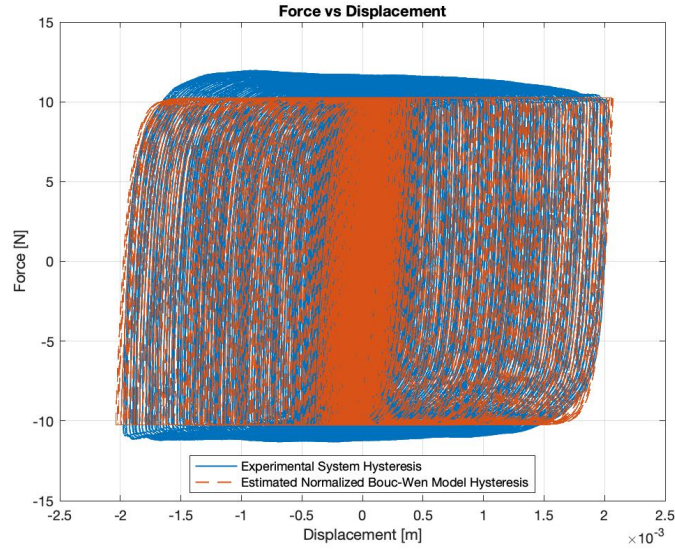Bouc-Wen Model with the Lowest MSE Trained using Signal I

Figure 5.16. Comparison of Hysteresis Loops in Method 2 for Normalized
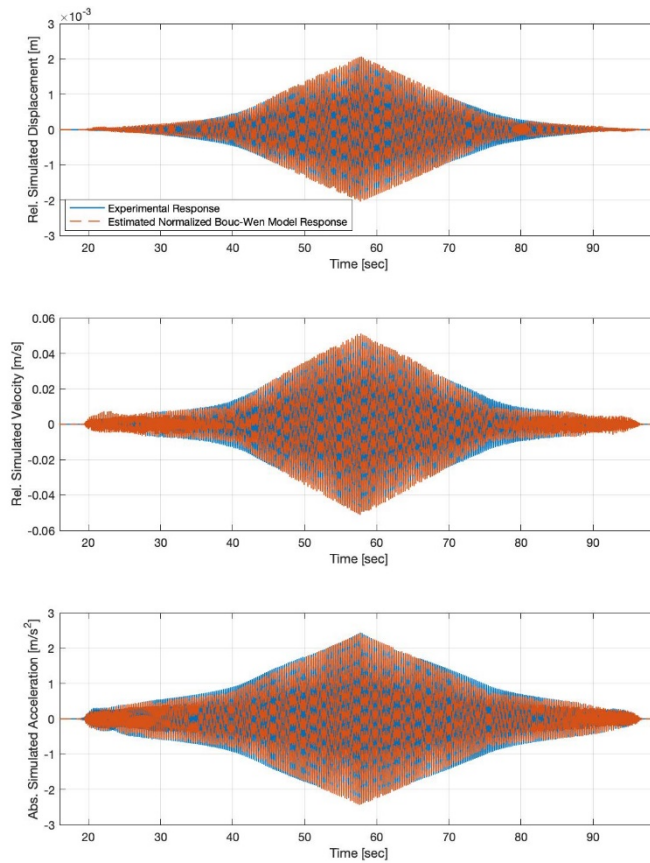Bouc-Wen Model with the Lowest MSE Trained using Signal I

Figure 5.17. Comparison of State Estimates in Method 2 for Normalized
Bouc-Wen Model with the Lowest MSE Trained using Signal I

b. *Modified Dahl Model*

The contribution of hysteresis force towards total force in the system for the modified Dahl model with the lowest MSE is shown in Figure 5.18. Figure 5.19 shows the estimated force-displacement hysteresis loop of the model. The estimated force remains very close to the actual force near the positive side of the displacement. A small underestimation in the force is observed near the negative side of the displacement. This difference still remains within an acceptable limit considering only displacement and acceleration responses were used for model training. The displacement, velocity and acceleration response are shown in Figure 5.20. A slight underestimation in acceleration response is observed for this model.

Figure 5.18. Force Contribution in Method 2 for Modified Dahl
Model with the Lowest MSE Trained using Signal I

131

Figure 5.19. Comparison of Hysteresis Loops in Method 2 for
Modified Dahl Model with the Lowest MSE Trained using Signal I

Figure 5.20. Comparison of State Estimates in Method 2 for Modified
Dahl Model with the Lowest MSE Trained using Signal I

c. *Modified LuGre Model*

Figure 5.21 shows the contribution of hysteretic force for modified LuGre model with the lowest MSE towards the total force in the system. The force-displacement hysteresis response is shown in Figure 5.22. The estimated force for the model remains very close to the true force in the system. A maximum difference of around 1 N is observed for the positive side of the force with negative displacement. An initial comparison with other models suggests that the overall force estimate of this model is one of the closest to the true value in the system. The displacement, velocity and acceleration response of the model is shown Figure 5.23. A slight underestimation in acceleration response is observed over the length of the input signal. The displacement and velocity estimates remain very close to the true structural response.
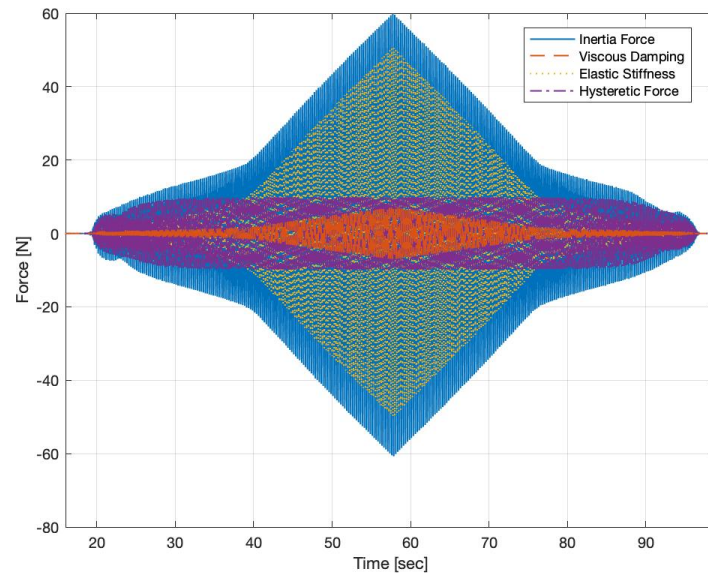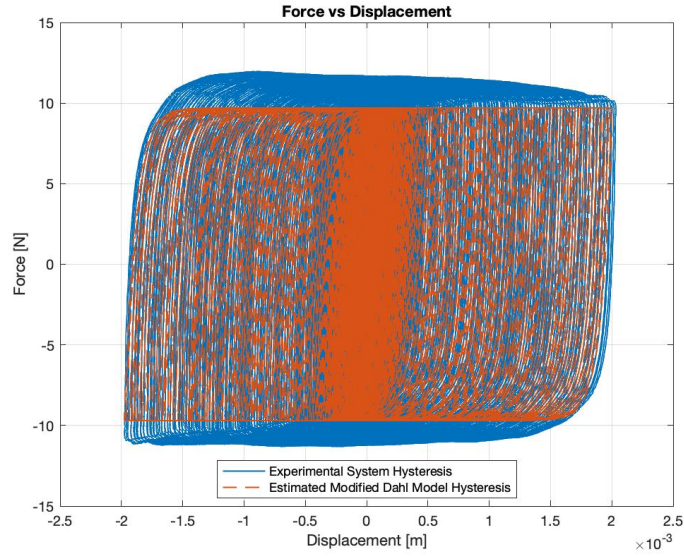

Figure 5.21. Force Contribution in Method 2 for Modified
LuGre Model with the Lowest MSE Trained using Signal I

Figure 5.22. Comparison of Hysteresis Loops in Method 2 for
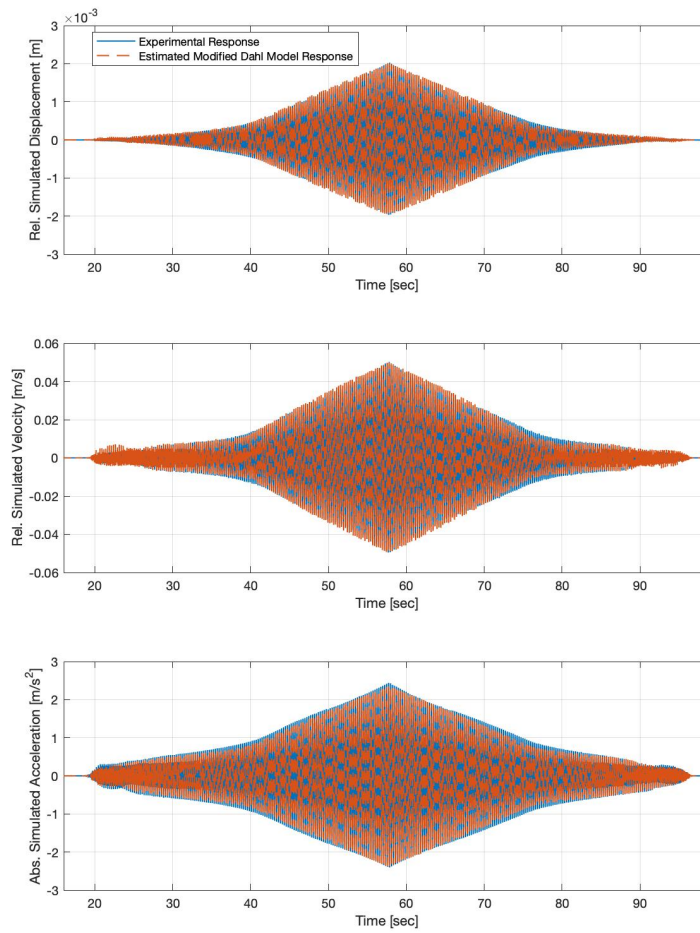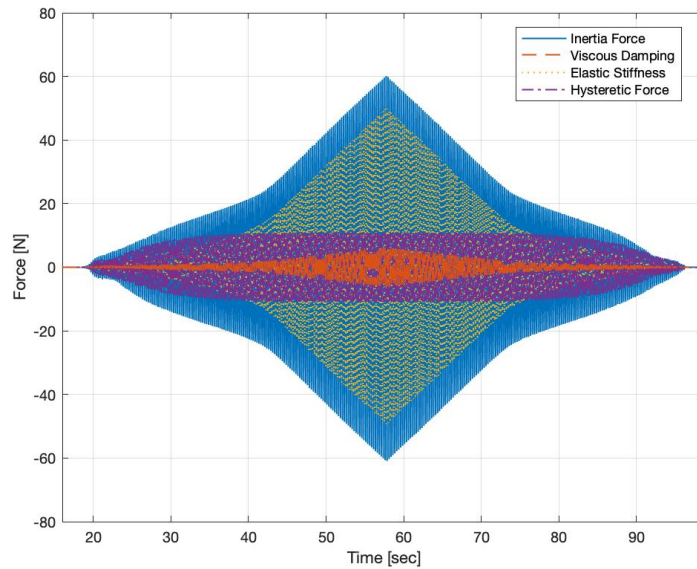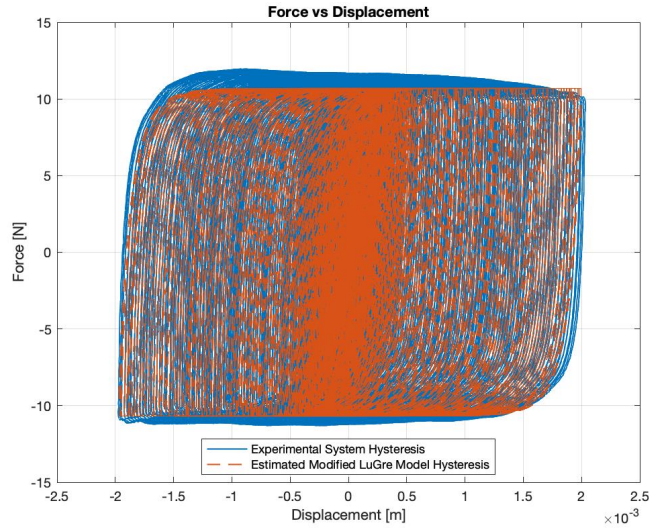Modified LuGre Model with the Lowest MSE Trained using Signal I
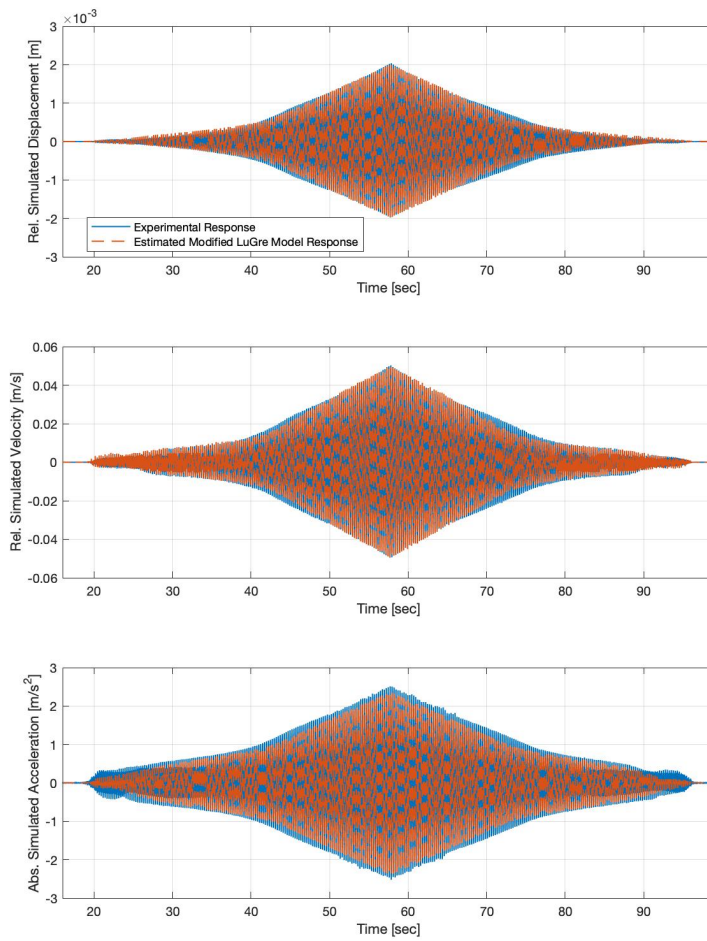

Figure 5.23. Comparison of State Estimates in Method 2 for Modified
LuGre Model with the Lowest MSE Trained using Signal I

5.5   Model Selection

The basis for model selection and comparison remains similar to the numerical model selection performed in Chapter 3. A candidate model with the lowest MSE for each of the mechanical forms is selected from the validation step. The three models are then compared to each other to select the overall best model based on the lowest MSE. This procedure is performed with both methods 1 and 2 and thus, two models are obtained individually for these methods. The efficiency of UKF estimates in method 1 plays an important role for real-life scenarios where the structural response is only available for one signal (for example, an earthquake). The results from method 1 thus help to understand the behavior of UKF for training and validation with only one signal.

Tables 5.3 shows the parameters of the best normalized Bouc-Wen model obtained from methods 1 and 2. It is observed that the model parameters remain same and a single model provides results with the lowest MSE for both methods. The damping, c, of this model is $117.59\ N \cdot s/m$ and the stiffness, k, is estimated to be $25090\ N/m$. The initial stiffness, k_z, is $10.25\ N$ and the initial stiffness of z given by ρ is $11337\ N$. The value of n is 1.12 and the value of σ is 0.95.

Table 5.3. Normalized Bouc-Wen Model with the Lowest MSE in Methods 1 and 2

Method	Training Signal	Validation Signal	c	k (x 10^4)	k_z	ρ (x 10^3)	n	σ
1	I	I	117.59	2.5090	10.25	11.337	1.12	0.95
2	I	II	117.59	2.5090	10.25	11.337	1.12	0.95

The parameters of the modified Dahl model with the lowest MSE in methods 1 and 2 is shown in Table 5.4. Two separate candidate models are obtained for methods 1 and 2. The damping, c, of these models remain between 100 and 150 $N \cdot s/m$ and the stiffness, k, remains close to 25000 N/m. The Coulomb frictional force remains close to 10 N and σ remains near 11000.

Table 5.4. Modified Dahl Model with the Lowest MSE in Methods 1 and 2

Method	Training Signal	Validation Signal	c	k (x 10^4)	F_d	σ (x 10^4)
1	I	I	111.74	2.4973	10.56	1.0579
2	I	II	140.82	2.5282	9.70	1.1473

Table 5.5 shows the parameters of two candidate modified LuGre models with the lowest MSE obtained from methods 1 and 2. The damping, c, of these models remain close to 100 $N \cdot s/m$ and the stiffness, k, remains close to 25000 N/m. The value of β is dispersed more than the other parameters and remains between 50000 and 90000 N/m. The value of α remains in the range of 5000 and 7500 m^{-1}. The generalized damping, ε, is close to 200 $N \cdot s/m$ for these models.

Table 5.5. Modified LuGre Model with the Lowest MSE in Methods 1 and 2

Trial	Method	Training Signal	Validation Signal	c	k (x 10^4)	β (x 10^4)	ε	α (x 10^3)
1	1	I	I	95.59	2.4976	8.1962	194.31	7.281
2	2	I	II	122.29	2.5034	5.9987	222.86	5.614

A comparison of errors for each of the best mechanical models trained and validated using signal I is shown in Table 5.6. The MSE and the force error with respect to time and displacement for each of these models are tightly distributed. The value of the MSE is high due to the standard deviation of displacement and acceleration response in the denominator of the equation for MSE. The displacement, velocity and acceleration response for these models is close to the actual observed experimental response. The lowest MSE is observed for the modified Dahl model. Therefore, this model is chosen to be the best candidate MR damper model in method 1. The force error with respect to time and displacement is also the lowest for this model when compared to other mechanical models.

Table 5.6. MR Damper Mechanical Models with the Lowest MSE in Method 1

Model (Method 1)	MSE (x 10^5)	E_t (x 10^{-2})	E_x (x 10^{-2})
Normalized Bouc-Wen	54.88	30.13	2.93
Modified Dahl	54.86	29.59	2.79
Modified LuGre	56.71	30.40	2.86

Table 5.7 compares the error for each of the best candidate model obtained from method 2. In addition, the error with these models when compared to the response of the structure for signals III, IV and V is shown in Table 5.8 (Figures in Appendix). Again, these error values are closely distributed between these models. The lowest MSE from Table 5.7 is recorded for the modified Dahl model and thus, this model is selected as the best candidate MR damper model for method 2. The force error with respect to time is also the lowest for this model. The force error with respect to displacement is highest for this model, however, it is still small and remains in acceptable limits for the selection of this model.

Table 5.7. MR Damper Mechanical Models with the Lowest MSE in Method 2

Model (Method 2)	MSE (x 10^5)	E_t (x 10^{-2})	E_x (x 10^{-2})
Normalized Bouc-Wen	2.93	19.09	1.39
Modified Dahl	1.62	18.10	1.61
Modified LuGre	2.49	25.14	1.57

Table 5.8. Comparison of Errors from Different Signals for MR Damper Mechanical Models with the Lowest MSE in Method 2

Validation Signal	Model	MSE $(\times 10^5)$	E_t $(\times 10^{-2})$	E_x $(\times 10^{-2})$
III	Normalized Bouc-Wen	9.65	30.65	1.79
	Modified Dahl	10.86	32.15	1.99
	Modified LuGre	12.32	47.42	2.35
IV	Normalized Bouc-Wen	18.15	45.07	2.65
	Modified Dahl	19.78	45.51	3.10
	Modified LuGre	19.18	48.78	2.72
V	Normalized Bouc-Wen	29.63	42.74	3.73
	Modified Dahl	38.28	45.52	4.63
	Modified LuGre	35.31	38.45	3.47

Thus, the parameters of modified Dahl model given in Table 5.4 are the parameters for the selected MR damper models from methods 1 and 2. The model from method 2 will be preferred over the model from method 1 if multiple sets of response data from different signals is available for the structure. This selection is based on the lower MSE of the model in method 2. In the event of limited availability of the data, the model from method 1 still performs comparatively well and can be selected as the best model. The inference history of parameters for this selected MR damper for methods 1 and 2 is shown in Figures 5.24 and 5.25, respectively. The parameter σ in Figure 5.24 converges towards the final estimated value in about 10 seconds and remains close to this value for the rest of the signal. This behavior of σ is mainly because of the sensitivity of this parameter for a small variation in input signal. However, the parameter converges well in the training of the best model in method 2 as shown in Figure 5.25. A quick convergence of other parameters to final estimated values is also evident from these figures. It is observed that the parameters converge to the final estimated value during initial 5-10 seconds of the input signal and remain close to the final estimated value for rest of the time during the input excitation.
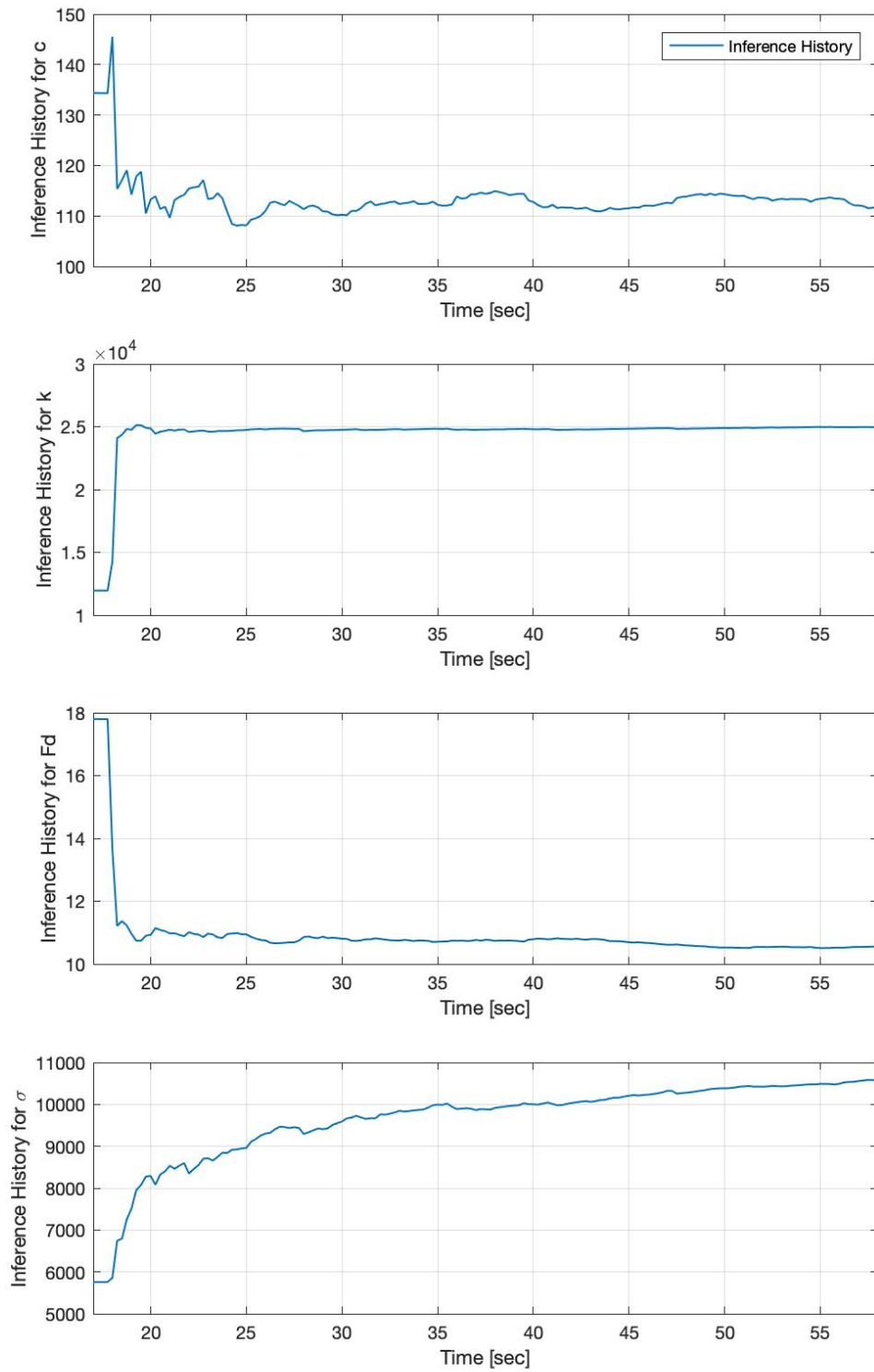
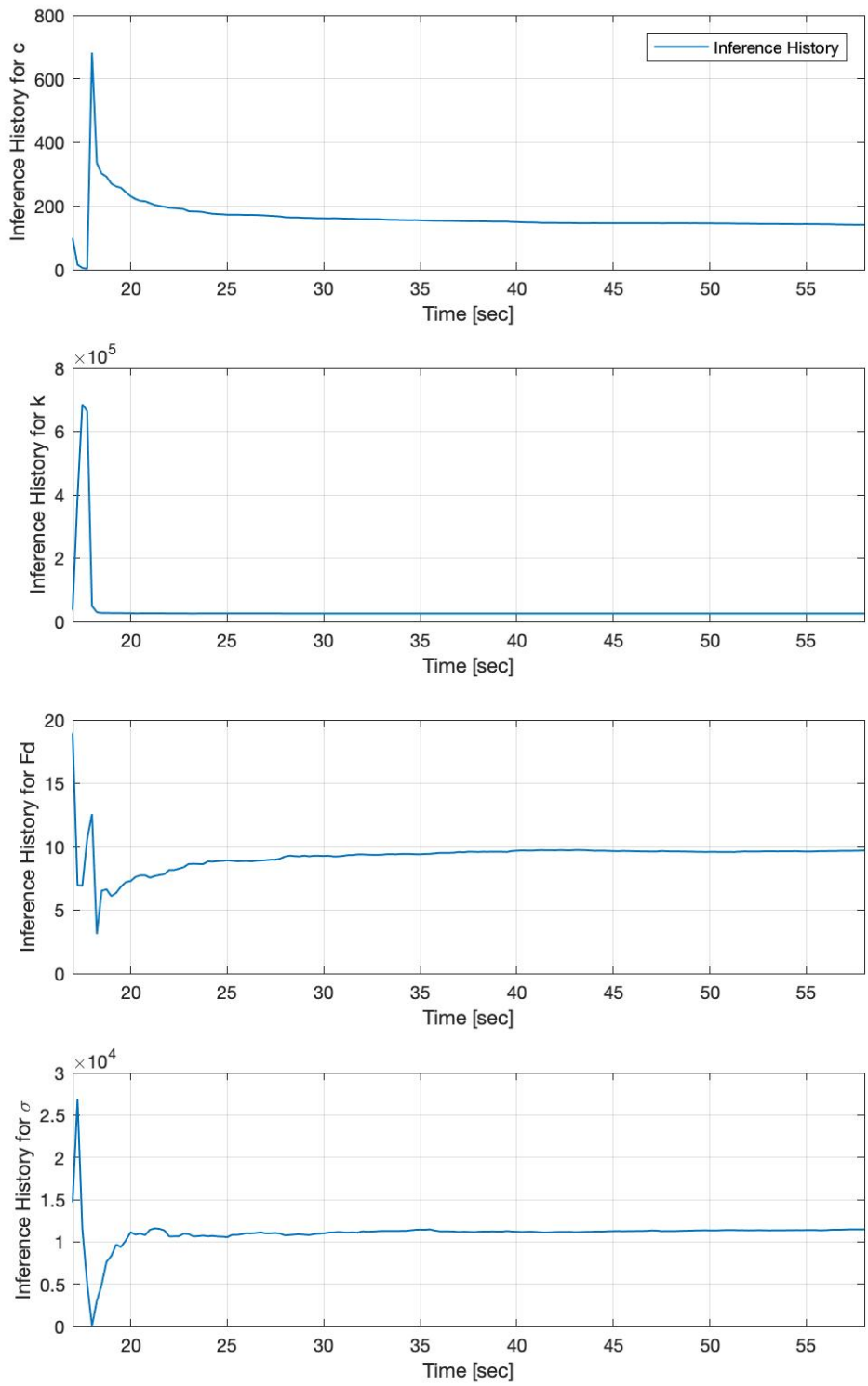Figure 5.24. Convergence History of Parameters for the Selected Model from Method 1

Figure 5.25. Convergence History of Parameters for the Selected
Model from Method 2

5.6   Summary

The findings of the chapter on experimental model selection can be summarized as:

- The MR damper shows very different behavior for displacement less than 2 mm and more than 2 mm. (Section 5.2)

- The model selection process is performed for the input signals producing displacement of more than 2 mm. (Section 5.2)

- The modified Dahl model has the highest percentage of trained candidate models and the modified LuGre model has the lowest percentage of trained candidate models. (Section 5.3)

- The UKF estimates for each mechanical form of the model in methods 1 and 2 is close to the true response of the system. (Section 5.4)

- The UKF force estimates are underestimated in some cases as only displacement and acceleration response is used for model training. (Section 5.4)

- The parameters of the modified Dahl model have the lowest MSE in both methods 1 and 2. (Section 5.5)

- The selected model with method 1 is found to still be effective when a structural response to only one signal is available (for example, an earthquake). (Section 5.5)

6. CONCLUSION AND FUTURE WORK

The conclusions from this thesis on Bayesian model selection are summarized in Section 6.1 of this chapter. The recommendations for future work on model selection are made in Section 6.2.

6.1   Conclusions

The study on experimental nonlinear device selection suggests that inducing nonlinearity in an experimental structure is simple. A number of devices emulating nonlinearity in the experimental structure are available. However, it is difficult to control, quantify and align these devices with high repeatability, efficiency and ease of implementation in the experimental structure. The nonlinearity provided by the devices is normally due to cubic, trigonometric or complex differential terms in their EOM. It is not possible for a single device to satisfy all requirements for nonlinearity and hence, several factors were prioritized to select a most suitable device for the study. A MR damper provides controllable and repeatable nonlinearity with a complex EOM. This device was selected as a suitable device to propagate nonlinearity for the current nonlinear identification study. It is inferred that a proper alignment of the MR damper is necessary while setting it up on the experimental structure. A poorly aligned damper produces improper force-displacement hysteresis response. The variables (damper fluid, electric current, paddle displacement, temperature, paddle and foam thickness) of MR damper play a major role in its behavior and should always be set within the specified range for each.

The experimental setup of the chosen MR damper was identified using three mechanical models, each trained and validated using input excitation signals, and structural displacement and acceleration response. The identification algorithm is based on Bayesian filtering technique. This filtering technique approximates states of general probabilistic state space models that are represented by sequence comprising of conditional probability distributions. The Markovian property of states followed in this technique suggests that the current and future states are independent of prior states in the system given states at the previous time step. In addition, the current measurements are independent of prior measurements and states given the current state of the system. The Kalman filter, EKF, constrained EKF and UKF are normally used filtering

techniques to predict system states and parameters. The UKF is the slowest of all nonlinear algorithms but is highly accurate and useful for systems with high nonlinearity. Therefore, the MR damper model identification study was performed using the UKF.

The model identification is performed by training and validation steps. The parameters of the UKF identification algorithm α_h, β_h and κ play a major role in getting good estimates for the trained models. The model training should be performed with a signal that produces substantial dynamic excitation in the system. This dynamic excitation is needed for the identification algorithm to estimate states and parameters of the system accurately. The majority of parameters of the trained models lie in a narrow range. The modified Dahl model gives the highest number of trained models and the modified LuGre model gives the lowest number of trained models for a similar prior distribution from indices of dispersion. The number of trained models is often less than the starting number of distributions on parameters. The estimation algorithm fails sometimes because of lack of convergence in the covariance matrix leading to poorly conditioned matrices. The parameters for trained models usually converge to final estimated value in initial five to ten seconds of excitation from the input signal.

The model validation is usually performed with different input excitation signals and the selection of this signal depends on the validation method used. The model with the lowest MSE also depends on the validation signal used and can be different for multiple forms of the validation signal. Model validation with the same signal as used for training is important for real-life scenarios where limited data for structural response is available. The model selection in the current study was performed on the basis of the lowest MSE between all mechanical forms of the model validated using a similar input excitation signal. The MSE and force error for each best candidate mechanical form of the model are closely distributed. The modified Dahl model gives the lowest MSE for both methods 1 and 2.

The lessons learned from the model selection study performed in this thesis are important for similar studies to be performed for other devices emulating nonlinearity in experimental structures and for real-life scenarios. This study will serve as a basis to research more on nonlinear damage identification for full-scale structures using Bayesian technique. The linear approach for damage identification currently used limits the knowledge of failure analysis and hence asks for more detailed nonlinear analysis. The identification approach of the current model selection process performed on the small-scale structure can be extended to full-scale systems since the

dimensionality of the current problem was analogous to a full-scale system, without undue model uncertainty.

6.2   Future Work

The model selection process demonstrated in this thesis was performed by keeping the parameters of the UKF identification algorithm α_h, β_h and κ constant. A small deviation in values of these parameters can lead to changes in the convergence behavior of the algorithm. However, a detailed study on the behavior of the algorithm with changing parameters is needed for the mechanical models of the MR damper used in this study. In addition, the model training was performed by a constant set of indices of dispersion. A more detailed analysis with higher indices of dispersion on prior distributions is recommended to reduce error due to convergence and increase the percentage of trained models. The variance on each parameter in the current study was increased simultaneously instead of taking a staggered configuration for indices of dispersion with different combinations of variance values for each parameter. The number of prior distributions on parameters will increase manifold and the computational efficiency of the algorithm will decrease in the latter. A study on the percentage of trained models and the accuracy of UKF estimates with staggered variance values is needed. Lastly, the efficiency of this UKF algorithm for MR damper model selection is to be compared with other estimation methods like constrained UKF, CEKF and particle filter methods.

A comparison of the UKF estimates with several other experimental nonlinear devices can also be made. A variable friction damper was developed in the IISL during the preliminary device selection study. A sandwich configuration of the variable friction damper with angle plates and Teflon produced repeatable and controllable nonlinearity. The friction between these plates was varied by changing the width of the rubbing plate. This preliminary study was performed using a small shaker with the damper attached to it. The force and displacement response were measured using the load cell and LVDT. A separate nonlinear structural identification can be done using this device installed on the current SDOF experimental structure. In addition, the model selection study can also be done on a 3 DOF setup with varying number of MR dampers or other nonlinear devices.

APPENDIX
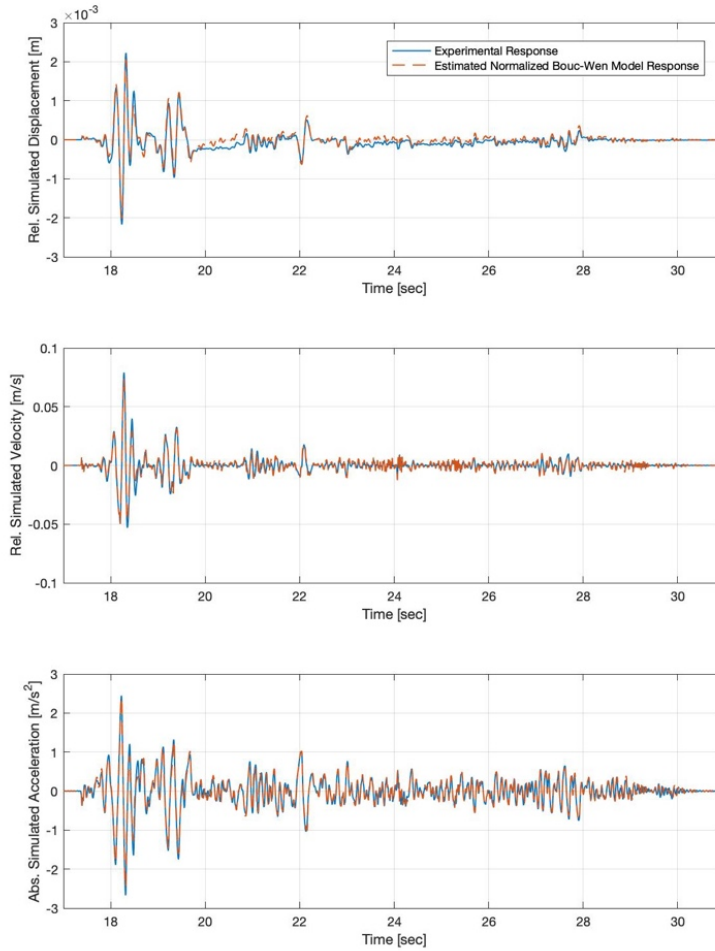
1. Normalized Bouc-Wen Model

Figure A.1. Comparison of State Estimates in Signal III for Normalized Bouc-Wen
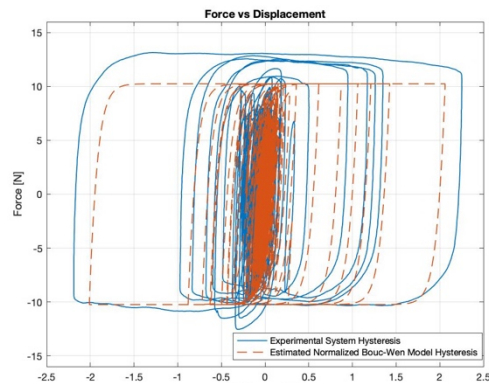Model with the Lowest MSE Trained using Signal I

Figure A.2. Comparison of Hysteresis Loops in Signal III for Normalized Bouc-Wen
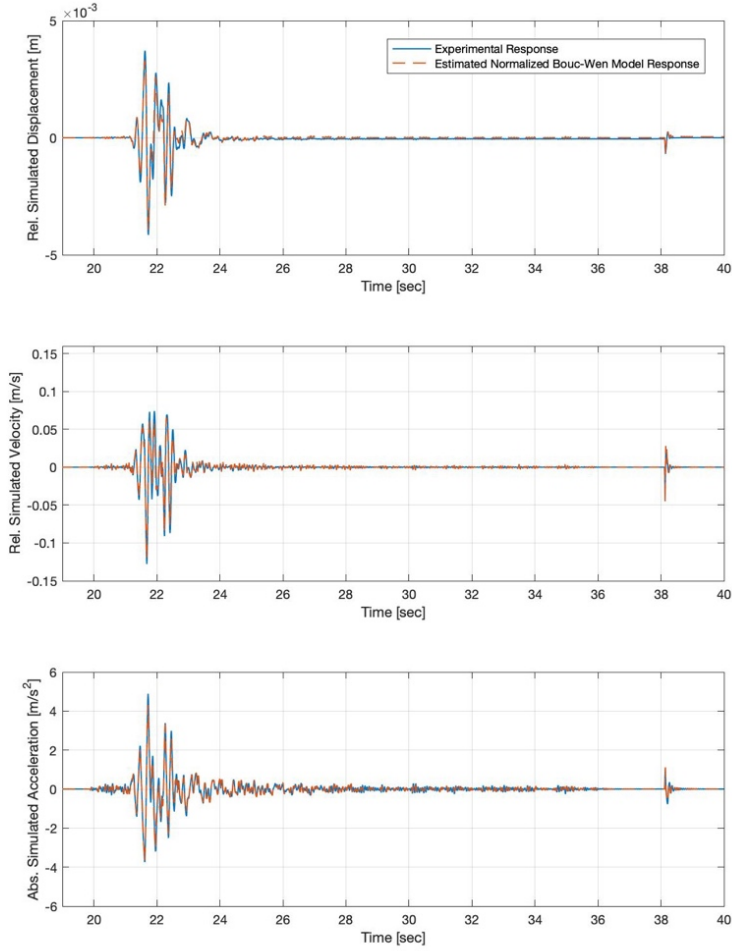Model with the Lowest MSE Trained using Signal I

Figure A.3. Comparison of State Estimates in Signal IV for Normalized Bouc-Wen Model with the Lowest MSE Trained using Signal I
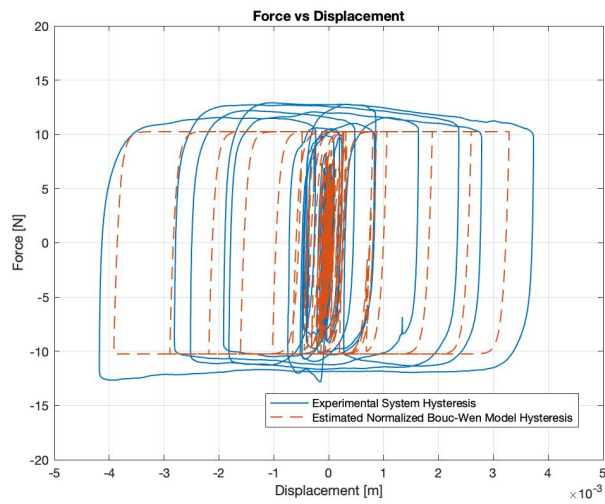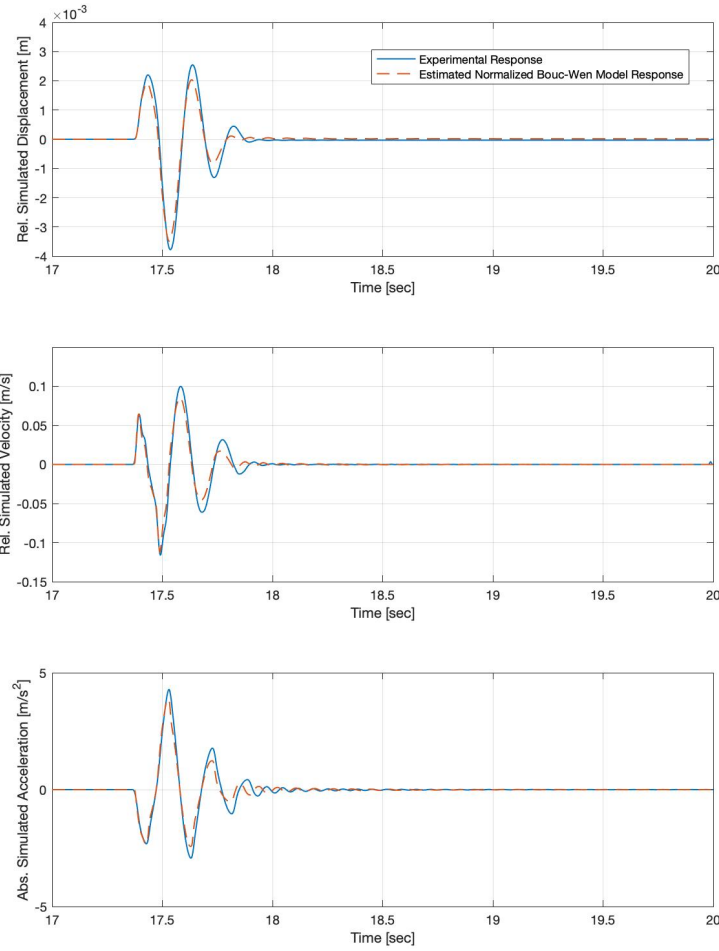

Figure A.4. Comparison of Hysteresis Loops in Signal IV for Normalized Bouc-Wen Model with the Lowest MSE Trained using Signal I

146

Figure A.5. Comparison of State Estimates in Signal V for Normalized Bouc-Wen
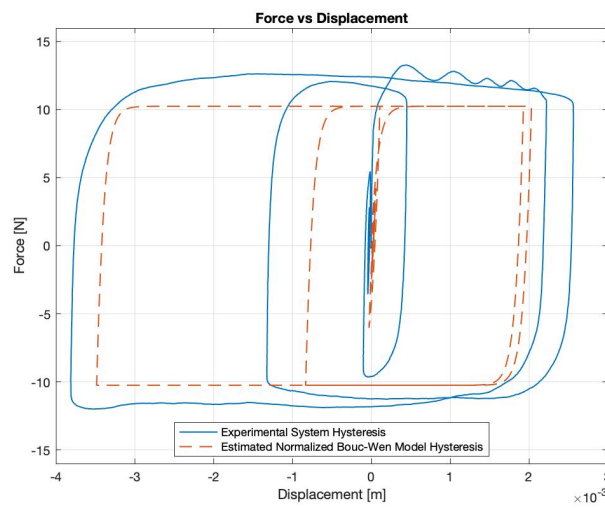Model with the Lowest MSE Trained using Signal I

Figure A.6. Comparison of Hysteresis Loops in Signal V for Normalized Bouc-Wen
Model with the Lowest MSE Trained using Signal I

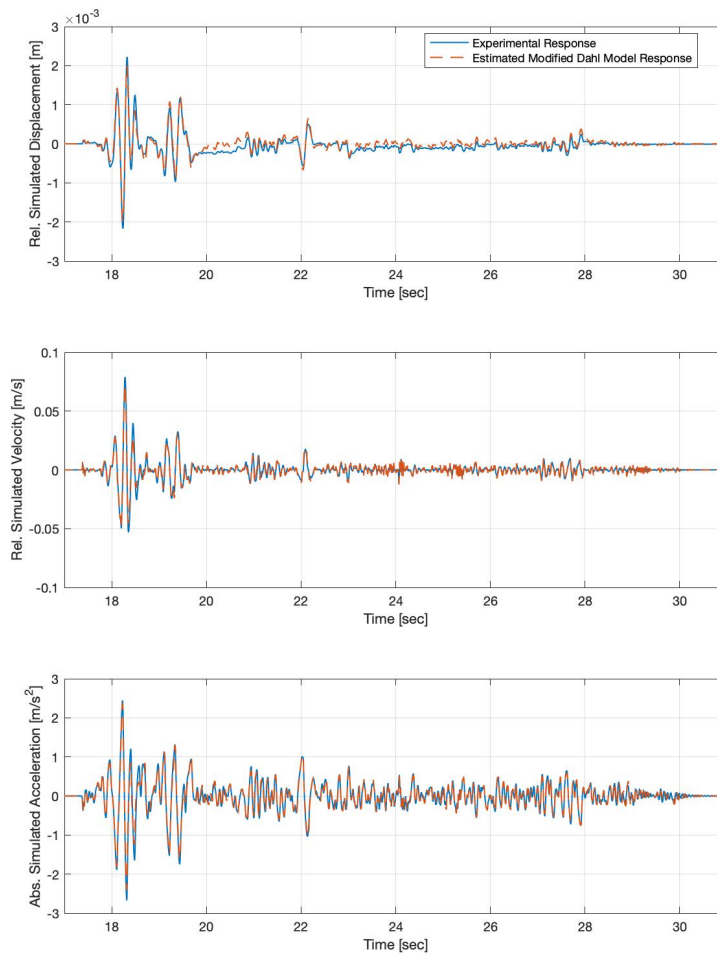## 2. Modified Dahl Model

Figure A.7. Comparison of State Estimates in Signal III for Modified Dahl Model with the Lowest MSE Trained using Signal I
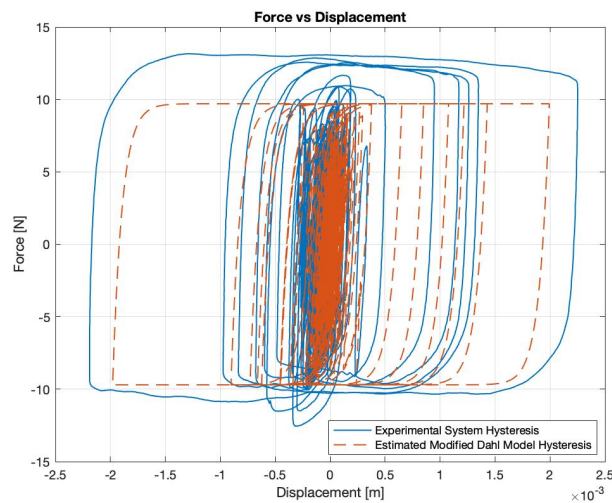

Figure A.8. Comparison of Hysteresis Loops in Signal III for Modified Dahl Model with the Lowest MSE Trained using Signal I

Figure A.9. Comparison of State Estimates in Signal IV for Modified Dahl Model with the Lowest MSE Trained using Signal I

Figure A.10. Comparison of Hysteresis Loops in Signal IV for Modified Dahl Model with the Lowest MSE Trained using Signal I
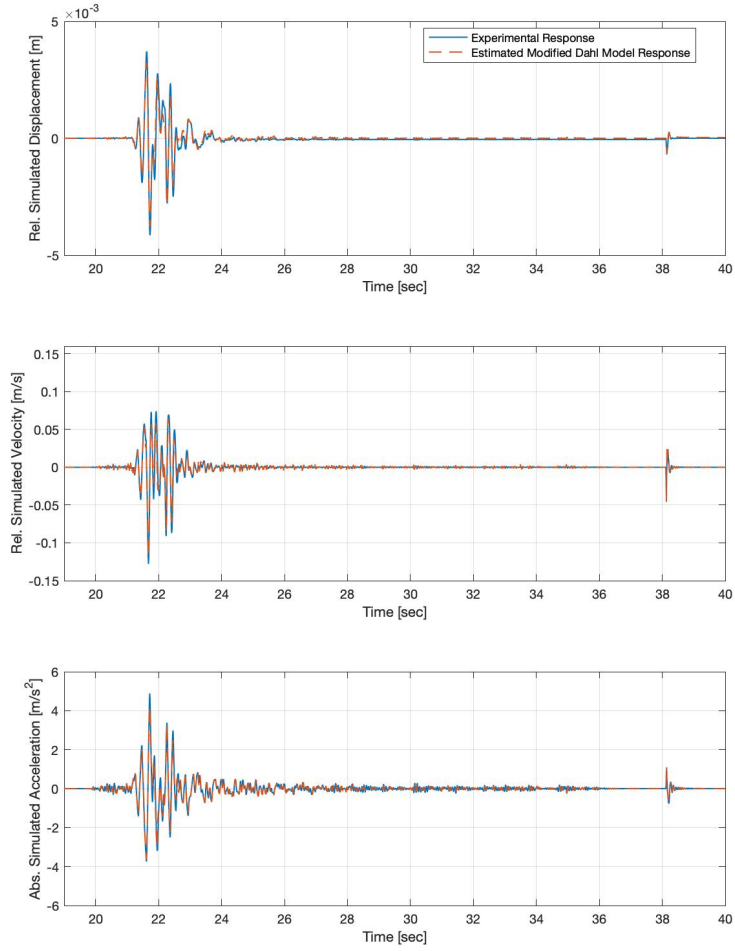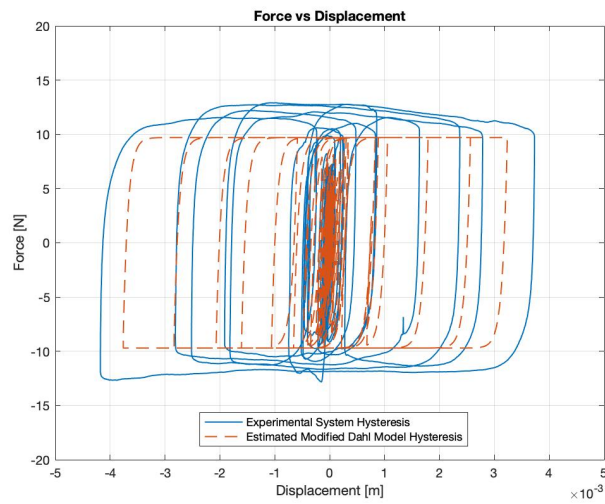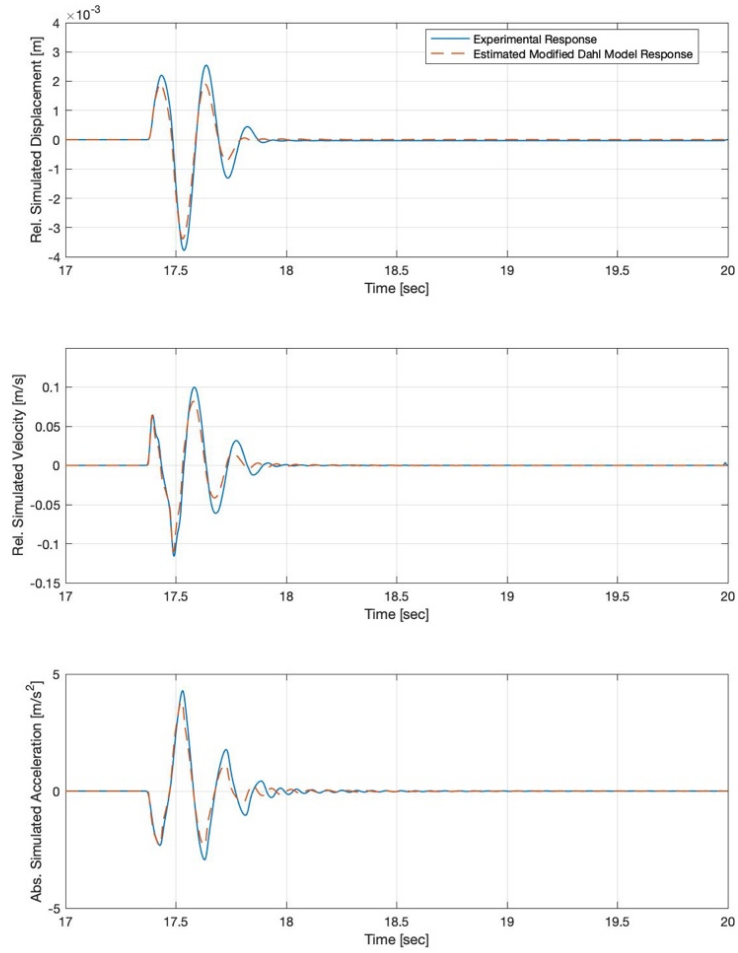
Figure A.11. Comparison of State Estimates in Signal V for Modified Dahl Model
with the Lowest MSE Trained using Signal I

Figure A.12. Comparison of Hysteresis Loops in Signal V for Modified Dahl Model with
the Lowest MSE Trained using Signal I

3. Modified LuGre Model

Figure A.13. Comparison of State Estimates in Signal III for Modified LuGre Model
with the Lowest MSE Trained using Signal I

Figure A.14. Comparison of Hysteresis Loops in Signal III for Modified LuGre Model
with the Lowest MSE Trained using Signal I

Figure A.15. Comparison of State Estimates in Signal IV for Modified LuGre Model
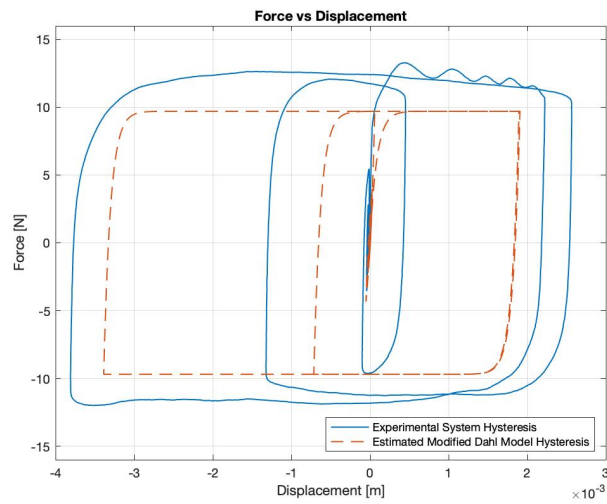with the Lowest MSE Trained using Signal I

Figure A.16. Comparison of Hysteresis Loops in Signal IV for Modified LuGre Model
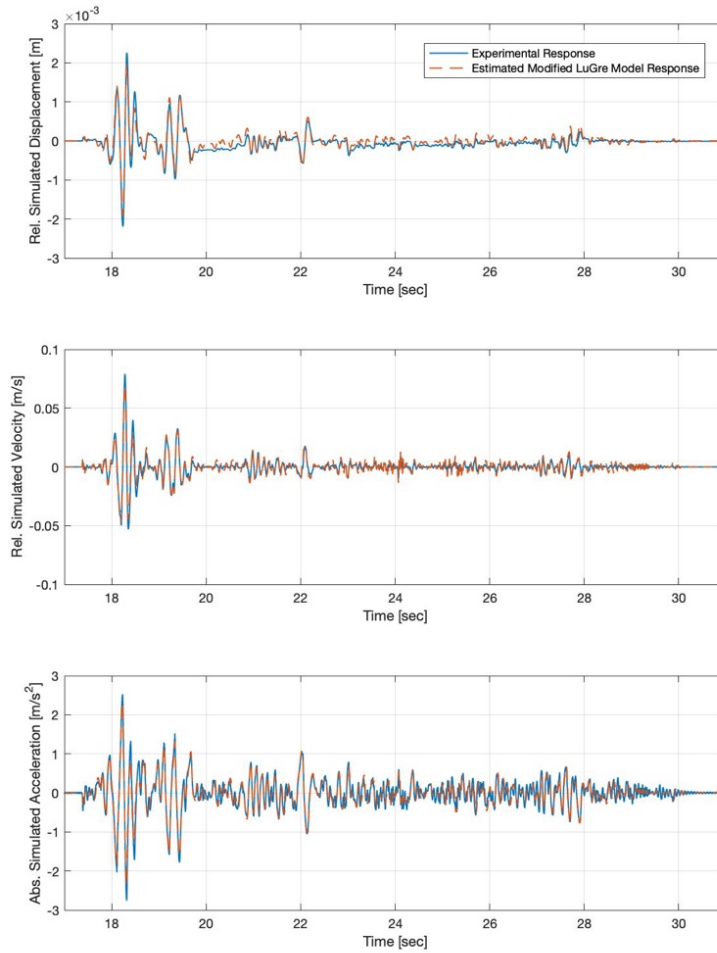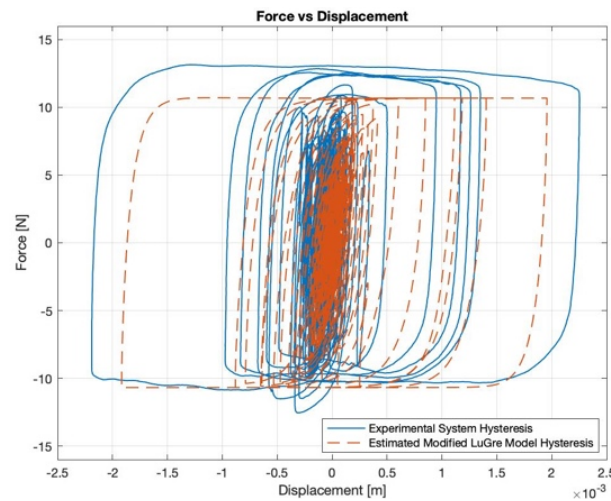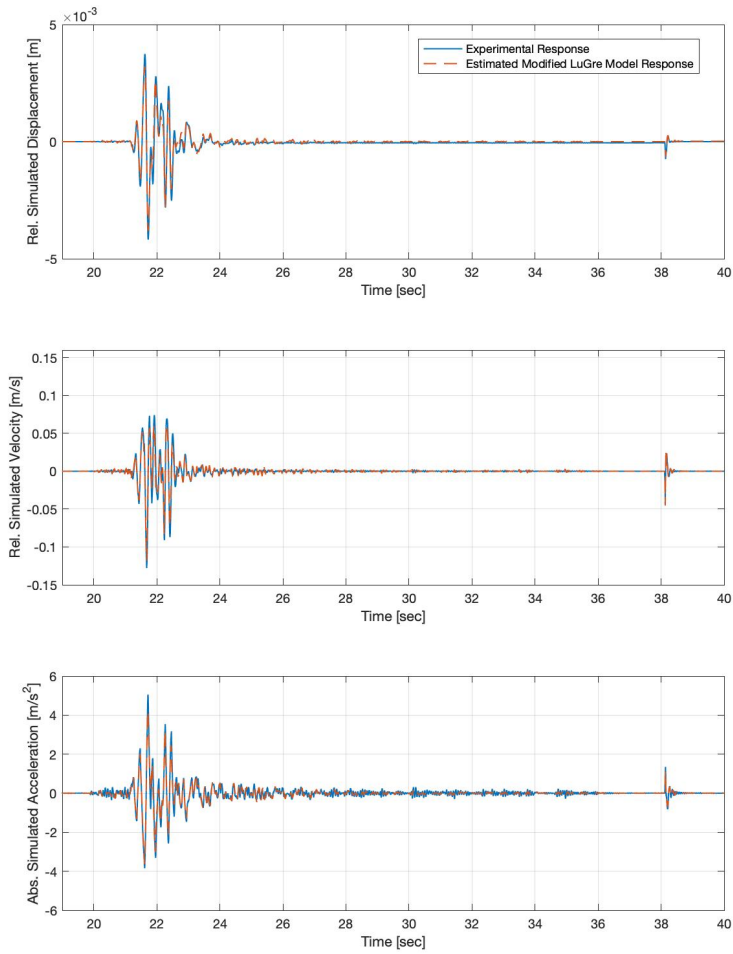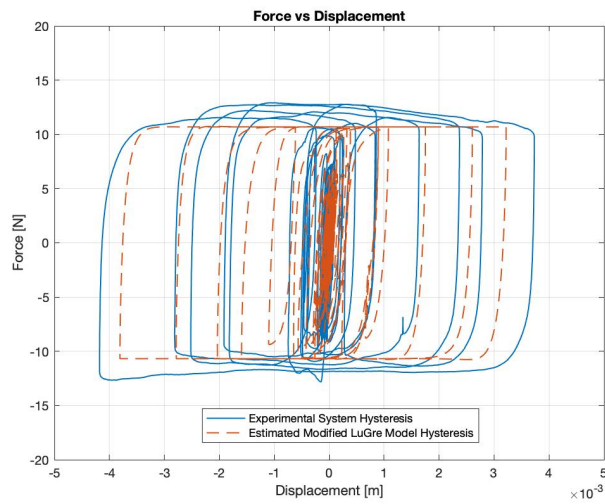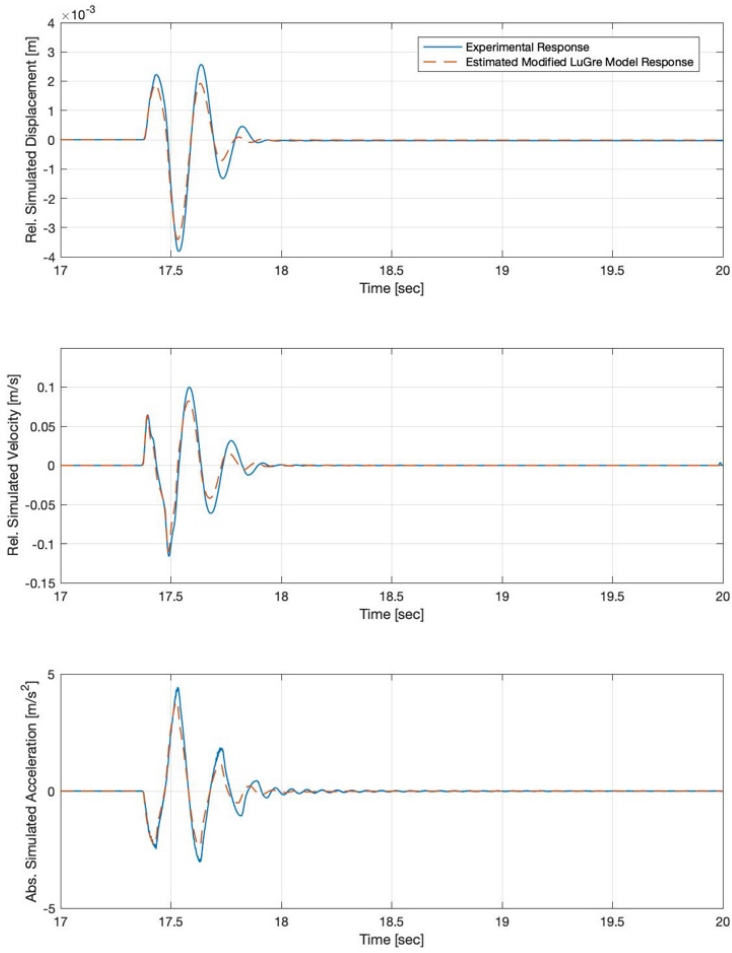with the Lowest MSE Trained using Signal I

Figure A.17. Comparison of State Estimates in Signal V for Modified LuGre Model
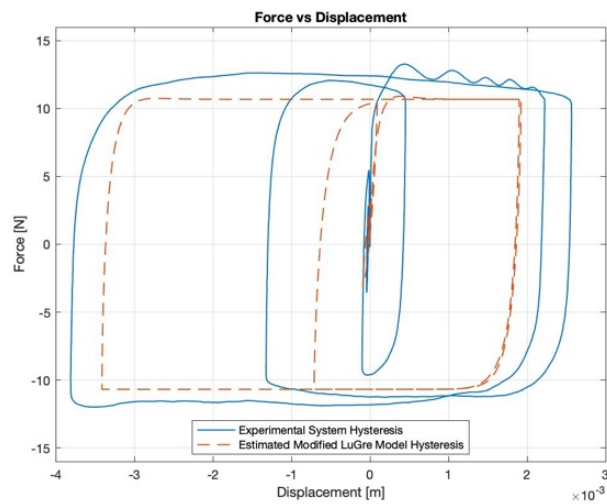with the Lowest MSE Trained using Signal I

Figure A.18. Comparison of Hysteresis Loops in Signal V for Modified LuGre Model
with the Lowest MSE Trained using Signal I

153

REFERENCES

Amjadian, M., & Agrawal, A. K. (2019). Seismic response control of multi-story base-isolated buildings using a smart electromagnetic friction damper with smooth hysteretic behavior. *Mechanical Systems and Signal Processing*, *130*, 409–432. https://doi.org/10.1016/j.ymssp.2019.05.018

Andersen, D., Starosvetsky, Y., Vakakis, A., & Bergman, L. (2012). Dynamic instabilities in coupled oscillators induced by geometrically nonlinear damping. *Nonlinear Dynamics*, *67*(1), 807–827. https://doi.org/10.1007/s11071-011-0028-0

Bamler, R., & Mandt, S. (2017). Structured Black Box Variational Inference for Latent Time Series Models. http://arxiv.org/abs/1707.01069

Beck, J. L., & Yuen, K. (2004). Model Selection Using Response Measurements: Bayesian Probabilistic Approach. *Journal of Engineering Mechanics, 130*, 192-203. https://doi.org/10.1061/ASCE0733-93992004130:2192

Bunyan, J., Moore, K. J., Mojahed, A., Fronk, M. D., Leamy, M., Tawfick, S., & Vakakis, A. F. (2018). Acoustic nonreciprocity in a lattice incorporating nonlinearity, asymmetry, and internal scale hierarchy: Experimental study. *Physical Review E*, *97*(5). https://doi.org/10.1103/PhysRevE.97.052211

Canudas De Wit, C., & Lischinsky, P. (1995). A New Model for Control of Systems with Friction. In *IEEE Transactions on Automatic Control* (Vol. 40, Issue 3).

Chang S.C., & Hu, J.F. (2016). Nonlinear Dynamics and Control in an Automotive Brake System. *Advances in Automobile Engineering*, *05*(01). https://doi.org/10.4172/2167-7670.1000135

Chang, C. M., Strano, S., & Terzo, M. (2016). Modelling of Hysteresis in Vibration Control Systems by means of the Bouc-Wen Model. In *Shock and Vibration* (Vol. 2016). Hindawi Limited. https://doi.org/10.1155/2016/3424191

Chatzi, E. N., & Smyth, A. W. (2009). The unscented Kalman filter and particle filter methods for nonlinear structural system identification with non-collocated heterogeneous sensing. *Structural Control and Health Monitoring*, *16*(1), 99–123. https://doi.org/10.1002/stc.290

Dahl, P. R. (1976). Solid friction damping of mechanical vibrations. *AIAA Journal*, *14*(12), 1675–1682. https://doi.org/10.2514/3.61511

Ealangi, I. (2010). Earthquake Protection of Buildings by Seismic Isolation. Devices and Concepts. In *Young Researchers Conference*.

Erazo, K., Sen, D., Nagarajaiah, S., & Sun, L. (2019). Vibration-based structural health monitoring under changing environmental conditions using Kalman filtering. *Mechanical Systems and Signal Processing*, *117*, 1–15. https://doi.org/10.1016/j.ymssp.2018.07.041

Gordon, N. J., Salmond, D. J., & Smith, A. F. M. (1993). Novel approach to nonlinear/non-Gaussian Bayesian state estimation. *IEE Proceedings – F, 140*, 2.

Ikhouane, F. al, & Rodellar, J. (2005). On the Hysteretic Bouc-Wen Model Part I: Forced Limit Cycle Characterization. In *Nonlinear Dynamics*, *42*, 63-78, Springer.

Ismail, M., Ikhouane, F., & Rodellar, J. (2009). The hysteresis Bouc-Wen model, a survey. *Archives of Computational Methods in Engineering*, *16*(2), 161–188. https://doi.org/10.1007/s11831-009-9031-8

Jiménez, R., & Álvarez-Icaza, L. (2005). LuGre friction model for a magnetorheological damper. *Structural Control and Health Monitoring*, *12*(1), 91–116. https://doi.org/10.1002/stc.58

Kalman, R.E. (1960). A new approach to linear filtering and prediction problems. *Journal of Basic Engineering, 82(1),* 35-45. https://doi.org/ 10.1115/1.3662552

Karami, K., Manie, S., Ghafouri, K., & Nagarajaiah, S. (2019). Nonlinear structural control using integrated DDA/ISMP and semi-active tuned mass damper. *Engineering Structures*, *181*, 589–604. https://doi.org/10.1016/j.engstruct.2018.12.059

Kim, Y., Hurlebaus, S., Sharifi, R., & Langari, R. (2009). Nonlinear Identification of MIMO Smart Structures. *Proceedings of the ASME 2009 Dynamic Systems and Control Conference*, *ASME*, *1*, 33-40, https://doi.org/10.1115/DSCC2009-2715

Kontoroupi, T., & Smyth, A. W. (2017). Online Bayesian model assessment using nonlinear filters. *Structural Control and Health Monitoring*, *24*(3). https://doi.org/10.1002/stc.1880

Lei, Y., Xia, D., Erazo, K., & Nagarajaiah, S. (2019). A novel unscented Kalman filter for recursive state-input-system identification of nonlinear systems. *Mechanical Systems and Signal Processing*, *127*, 120–135. https://doi.org/10.1016/j.ymssp.2019.03.013

Li, D., & Wang, Y. (2021). Parameter identification of a differentiable Bouc-Wen model using constrained extended Kalman filter. *Structural Health Monitoring*, *20*(1), 360–378. https://doi.org/10.1177/1475921720929434

Lund, A., Dyke, S. J., Song, W., & Bilionis, I. (2019). Global sensitivity analysis for the design of nonlinear identification experiments. *Nonlinear Dynamics*, *98*(1), 375–394. https://doi.org/10.1007/s11071-019-05199-9

Lund, A., Dyke, S. J., Song, W., & Bilionis, I. (2020). Identification of an experimental nonlinear energy sink device using the unscented Kalman filter. *Mechanical Systems and Signal Processing, 136*. https://doi.org/10.1016/j.ymssp.2019.106512

Ma, F., Zhang, H., Bockstedte, A., Foliente, G. C., & Paevere, P. (2004). Parameter analysis of the differential model of hysteresis. *Journal of Applied Mechanics, Transactions ASME*, *71*(3), 342–349. https://doi.org/10.1115/1.1668082

McFarland, D. M., Bergman, L. A., & Vakakis, A. F. (2005). Experimental study of non-linear energy pumping occurring at a single fast frequency. *International Journal of Non-Linear Mechanics*, *40*(6), 891–899. https://doi.org/10.1016/j.ijnonlinmec.2004.11.001

Meiliang, W., & Smyth, A. W. (2007). Application of the unscented Kalman filter for real-time nonlinear structural system identification. *Structural Control and Health Monitoring*, *14*(7), 971–990. https://doi.org/10.1002/stc.186

Muto, M., & Beck, J. L. (2008). Bayesian updating and model class selection for hysteretic structural models using stochastic simulation. *JVC/Journal of Vibration and Control*, *14*(1–2), 7–34. https://doi.org/10.1177/1077546307079400

Nishitani, A., Nitta, Y., Ishibashi, Y., & Itoh, A. (1999). Semi-Active Structural Control with Variable Friction Dampers. *Proceedings of the American Control Conference, San Diego, CA, USA*, *2*, 1017-1021. https://doi.org/10.1109/ACC.1999.783194

Olivier, A., & Smyth, A. W. (2017). On the performance of online parameter estimation algorithms in systems with various identifiability properties. *Frontiers in Built Environment*, *3*. https://doi.org/10.3389/fbuil.2017.00014

Oyelade, A. O. (2020). Experiment study on nonlinear oscillator containing magnetic spring with negative stiffness. *International Journal of Non-Linear Mechanics*, *120*. https://doi.org/10.1016/j.ijnonlinmec.2019.103396

Peeters, M., Kerschen, G., & Golinval, J. C. (2011). Modal testing of nonlinear vibrating structures based on nonlinear normal modes: Experimental demonstration. *Mechanical Systems and Signal Processing*, *25*(4), 1227–1247. https://doi.org/10.1016/j.ymssp.2010.11.006

S. Sarkka, in: Bayesian Filtering and Smoothing, Cambridge University Press, 2013, https://doi.org/10.1017/CBO9781139344203.

Spencer Jr, B., Dyke, S., Sain, M., & Carlson, J. (1997). Phenomenological Model for Magnetorheological Dampers. *Journal of Engineering Mechanics, 123*(3), 230-238. https://doi.org/10.1061/(ASCE)0733-9399(1997)123:3(230)

Spencer Jr, B., & Nagarajaiah, S. (2003). State of the Art of Structural Control. *Journal of Structural Engineering, 129*(7), 845-856. https://doi.org/10.1061/(asce)0733-9445(2003)129:7(845)

Starosvetsky, Y., & Gendelman, O. V. (2008). Dynamics of a strongly nonlinear vibration absorber coupled to a harmonically excited two-degree-of-freedom system. *Journal of Sound and Vibration*, *312*(1–2), 234–256. https://doi.org/10.1016/j.jsv.2007.10.035

Ungarala, S., Dolence, E., & Li, K. (2007). Constrained Extended Kalman Filter for Nonlinear State Estimation. *IFAC Proceedings Volumes, 40*(5), 63-68. https://doi.org/10.3182/20070606-3-mx-2915.00058

Wan, E. A., & Nelson, A. T. (1997). Dual Kalman Filtering Methods for Nonlinear Prediction, Smoothing, and Estimation. *Advances in Neural Information Processing Systems,* 793-799.

Wan, E. A., and Van Der Merwe, R. (2000). The unscented Kalman filter for nonlinear estimation. *In Proceedings of the IEEE 2000 Adaptive Systems for Signal Processing, Communications, and Control Symposium 2000. AS-SPCC (Lake Louise: IEEE)*, 153–158. https://doi.org/10.1109/ASSPCC.2000.882463

Xu, B., Deng, B. C., Li, J., & He, J. (2019). Structural nonlinearity and mass identification with a nonparametric model using limited acceleration measurements. *Advances in Structural Engineering*, *22*(4), 1018–1031. https://doi.org/10.1177/1369433218792083

Zhu, X., & Lu, X. (2011). Parametric identification of Bouc-Wen model and its application in mild steel damper modeling. *Procedia Engineering*, *14*, 318–324. https://doi.org/10.1016/j.proeng.2011.07.039